Non Linear Optimal Control Strategies For Geostationary Spacecraft Orbit Station Keeping Using Electrical Propulsion Only

Thesis
to achieve the degree
Master of Science

submitted by

Maximilian Roth
born on 10th March 1990 in Karlstadt, Germany

Department of Cybernetics
Institute for Electrical Engineering
Czech Technical University
2016

Co-funded by the
Erasmus+ Programme
of the European Union

LULEÅ
TEKNISKA
UNIVERSITET

Czech Technical University in Prague
Faculty of Electrical Engineering

Department of Control Engineering

DIPLOMA THESIS ASSIGNMENT

Student: **Maximilian Roth**

Study programme: Cybernetics and Robotics
Specialisation: Systems and Control

Title of Diploma Thesis: **Non Linear Optimal Control Strategies For Geostationary Spacecraft Orbit Station Keeping Using Electric Propulsion Only**

Guidelines:

The main objective of this thesis is indeed to develop optimal control strategies in order to keep a geostationary spacecraft within its allocated control box using electric propulsion only which is done for "SCISYS Deutschland GmbH" under technical supervision of Pau Hebrero Casasayas. The work shall first investigate "state-of-the-art" solutions which are currently in development or already used operationally.

1. It shall then focus on the modelling and appropriate parameterisation of the free non-linear orbit dynamics equations (including all the relevant perturbations).
2. It shall then properly formulate the optimal control problem under all the applicable constraints, making use of electric propulsion as the only control force.
3. It shall then implement and validate (also through simulation) numerical algorithms to solve the subject problem, targeting numerical robustness and efficiency because of the intended future operational use.

Bibliography/Sources:

[1] F. Topputo, F. Bernelli-Zazzera. Optimal Low-Thrust Station Keeping of Geostationary Satellites.
[2] Damiana Losa. High vs Low Thrust Station Keeping Maneuver Planning for Geostationary Satellites. Automatic. École Nationale Supérieure des Mines de Paris, 2007. English.

Diploma Thesis Supervisor: doc. Martin Hromčík Ing., Ph.D.

Valid until the summer semester 2016/2017

L.S.

prof. Ing. Michael Šebek, DrSc.
Head of Department

prof. Ing. Pavel Ripka, CSc.
Dean

Prague, February 24, 2016

Submitted on 14th August 2016

Supervisor: doc. Martin Hromčík Ing., Ph.D.

Abstract

This thesis concentrates on the non-linear optimisation of the station keeping problem of a low-thrust geostationary satellite and provides with the Approximate Sequence of Riccati Equation (ASRE) optimisation method a tool to decrease the total fuel consumption to a global minimum.
Creating a perturbation model for geostationary satellites with only electrical propulsion systems and describing an optimal control algorithm called Approximated Sequence of Riccati Equations with the transition method approach which guarantees convergence to its global optimum are necessary to design an accurate simulation of the station keeping problem. Therefore, these are combined with the spacecraft dynamics and the optimisation method to calculate a global optimal fuel consumption in a fixed time horizon. As far as the author knows the description of the ASRE algorithm with transition matrix approach is the detailed, public available one. It is the first time that the umbra and penumbra are considered for the perturbation model for the used optimisation method. For the verification of the final fuel consumption, the results of common literature, like Losa [14], are used to demonstrate the functionality of the used optimisation. The findings of this thesis illustrate the complexity of the non-linear station keeping problem as well as the Approximated Sequence of Riccati Equations optimisation method for geostationary satellites can compete with already available solutions. Furthermore, the derivation of the State-Dependent Riccati Equations to the Approximated Sequence of Riccati Equations is discussed and approaches to decrease the propellant consumption are considered like changing the mathematical factorisations or constraining the problem in another way. The expectations of the optimisation approach are absolutely fulfilled, but the final result has to go through more optimisations of the adjustable variables to achieve better results than provided by common literature.
To conclude, the used optimisation method has the power to provide a very low propellant consumption profile for geostationary station keeping, but in the future some further improvements to the free parameters of the optimisation have to be done.

Keywords

Approximate Sequence of Riccati Equations. ASRE. Optimal control. Optimal control with transition matrix. Low-thrust station keeping. Flight dynamics. Perturbation.

Acknowledgement

First, I would like to express my gratitude to my technical supervisors Pau Hebrero Casasayas and Livio Tucci at *SCISYS Deutschland GmbH*. Their guidance, patience and support during this time were fundamental to complete this work.
My thanks also go to Martin Hromčík who made it possible to write the thesis abroad and to everyone of the SpaceMaster programme. In addition, I would like to thank the support of the Education, Audiovisual and Culture Executive Agency of the Commission of the European Communities under the Erasmus Mundus Framework.
Finally, but importantly, I would like to thank my parents, girlfriend and friends for their unending support during these years abroad. This would not have been possible without you.

Declaration

I, Maximilian Roth, declare that this thesis titled, 'Non-Linear Optimal Control Strategies For Geostationary Spacecraft Orbit Station Keeping Using Electrical Propulsion Only' and the work presented in it are my own. I confirm that:

- This work was done wholly or mainly while in candidature for a research degree at this University.
- Where any part of this thesis has previously been submitted for a degree or any other qualification at this University or any other institution, this has been clearly stated.
- Where I have consulted the published work of others, this is always clearly attributed.
- Where I have quoted from the work of others, the source is always given. With the exception of such quotations, this thesis is entirely my own work.
- I have acknowledged all main sources of help.
- Where the thesis is based on work done by myself jointly with others, I have made clear exactly what was done by others and what I have contributed myself.

Darmstadt, 14th August 2016

Maximilian Roth

Contents

Page

List of Figures **ix**

List of Tables **xii**

1 Introduction **1**
1.1 Related Work . . . 2
1.2 Outline . . . 3

2 Background **5**
2.1 Orbit elements . . . 5
2.1.1 Classical Orbital Elements . . . 5
2.1.2 Equinoctial Orbital Elements . . . 5
2.2 Coordinate Reference Frames . . . 6
2.2.1 Earth-Centred Inertial . . . 7
2.2.2 Earth-Centred Earth-Fixed . . . 8
2.2.3 Radial Tangential Normal . . . 9
2.3 Fuel consumption . . . 10

3 Perturbations **11**
3.1 Earth Gravity Attraction . . . 11
3.1.1 Non-normalised Earth Gravity Attraction . . . 12
3.1.2 Normalised Earth's Gravity Attraction . . . 16
3.2 Gravity Attraction of Celestial Bodies . . . 19
3.3 Solar Radiation Pressure . . . 21
3.3.1 Neglection of Umbra and Penumbra . . . 21
3.3.2 Umbra and Penumbra . . . 21

4 Approximate Sequence of Riccati Equations **26**
4.1 State-dependent Riccati Equations . . . 26
4.1.1 Theory . . . 26
4.1.2 State-Dependent Coefficient Matrix . . . 27
4.1.3 Controllability . . . 27
4.1.4 Observability . . . 28
4.1.5 Linear Quadratic Control . . . 29
4.1.6 Control Structure . . . 29
4.1.7 Degrees of Freedom . . . 30

4.2 Approximate Squence of Riccati Equations . . . 31
4.2.1 Background . . . 31
4.2.2 Linear Quadratic Optimal Control . . . 32
4.2.3 Theory . . . 32
4.2.4 Solving the Approximate Squence of Riccati Equations . . . 33
4.3 Approximate Squence of Riccati Equations with Transition Matrix Approach . . . 34
4.3.1 Non-linear constrained problems . . . 35
4.3.1.1 Hard-constrained Problem . . . 35
4.3.1.2 Soft-constrained Problem . . . 35
4.3.1.3 Mixed-constrained Problem . . . 36
4.3.2 Implementation of the Approximate Sequence of Riccati Equations with Transition Matrix Approach . . . 38
4.3.3 Example of Approximate Sequence of Riccati Equations . . . 39

5 Spacecraft Dynamics **50**
5.1 Dynamic Equation of Motion in Spherical Coordinates . . . 50
5.2 Unperturbed and Uncontrolled Nominal Dynamics . . . 52
5.3 Perturbed and Uncontrolled Nominal Dynamics . . . 52
5.4 Factorisation of the System Matrix . . . 53
5.5 Perturbed and Controlled Nominal Dynamics . . . 54

6 Valdiation and Results **56**
6.1 Free Drift . . . 57
6.2 Control . . . 60
6.3 Free Drift and Control . . . 65
6.4 Optimisation of Weighting Matrices . . . 68
6.5 Optimised Control . . . 73
6.6 Different Factorisations . . . 76
6.7 Comparison . . . 80

7 Conclusion **84**
7.1 Thesis Contributions . . . 84
7.2 Future Work . . . 85

A Q-Matrix **87**

B Symbols **90**

C Acronyms **92**

D Bibliography **93**

List of Figures

2.1 Classical orbital elements 6
2.2 Earth-Centered Inertial (ECI) reference coordinate frame 7
2.3 Earth-Centred Earth-Fixed (ECEF) reference coordinate frame 9
2.4 Radial-Tangential-Normal (RTN) reference coordinate frame 10

3.1 Norm of all perturbations including SRP, Sun and Moon attraction as well as Tesserals and Zonals up to order and degree of three for one year at longitude of 60 deg 11
3.2 Drift change due to Earth's gravity field seen from North pole according to Soop [22] . . . 13
3.3 Third body disturbance of spacecraft 20
3.4 Norm of moon perturbation for geostationary spacecraft for one year at longitude of 60 deg 20
3.5 Shadow model according to Montenbruck [18] 23
3.6 Norm of solar radiation pressure acceleration including eclipse acting on a spacecraft in height of 1000 km at the same moment with different longitude values 25

4.1 Error behaviour of factorisation $\mathbf{A}_{\alpha 1}$ in a hard constrained non-linear problem 41
4.2 Hard constraints of factorisation $\mathbf{A}_2$ and $\mathbf{A}_3$ 43
4.3 Hard constrained problem solved by different factorisations 44
4.4 Hard constraints of factorisation $\mathbf{A}_{\alpha 1}$ for different iterations 45
4.5 Soft constraints of factorisation $\mathbf{A}_2$ and $\mathbf{A}_3$ 48
4.6 Soft constraints of different factorisations 49

6.1 Free Drift of spacecraft in two weeks with Euler integration (600 s): distance to Earth over time 58
6.2 Free Drift of spacecraft in two weeks with Euler integration (600 s): longitude over time . 58
6.3 Free Drift of spacecraft in two weeks with Euler integration (600 s): latitude over time . . 59
6.4 Free Drift of spacecraft in two weeks with Euler integration (600 s): longitude vs latitude 59
6.5 Position of spacecraft with two hard constraints (r, ϵ) with Euler integration (60 s): distance to Earth over time 61
6.6 Position of spacecraft with two hard constraints (r, ϵ) with Euler integration (60 s): longitude deviation over time 61
6.7 Position of spacecraft with two hard constraints (r, ϵ) with Euler integration (60 s): latitude over time 62
6.8 Position of spacecraft with two hard constraints (r, ϵ) with Euler integration (60 s): latitude over longitude deviation 62
6.9 Velocity of spacecraft with two hard constraints (r, ϵ) with Euler integration (60 s): radial velocity over distance to Earth 63

6.10 Velocity of spacecraft with two hard constraints (r, ϵ) with Euler integration (60 s): tangential velocity over longitude deviation . . . 63
6.11 Velocity of spacecraft with two hard constraints (r, ϵ) with Euler integration (60 s): normal velocity over latitude . . . 64
6.12 Thrust control profile of non-linear system with two hard constraints (r, ϵ) with Euler integration (60 s) . . . 64
6.13 Spherical position of spacecraft after free drifts and controlled manoeuvres with only hard constraints and Euler integration (600 s): distance to Earth over time . . . 66
6.14 Spherical position of spacecraft after free drifts and controlled manoeuvres with only hard constraints and Euler integration (600 s): longitude deviation over time . . . 66
6.15 Spherical position of spacecraft after free drifts and control manoeuvres with only hard constraints and Euler integration (600 s): latitude over time . . . 67
6.16 Spherical position of spacecraft after free drifts and control manoeuvres with only hard constraints and Euler integration (600 s): latitude over longitude deviation . . . 67
6.17 Spacecraft after free drifts and control manoeuvres with only hard constraints and Euler integration (600 s): thrust control profile . . . 68
6.18 Optimisation of weighting matrix $\mathbf{S}$ with one hard constraint (r) and Euler integration (600 s): final longitude deviation values . . . 70
6.19 Optimisation of weighting matrix $\mathbf{S}$ with one hard constraint (r) and Euler integration (600 s): final latitude values . . . 70
6.20 Optimisation of weighting matrix $\mathbf{S}$ with one hard constraint (r) and Euler integration (600 s): final radial drift values . . . 71
6.21 Optimisation of weighting matrix $\mathbf{S}$ with one hard constraint (r) and Euler integration (600 s): final tangential drift values . . . 71
6.22 Optimisation of weighting matrix $\mathbf{S}$ with one hard constraint (r) and Euler integration (600 s): final normal drift values . . . 72
6.23 Optimisation of weighting matrix $\mathbf{S}$ with one hard constraint (r) and Euler integration (600 s): Δv . . . 72
6.24 Optimisation of weighting matrix $\mathbf{S}$ with one hard constraint (r) and Euler integration (600 s): mass of used fuel . . . 73
6.25 Free Drift and control of spacecraft with optimised weighting matrices with only hard constraints and Euler integration (600 s): distance to Earth vs. time . . . 74
6.26 Free Drift and control of spacecraft with optimised weighting matrices with only hard constraints and Euler integration (600 s): longitude deviation vs. time . . . 74
6.27 Free Drift and control of spacecraft with optimised weighting matrices with only hard constraints and Euler integration (600 s): latitude vs. time . . . 75
6.28 Free Drift and control of spacecraft with optimised weighting matrices with only hard constraints and Euler integration (600 s): latitude vs. longitude deviation . . . 75
6.29 Free Drift and control of spacecraft with optimised weighting matrices with only hard constraints and Euler integration (600 s): thrust control profile . . . 76
6.30 Free Drift and control of a spacecraft via factorisation $\mathbf{A}_1$ for one month with only hard constraints and Euler integration (600 s) . . . 79

6.31 Free Drift and control of a spacecraft with ones in the parameter factorisation for one month with only hard constraints and Euler integration (600 s) 79
6.32 Free Drift and control of a spacecraft with random parameter factorisation for one month with only hard constraints and Euler integration (600 s) 80
6.33 Distance to Earth over longitude for one year for a geostationary satellite with the random parameter factorisation with only hard constraints and Euler integration (1200 s) 81
6.34 Latitude over longitude deviations for one year for a geostationary satellite with the random parameter factorisation with only hard constraints and Euler integration (1200 s) . . 81
6.35 Thrust in radial direction for one year for a geostationary satellite with the random parameter factorisation with only hard constraints and Euler integration (1200 s) 82
6.36 Thrust in tangential direction for one year for a geostationary satellite with the random parameter factorisation with only hard constraints and Euler integration (1200 s) 82
6.37 Thrust in normal direction for one year for a geostationary satellite with the random parameter factorisation with only hard constraints and Euler integration (1200 s) 83

A.1 Optimisation of weighting matrix $\mathbf{Q}$ 87
A.2 Optimisation of weighting matrix $\mathbf{Q}$ 88
A.3 Optimisation of weighting matrix $\mathbf{Q}$ with one hard constraint (r) and Euler integration (600 s 89

List of Tables

3.1 Legendre polynomials and geopotential coefficients up to order and degree three (see Losa [14]) . . . 14
3.3 Induced acceleration by the Earth gravity attraction in inertial Cartesian coordinates . . . 14
3.3 Induced acceleration by the Earth gravity attraction in inertial Cartesian coordinates (continued) . . . 15
3.3 Induced acceleration by the Earth gravity attraction in inertial Cartesian coordinates (continued) . . . 16
3.2 Gravitational potential for Earth in ECI frame . . . 17
3.4 Normalised geopotential coefficients up to order and degree three in units of 10^{-6} . . . 18
3.5 Induced acceleration by the Earth gravity attraction in inertial Cartesian coordinates . . . 18
3.6 Perturbing acceleration of Moon and Sun in inertial Cartesian coordinates . . . 20
3.7 Solar radiation pressure in inertial Cartesian frame . . . 22

4.1 Error progress of the infinity norm of the actual iteration compared with the previous iteration of factorisation $\mathbf{A}_{\alpha 1}$ in a hard constrained non-linear problem . . . 42
4.2 Number of iterations and cost function of different factorisations for hard-constrained problem 46
4.3 Number of iterations and cost function of different factorisations in soft constrained problem 47

5.1 Factorisation of satellite dynamics . . . 54

1 Introduction

Traditionally geostationary spacecrafts orbiting the Earth hold their position with chemical thrusters. These thrusters are well-known and provide a high Δv which allows them to fire once every two weeks in order to stay close at the chosen nominal longitude in the geostationary orbit. A low specific impulse and a low effective exhaust velocity are the main disadvantages of chemical thrusters. Due to Tsiolkovsky's rocket equation thrusters based on chemical propulsion systems need a lot of fuel. In contrast, modern low-thrust spacecrafts provide a very high specific impulse with a large effective exhaust velocity. The provided thrust is smaller than chemically produced thrust. However, electrical thrusters can be fired for longer times and the main limiter is the available electrical power.
Therefore, different researchers are trying to optimise the propellant consumption of station keeping of geostationary satellites with chemical thrusters to a minimum. However, the satellite providers are changing their way of thinking towards electrical propulsion systems for geostationary spacecrafts because of the high fuel consumption of satellites with chemical propulsion systems. The main disadvantage of electrical ones is that they need up to six months in the geostationary transfer orbit and get a high dose of radiation in the Van-Allen belt. In this time, the spacecraft is not available for the customer and provider. On the other hand, spacecrafts with electrical propulsion systems need less fuel compared to ones with chemical systems – the high exhaust velocity and high specific impulse decrease the amount of fuel to an optimal minimum although their available thrust is very low. This propellant saving can be directly transferred to lower costs of the start of the spacecraft or can grant the possibility to bring more payload up in the geostationary orbit. Alternatively, the spacecraft can stay in orbit with the same amount of fuel.
To reduce this long period in the geostationary transfer orbit, modern control algorithms can decrease the transfer time to a good trade-off between used propulsion and time. Those algorithms are optimising the station keeping procedure of electric thrusted satellites, too. According to international contracts, the geostationary spacecraft has to stay inside of its control box. External forces are acting on the satellite. Thus, the satellite provider has to guarantee that live-time station keeping is assured. The most important forces are the attraction of Sun and Moon as well as the solar radiation pressure. The Earth seen as a point mass is holding the spacecraft in its perfect orbit – under the assumption that the velocity and the radius are ideal. However, the Earth influences the spacecraft with its non-homogeneous shape. This Earth induced perturbation can be modelled with the help of Zonals and Tesserals and is often called natural drift. All these forces are acting on the satellite and are trying to bring it out of its perfect orbit. To guarantee that the spacecraft will stay inside its control box, which is normally 0.1 deg for the longitude and latitude deviation, and to save propellant the thrusters have to be controlled in an optimal way.
Therefore, this thesis improves and validates an already available method to optimise the fuel consumption for low-thrust geostationary station keeping. This is achieved by increasing the accuracy of the perturbation model by the effect of the eclipse and presenting different mathematical factori-

sations of the station keeping problem. Furthermore, different simulations show the possibility to optimise the non-linear station keeping problem in an optimal way.

1.1 Related Work

Due to the re-thinking of the propulsion system of geostationary satellites, control engineers started to work on new approaches. In 1980, Eckstein [4] proved that it is possible to solve the optimal station keeping problem with low-thrust propulsion systems. The innovation was that the spacecraft model could be linearised and solved in a discrete way. The advantage of this new approach: it can compete with classical methods even under the presence of constraints.
The next step was done by T. Çimen [11, 12]. His work based on J. R. Cloutier's research in the late 90's and in the beginning of the 21st century. Cloutier wrote many famous papers about State-Dependent Riccati Equations (SDRE) [1, 2, 3]. This approach of Riccati equations breaks down the non-linear system to a factorised model which grants additional degrees of freedom depending on the factorisation. The weighting matrices, which are not existing in the classical optimal problem solvers, are providing the possibility to add constraints to the solver as well as having some more free parameters. Furthermore, it was demonstrated that the SDRE method is robust and asymptotically stable.
In 2004, Çimen [12] introduced a new proposal to solve non-linear finite-time optimal tracking problems – the Approximate Sequence of Riccati Equation (ASRE) method. He proved that under mild conditions his approach converges to the global optimum of the non-linear problem. In contrast to other SDRE methods the ASRE approach is a fixed time problem. This means that the non-linear problem can either be solved (globally) optimally in a fixed amount of time as a two-point boundary problem or it has no optimal solution for the chosen time slot. Another benefit is this application can be performed offline to calculate the optimal control cycle. Therefore, storage capabilities and pre-computing have to be available. Then, the final optimal controller can be used in the online control.
F. Topputo and F. Bernelli-Zazzera started to improve the ASRE approach and in 2011 they presented at the 3rd CEAS Air&Space Conference their approach for optimal low-thrust station keeping for geostationary satellites [25]. They used the general ASRE method by Çimen which consists of time-varying linear quadratic regulators. The two-point boundary value problem was solved with the help of a transition matrix approach which was further improved by M. Pasta [19]. Therefore, they separated the constrained states of the non-constrained states and made a feed-forward integration to get the solution of the state transition matrix. This intermediary result is used to calculate the initial co-state vector which can be used to determine the optimal control profile of the non-linear problem. This proposal is very robust and can handle strict constraints.
Many other researchers like Weiss [29], Sukhanov [24] and Losa [14] are trying to achieve better optimisation algorithm with different approaches. For example, in 2015 Weiss showed that it is possible to use autonomous model predictive control algorithms for closed-loop station keeping of low-thrust geostationary satellites. This method provides a high robustness and reliability while it can reduce the operational costs because the Δv is reduced. In contrast to this, Sukhanov suggests a mathematical method for station keeping of low-thrust satellites which is based on linearising the satellite's motion to a close reference orbit. This approach sees the non-linear model as a two-body

problem and respects the constraints on the thrust direction.
Another promising method is described by D. Losa [14, 15, 16]. She used different schemes to solve the low-thrust station keeping problem: In 2005, the differential inclusion approach which is a direct method was presented and verified. This proposal discretises the control time history or the state variable time history. If the problem consists of state functions and their derivatives, the control variables can be eliminated from the control problem. To handle mixed constrained non-linear problems, she suggested a decomposition method in 2006. This direct method consists of linear and non-linear optimal control problems. It is able to handle on-off thruster constraints and other constraints. In her dissertation in 2007, Losa combined the previous attempts and showed direct solutions for the fixed horizon and the receding horizon optimisation for geostationary low-thrust station keeping. A linearisation around the station keeping point which is seen as an equilibrium point is used. In the end, she verified her solution without constraining the thrusters, but she showed how to model the thrust constraints, too. In 2016, C. Gazzino and D. Losa provided a paper to solve the station keeping problem while splitting the control problem to two separate problems [5]. First, an indirect method is used to solve a classical optimal control problem by taking the result of a direct solution of the problem without any constraints. Second, two ways of using the constraints are discussed. The authors conclude that further research on this approach has to be done because the formulation of the Pontryagin's Maximum Principle with mixed control-state constraints has not been considered.
Due to the many different approaches, one method which is promising the most further improvements has to be chosen. The solver proposed by Topputo and the other one by Losa are seen as the most favourable ones by the author of this thesis. Topputo provides a relatively new proposal which converges to its (global) optimum and Losa uses a direct as well as an indirect method which are well-known. Both approaches can tackle constrained problems which are already described like the thrusters or maximum deviation of the longitude. Topputo has a long list of possible further upgrades of the method like better factorisations and optimising the weighting matrices. On the other side, Losa's newest paper [5] describes only one remaining issue: the Pontryagin's Maximum Principle with mixed control-state constraints should be analysed. Another difference between the promising methods is Topputo uses a pseudo-linearised factorisation which has a non-unique solution for a station keeping problem for geostationary satellites. Losa has to linearise the non-linear problem around an equilibrium point which is the nominal station keeping point. The problem of Losa's linearisation is that the model has just an accuracy up to a Taylor expansion of order one. Therefore, Losa has to calculate the whole system in Cartesian coordinates while Topputo can stay with spherical ones.
After the previous consideration, the thesis will use and improve Topputo's ASRE method with the transition matrix approach. In summary, his scheme guarantees a global optimal control profile, possibility of further improvements and many chances to fine tune the optimisation like changing the weighting matrices or factorisations.

1.2 Outline

This work is structured in the following way to guarantee the reader a comprehensible picture of the usage of the ASRE method for a geostationary station keeping problem:

In Chapter 1, an introduction to the low-thrust station keeping problem for geostationary satellites is given. Furthermore, an explanation why the ASRE method is used.
In Chapter 2, basic understanding of the different coordinate reference frames and the orbital elements is provided. Also, a short description of how to calculate the fuel consumption can be found.
In Chapter 3, the perturbation model including the Earth, the Sun and the Moon as well as the solar radiation pressure with the eclipse constraints are derived. The Earth is modelled as a non-homogeneous sphere with Zonals and Tesserals up to order and degree of three. The celestial bodies, Sun and Moon, are regarded as point masses. The perturbation model has to be created as it has to be used for the final evaluation of the optimisation.
In Chapter 4, the ASRE method is derived. First, the SDRE are shown including their conditions. These are valid for the ASRE approach, too. From the normal ASRE approach, the improvement towards the transition matrix approach is described. Therefore, different constrained problems and an example to verify the method is given.
In Chapter 5, the dynamics of a geostationary spacecraft are given – first, in the unperturbed case and finally in the perturbed case. A possible factorisation of the dynamics is discussed including perturbations and the control of the input to the system.
In Chapter 6, first, it is shown that the perturbation model puts all the necessary disturbances to the spacecraft. Afterwards, the control algorithm is tested for the case of no perturbations. Then, it is presented that the control algorithm provides an optimal control profile for the perturbed case. One of the free parameters of the system are the weighting matrices. These are optimised and used to present an optimal control profile with better weighting matrices for the chosen factorisation. The large influence of the factorisation is discussed later. Finally, the best factorisation of the system including the best weighting matrices are compared to the result of Losa [14].
In Chapter 7, a summary of the work is presented as wells as ideas for further development and research.

2 Background

This chapter provides an overview of the orbital elements and the later used coordinate reference frames like the Earth-Centred Inertial. In the last-mentioned topic, the transformation from spherical to Cartesian coordinates and vice versa are discussed, too. Additionally, the rotation around the z-axis, which is important to rotate a rotating reference frame to an inertial one, is shown. For the calculation of the minimum fuel consumption, this chapter presents a way to determine the used propellant mass.

2.1 Orbit elements

In this thesis, the orbit elements are only described very briefly. More detailed information is provided in common literature like Losa [14], Sidi [21] and Soop [22].

2.1.1 Classical Orbital Elements

The Classical Orbital Elements (COE) were first described by Kepler. He defined them in an unperturbed Keplerian orbit: The COE can be seen in Fig. 2.1. For more details on the single elements

a	semi-major axis
e	eccentricity
i	inclination
Ω	right ascension of the ascending node
ω	argument of perigee
ν	true anomaly

the author refers to Losa [14].

2.1.2 Equinoctial Orbital Elements

The COE have singularities for spacecrafts in a geostationary orbit. The inclination i is quasi zero. The ascending node is not defined because the equatorial plane has no unique crossing line with the orbital plane. In fact, they are identical. Therefore, neither the argument of perigee nor the true anomaly are defined.
A new set of orbital parameters was chosen by Lagrange: the Equinoctial Orbital Elements (EOE). These parameters have no singularities for the geostationary orbit. They can be described using the

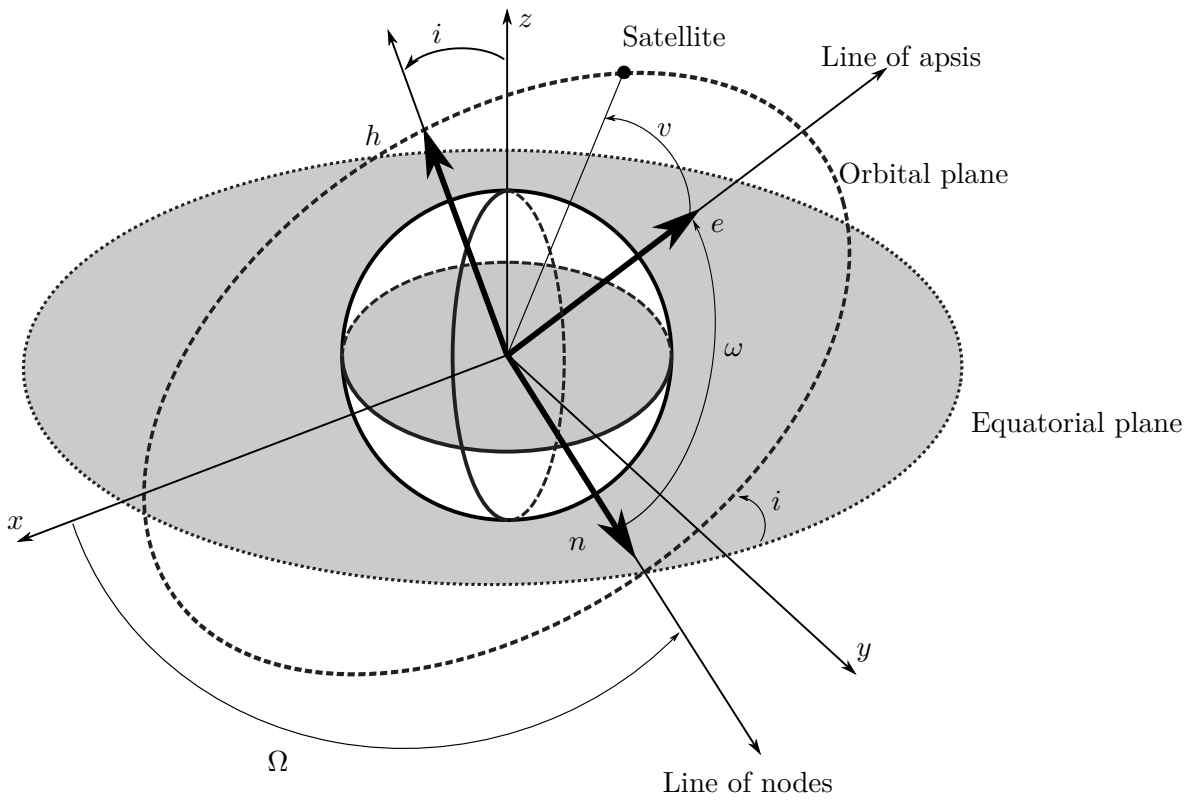

Figure 2.1: Classical orbital elements

COE:

$$\begin{bmatrix} a \\ P_1 \\ P_2 \\ Q_1 \\ Q_2 \\ l_\theta \end{bmatrix} = \begin{bmatrix} a \\ e\sin(\omega + I\Omega) \\ e\cos(\omega + I\Omega) \\ \tan(\frac{i}{2}\sin\Omega) \\ \tan(\frac{i}{2}\cos\Omega) \\ \Omega + \omega + M - \theta(t) \end{bmatrix}, \tag{2.1}$$

where I is a retrograde factor. It is $+1$ if the satellite is in a prograde orbit and it is -1 for retrograde orbits. $\theta(t)$ is the Greenwich Hour Angle (GHA) which depends on time and is changing with the rotation of the Earth – in 24hours it rotates 360° (see Section 3.1).[14]

2.2 Coordinate Reference Frames

In the following, the later used reference frames are discussed. They can be categorised in spacecraft fixed, Earth-Centred Earth-Fixed (ECEF) and the Earth-Centered Inertial (ECI) frame. This section is a summary of Losa [14] and Wertz [30]. The reference frames are commonly and well-described in literature, such as Wertz [30].

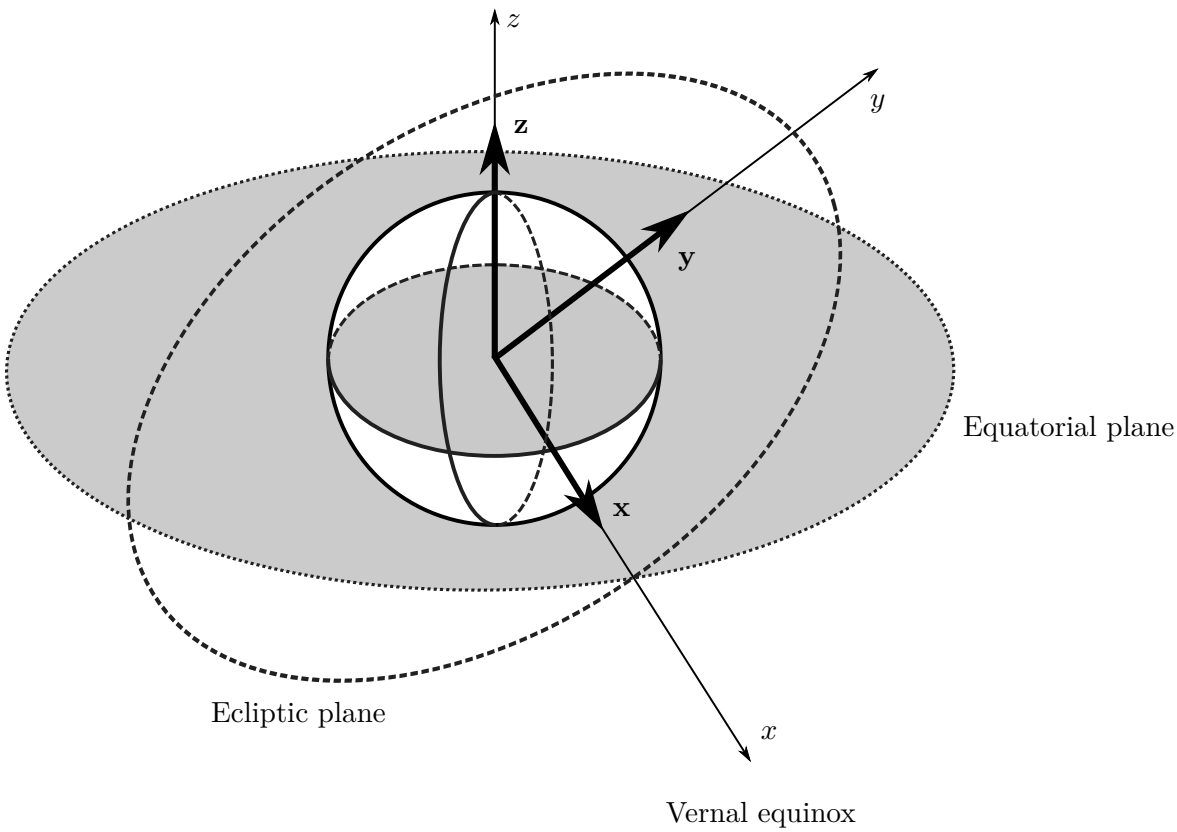

Figure 2.2: ECI reference coordinate frame

2.2.1 Earth-Centred Inertial

The Earth-Centered Inertial (ECI) lies in the ecliptic plane of the Sun and has its origin in the centre of the Earth. **x**, **y** and **z** are the unit vectors of the x, y and z axis. The x-axis is defined as the crossing of the equatorial plane with the ecliptic plane (see Fig. 2.2) which is also called the vernal equinox. The z-axis is the axis through the celestial North pole. The y-axis is standing perpendicularly on the x-z-plane to fulfil a right-handed coordinate system.[16]
The ECI reference frame is depending on the time. The J-2000 reference frame, which was introduced to give an exact reference on the 1st of January 2000 at 12:00 o'clock, is one possible inertial frame and is used in this thesis as the initial reference frame. To use it for newer dates, it is important to use the True-of-Date inertial system which does not neglect the nutation effect. The true of date reference frame follows the same concept as the J-2000 reference frame, but the axes differ slightly: the x-axis is at the current vernal equinox, the y-axis at the current equatorial plane and the z-axis is perpendicular to the other two axes. For all of the following calculations, the true of date reference frame is used whenever the ECI reference frame is mentioned.
In general, the ECI reference system is given in terms of Cartesian coordinates x, y and z which can be described in spherical terms

$$\begin{bmatrix} x \\ y \\ z \end{bmatrix} = \begin{bmatrix} r\cos\delta\cos\alpha \\ r\cos\delta\sin\alpha \\ r\sin\delta \end{bmatrix}, \tag{2.2}$$

where r is the distance from the centre of the Earth to the spacecraft, α is the angle between x-axis and the projection of r in the equatorial plane. δ is the angle between the projection of r in the equatorial plane and the real r.[14]
Expressing spherical coordinates from Cartesian coordinates:

$$\begin{bmatrix} r \\ \lambda \\ \phi \end{bmatrix} = \begin{bmatrix} \sqrt{x^2+y^2+z^2} \\ \arctan \dfrac{y}{x} \\ \arctan \dfrac{z}{\sqrt{x^2+y^2}} \end{bmatrix} \tag{2.3}$$

2.2.2 Earth-Centred Earth-Fixed

In contrast to the ECI reference frame, the Earth-Centred Earth-Fixed (ECEF) is rotating with the Earth and has its origin in the centre of the Earth. The x-axis is at the Greenwich meridian and the y-axis is perpendicular to the x-z plane to achieve a right-handed coordinate system, where the z-axis goes through the North pole (see Fig. 2.3). The radius r is defined as the distance from the centre of the Earth to the centre of gravity of the satellite. The latitude ϕ describes the angle between the radius vector and the x-y-plane which is the equatorial plane. The longitude θ is the angle between the projection of the vector from the centre of Earth to the spacecraft in the equatorial plane and the vernal equinox subtracted by the GHA (see Section 3.1).[14]
To convert the spherical coordinates with respect to the ECEF to the inertial frame with Cartesian coordinates, it is important to rotate the the ECEF and transform the spherical to Cartesian coordinates.

$$\begin{bmatrix} x \\ y \\ z \end{bmatrix} = \mathbf{R}_Z(\theta) \cdot \begin{bmatrix} r\cos\phi\cos\lambda \\ r\cos\phi\sin\lambda \\ r\sin\phi \end{bmatrix}, \tag{2.4}$$

where $\mathbf{R}_Z(\theta)$ is the rotation matrix around the z-axis. The rotation has just to be around the z-axis of an angle θ because the it is the same in ECI and ECEF.

$$\mathbf{R}_Z(\theta) = \begin{bmatrix} \cos\theta & -\sin\theta & 0 \\ \sin\theta & \cos\theta & 0 \\ 0 & 0 & 1 \end{bmatrix} \tag{2.5}$$

From Cartesian to spherical coordinates in the ECI reference frame, the following equations are useable:

$$\begin{bmatrix} r \\ \lambda \\ \phi \end{bmatrix} = \begin{bmatrix} \sqrt{x^2+y^2+z^2} \\ \arctan \dfrac{y\sin\theta + x\cos\theta}{y\cos\theta - x\cos\theta} \\ \arctan \dfrac{z}{\sqrt{x^2+y^2}} \end{bmatrix} \tag{2.6}$$

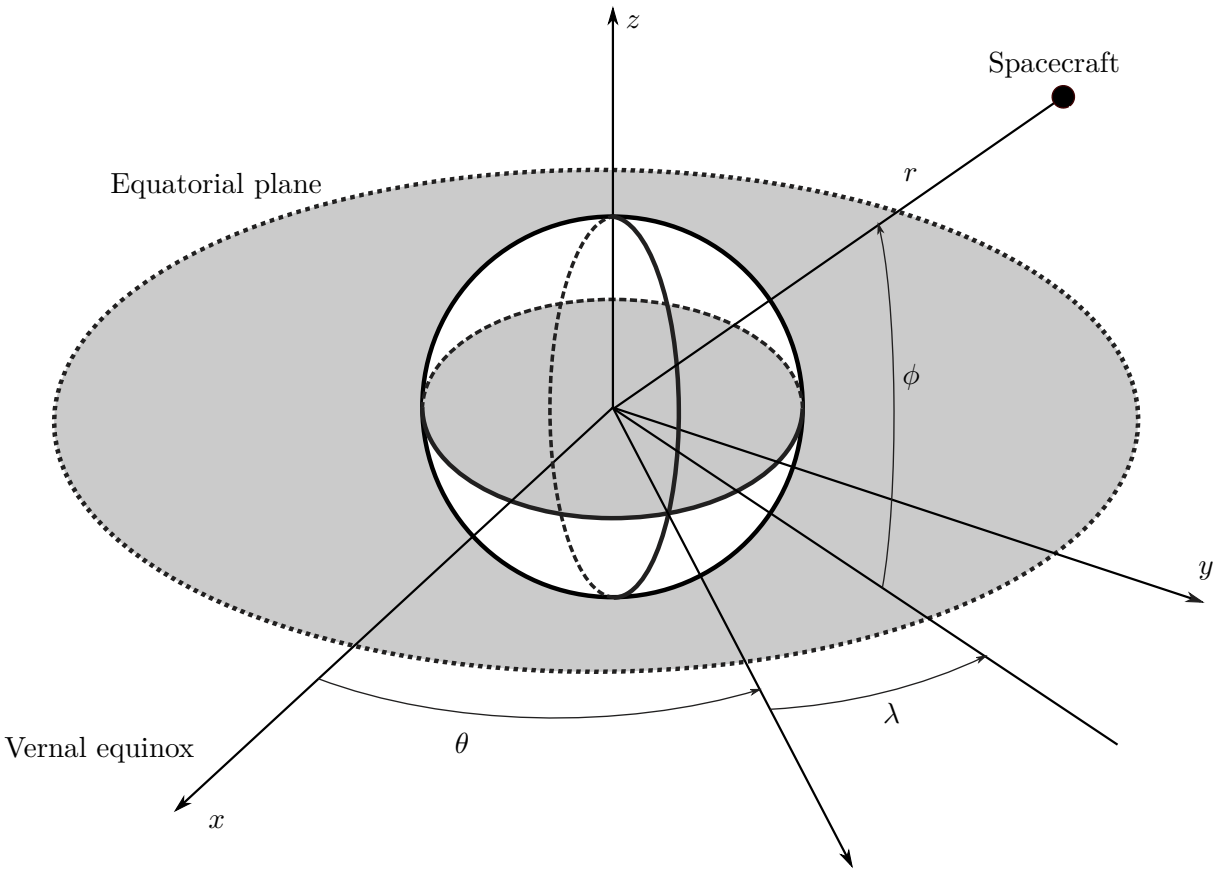

Figure 2.3: ECEF reference coordinate frame

2.2.3 Radial Tangential Normal

The Radial-Tangential-Normal (RTN) reference frame is in contrast to the coordinate frames described above a spacecraft based one. In general, it is used to express the perturbations acting on a spacecraft. The origin of the RTN is chosen to be fixed at the nominal position of the spacecraft. The radial-axis is facing at the negative direction of the spacecraft-Earth-vector. The tangential-axis is given by the flight direction and the normal-axis is perpendicular on the R-T-plane to build a right-handed coordinate system (see Fig. 2.4). The **R**, **T** and **N** are set as the unit vectors of the RTN reference frame.[15]

For geostationary satellites, the N-axis is pointing in the same direction as the z-axis of the ECI reference frame. Thus, to convert from ECI to RTN a rotation around the z-axis has to be performed. For non-geostationary orbits, the argument of perigee ω and the true anomaly v are used. In the geostationary case, the inclination i is zero and the true anomaly as well as the argument of perigee are not defined. Hence, the COE cannot be used – the EOE have to be used.

The detailed way to get the true longitude L and the according $\sin L$ and $\cos L$ can be found in Losa [14]. Using the rotation matrix in the EOE from Losa [14] leads to

$$\begin{bmatrix} \mathbf{R} \\ \mathbf{T} \\ \mathbf{N} \end{bmatrix} = \begin{bmatrix} \cos L & \sin L & 0 \\ \sin L & \cos L & 0 \\ 0 & 0 & 1 \end{bmatrix} \cdot \begin{bmatrix} \mathbf{X} \\ \mathbf{Y} \\ \mathbf{Z} \end{bmatrix}, \tag{2.7}$$

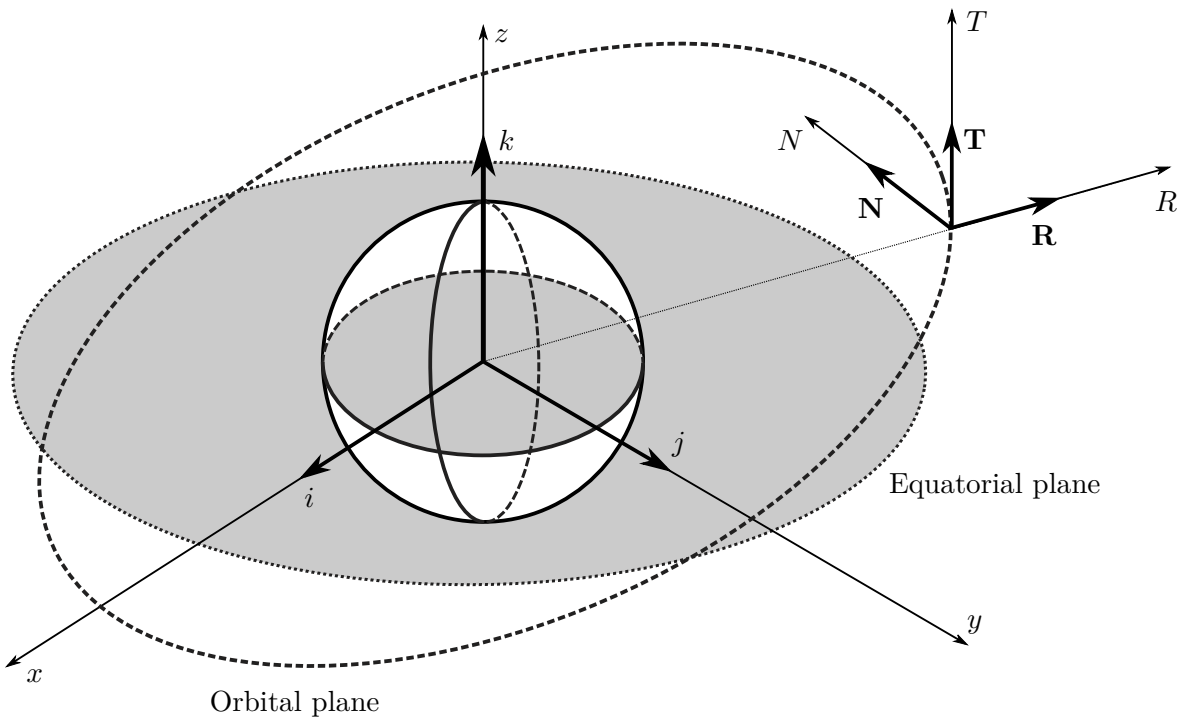

Figure 2.4: Radial-Tangential-Normal (RTN) reference coordinate frame

where

$$\sin L = \frac{\left(\sqrt{1-P_1^2-P_2^2}+1-P_2^2\right)\sin K + P_1P_2\cos K - P_1\left(1+\sqrt{1-P_1^2-P_2^2}\right)}{(1-P_1\sin K - P_2\cos K)\cdot\left(1+\sqrt{1-P_1^2-P_2^2}\right)} \tag{2.8}$$

$$\cos L = \frac{\left(\sqrt{1-P_1^2-P_2^2}+1-P_2^2\right)\cos K + P_1P_2\sin K - P_2\left(1+\sqrt{1-P_1^2-P_2^2}\right)}{(1-P_1\sin K - P_2\cos K)\cdot\left(1+\sqrt{1-P_1^2-P_2^2}\right)}. \tag{2.9}$$

The parameter K can be shown by

$$K = \Omega + \omega + E. \tag{2.10}$$

2.3 Fuel consumption

The fuel consumption for a geostationary spacecraft around the Earth can be calculated via Δv which is the maximum change of the velocity of the satellite. The total amount of needed fuel for a manoeuvre is according to Tsiolkovsky's rocket equation:

$$m_p = m \cdot \left(1 - e^{-\frac{\Delta v}{I_{sp} g}}\right), \tag{2.11}$$

where m_p is the mass of the used propellant, m is the initial spacecraft mass, I_{sp} is the specific impulse of the used propellant and g is the acceleration at the surface of the Earth.[19]

3 Perturbations

In general, many different forces act on satellites. In low Earth orbits, the main disturbances are the atmospheric drag and the gravity attraction of the Earth. While increasing the semi-major axis to a geostationary orbit, the acting forces will change. Now, the attraction of the Sun and the Moon have large influences on the system as well as the solar radiation pressure. Due to the larger distance from the Earth's surface and accordingly being far away from the dense atmosphere, the atmospheric drag can be neglected. In Fig. 3.1, the norm of all important perturbations for geostationary satellites can be found. Over one year, the norm stays in an arithmetic average of approximately $0.75 \cdot 10^{-8}$ km/s. The maxima and minima peaks have a nearly constant time between them.
In the following, the different perturbations are presented. The description of the dynamic model is well-known and a summary of common literature is shown in this chapter (compare with Losa [16], Montenbruck [18] and Sidi [21]). The necessary forces which are needed to create an accurate dynamic model for the station keeping of geostationary satellites are derived: (1) the gravity attraction of the Earth, (2) the attraction of the Sun and the Moon, and (3) the solar radiation pressure including the effect of the eclipse. It is important to mention that the attraction of other planets like Jupiter can be neglected.

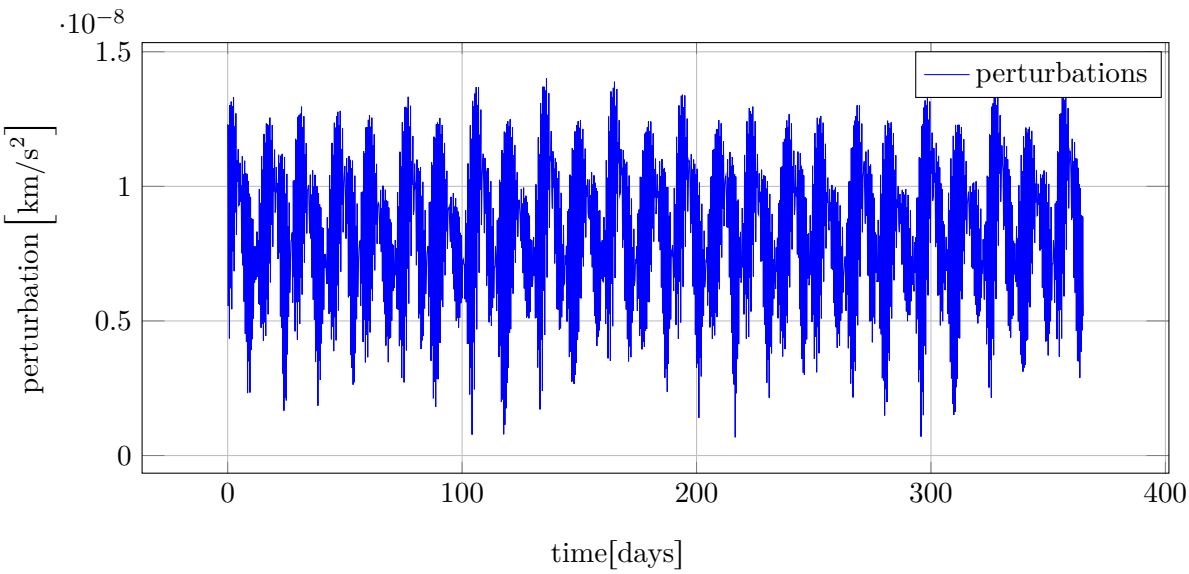

Figure 3.1: Norm of all perturbations including SRP, Sun and Moon attraction as well as Tesserals and Zonals up to order and degree of three for one year at longitude of 60 deg

3.1 Earth Gravity Attraction

There are and have been many space missions to collect data about the gravitational field of the Earth. Due to the non-homogeneous shape, which is often compared to a potato, the greatest gravitational

force of the Earth acting on a geostationary spacecraft orbiting the Earth is at 75.1°E and at 105.3°W – those two points are called *stable points*. At 161.9°E and at 11.5°W there are unstable points which means a spacecraft positioned there can, depending on the initial velocity, drift either to the east or west. In contrast, a geostationary satellite set to a stable point will remain at that position forever (see Fig. 3.2).[18]

3.1.1 Non-normalised Earth Gravity Attraction

In the case of the Earth being a homogeneous sphere or being seen as a point mass, the potential field can be described as

$$\ddot{r} = \nabla U, \tag{3.1}$$

where

$$U(r) = \frac{GM_{\oplus}}{r} = \frac{\mu_{\oplus}}{r} \tag{3.2}$$

is the potential function.
For more realistic models this assumption needs to be more precise. Thus, a non-homogeneous mass distribution and an oblate celestial body will be used

$$U(r, \lambda, \phi) = \frac{\mu_{\oplus}}{r} + B(r, \phi, \lambda), \tag{3.3}$$

"where $B(r, \phi, \lambda)$ is the appropriate spherical harmonic expansion used to correct the gravitational potential for the earth's nonsymmetric mass distribution"[21]. The gravity field, which can be derived from the geopotential, can be described as a function of zonal and tesseral components and of Legendre polynomials:

$$U(r, \phi, \lambda) = \frac{\mu_{\oplus}}{r} \sum_{n=0}^{\infty} \sum_{m=0}^{n} \frac{R_{\oplus}^{n}}{r^{n}} P_{nm}(\sin\phi)(C_{nm}\cos(m\lambda) + S_{nm}\sin(m\lambda)), \tag{3.4}$$

where $P_{nm}(\sin\phi)$ are the Legendre polynomials. C_{nm} and S_{nm} are the unitless geopotential coefficients which describe the mass distribution of the Earth (see Table 3.1). For $m \neq 0$ they specify the Tesserals which rely on the the longitude and latitude. In contrast, the Zonals are characterised for $m = 0$. There is no dependency on the longitude, but only on the latitude and the Zonals are often called "J"-terms according to the Joint Gravity Model (JGM) – the most significant one is the "J2"-term.[20]

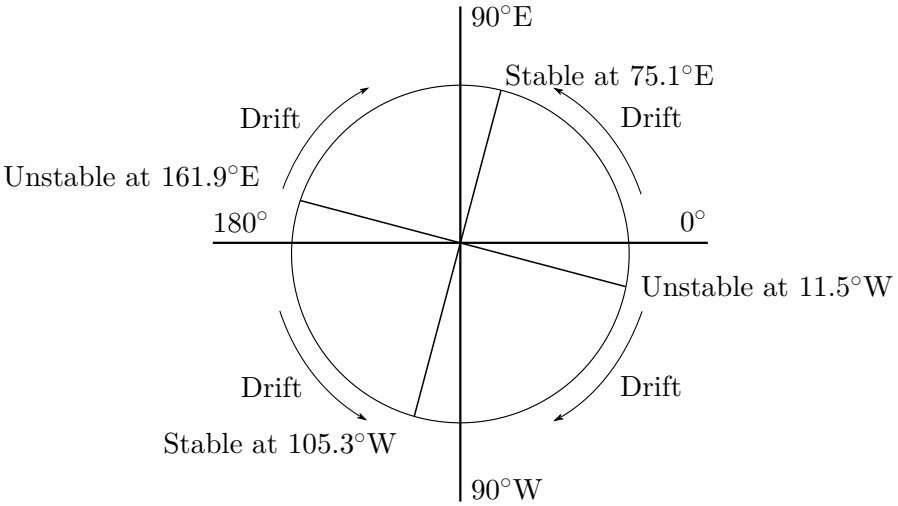

Figure 3.2: Drift change due to Earth's gravity field seen from North pole according to Soop [22]

Consequently Eq. (3.4) (compare with Losa [14]) can be written as

$$
\begin{aligned}
U(r,\phi,\lambda) = \frac{\mu_\oplus}{r} &+ \\
&+ \frac{\mu_\oplus R_\oplus^2}{r^3}\left(\frac{3}{2}\sin^2\phi - \frac{1}{2}\right) C_{20} + \\
&+ \frac{\mu_\oplus R_\oplus^2}{r^3}\left(3\cos^3\phi\right)\left(C_{22}\left(\cos^2\lambda - \sin^2\lambda\right) + 2S_{22}\sin\lambda\cos\lambda\right) + \\
&+ \frac{\mu_\oplus R_\oplus^3}{r^4}\left(\frac{5}{2}\sin^3\phi - \frac{3}{2}\sin\phi\right) C_{30} + \\
&+ \frac{\mu_\oplus R_\oplus^3}{r^4}\left(\frac{15}{2}\sin^2\phi\cos\phi - \frac{3}{2}\cos\phi\right)\left(C_{31}\cos\lambda + S_{31}\sin\lambda\right) + \\
&+ \frac{\mu_\oplus R_\oplus^3}{r^4}\left(15\sin\phi\cos^2\phi\right)\left(C_{32}\left(\cos^2\lambda - \sin^2\lambda\right) + 2S_{32}\sin\lambda\cos\lambda\right) + \\
&+ \frac{\mu_\oplus R_\oplus^3}{r^4}\left(15\cos^3\phi\right)\left(C_{33}\cos\lambda\left(1 - 4\sin^2\lambda\right) + S_{33}\sin\lambda\left(4\cos^2\lambda - 1\right)\right).
\end{aligned}
\tag{3.5}
$$

Now, Eq. (3.6) can be used to transform Eq. (3.5) in the ECI reference frame.

$$
\begin{aligned}
\sin\phi &= \frac{z}{\sqrt{x^2+y^2+z^2}} & \sin\lambda &= \frac{y\cos\theta - x\sin\theta}{\sqrt{x^2+y^2}} \\
\cos\phi &= \frac{\sqrt{x^2+y^2}}{x^2+y^2+z^2} & \cos\lambda &= \frac{x\cos\theta + y\sin\theta}{\sqrt{x^2+y^2}}
\end{aligned}
\tag{3.6}
$$

The geopotential function $U(r,\phi,\lambda)$ from Eq. (3.5), which is transformed to the ECI reference frame, can be described by

$$
U(x,y,z,\theta) = U_{00} + U_{20} + U_{22} + U_{30} + U_{31} + U_{32} + U_{33}. \tag{3.7}
$$

The components of Eq. (3.7) can be seen in table Table 3.2, where x, y, z are the inertial Cartesian coordinates and θ is the GHA. The GHA, which is the right ascension of the Greenwich meridian, is the angle between the Greenwich meridian and the mean vernal equinox of the date in the J-2000

Table 3.1: Legendre polynomials and geopotential coefficients up to order and degree three (see Losa [14])

n	m	C_{nm}	S_{nm}	$P_{nm}(\sin\phi)$
0	0	1.00	0.00	1
1	0	0.00	0.00	$\sin\phi$
1	1	0.00	0.00	$\cos\phi$
2	0	$-1.08 \cdot 10^{-3}$	0.00	$\frac{3}{2}\sin^2\phi - 0.5$
2	1	0.00	0.00	$3\cos\phi\sin\phi$
2	2	$1.57 \cdot 10^{-6}$	$-9.03 \cdot 10^{-7}$	$3\cos^2\phi$
3	0	$2.53 \cdot 10^{-6}$	0.00	$\frac{5}{2}\sin^3\phi - \frac{3}{2}\sin\phi$
3	1	$2.18 \cdot 10^{-6}$	$2.68 \cdot 10^{-7}$	$\frac{15}{2}\cos\phi\sin^2\phi - \frac{3}{2}\cos\phi$
3	2	$3.11 \cdot 10^{-7}$	$-2.12 \cdot 10^{-7}$	$15\cos^2\phi\sin\phi$
3	3	$1.02 \cdot 10^{-7}$	$1.98 \cdot 10^{-7}$	$15\cos^3\phi$

In this thesis the Zonals and Tesserals are chosen to be up to order and degree of three ($m = 3$ and $n = 3$).

reference frame (see Montenbruck [18]). It is given by

$$\Theta = 280.4606^\circ + 360.9856473^\circ \cdot d, \tag{3.8}$$

where d is the time in days since first of January 2000 at 12:00 o'clock. The terms which are not mentioned like U_{21} are zero.
The acceleration of the Earth attraction in the ECI frame can be derived from the potential function in the ECI frame

$$\begin{bmatrix} a_{eX} & a_{eY} & a_{eZ} \end{bmatrix}^T = \nabla_{xyz} U(x, y, z, \theta). \tag{3.9}$$

The gradient of the potential function Eq. (3.9) can be described as

$$\begin{bmatrix} a_{eX} \\ a_{eY} \\ a_{eZ} \end{bmatrix} = \mu_\oplus \begin{bmatrix} \alpha_{eX00} + R_\oplus^2\alpha_{eX20} + R_\oplus^2\alpha_{eX22} + R_\oplus^3\alpha_{eX30} + R_\oplus^3\alpha_{eX31} + R_\oplus^3\alpha_{eX32} + R_\oplus^3\alpha_{eX33} \\ \alpha_{eY00} + R_\oplus^2\alpha_{eY20} + R_\oplus^2\alpha_{eY22} + R_\oplus^3\alpha_{eY30} + R_\oplus^3\alpha_{eY31} + R_\oplus^3\alpha_{eY32} + R_\oplus^3\alpha_{eY33} \\ \alpha_{eZ00} + R_\oplus^2\alpha_{eZ20} + R_\oplus^2\alpha_{eZ22} + R_\oplus^3\alpha_{eZ30} + R_\oplus^3\alpha_{eZ31} + R_\oplus^3\alpha_{eZ32} + R_\oplus^3\alpha_{eZ33} \end{bmatrix}, \tag{3.10}$$

with α_{nm} being the derivative of $U(x, y, z, \theta)$ to x, y and z. It can be found in Table 3.3.

Table 3.3: Induced acceleration by the Earth gravity attraction in inertial Cartesian coordinates

α_{eX00}	$\frac{-x}{\rho^3}$
α_{eY00}	$\frac{-y}{\rho^3}$

Table 3.3: Induced acceleration by the Earth gravity attraction in inertial Cartesian coordinates (continued)

α_{eZ00}	$\frac{-z}{\rho^3}$
α_{eX20}	$\frac{3C_{20}x\left(x^2+y^2-4z^2\right)}{2\rho^7}$
α_{eY20}	$\frac{3C_{20}y\left(x^2+y^2-4z^2\right)}{2\rho^7}$
α_{eZ20}	$\frac{3C_{20}z\left(3x^2+3y^2-2z^2\right)}{2\rho^7}$
α_{eX22}	$\frac{6y\left(-4x^2+y^2+z^2\right)\psi_{22}^2+3x(-3x^2+7y^2+2z^2)\gamma_{22}^2}{\rho^7}$
α_{eY22}	$\frac{6x\left(x^2-4y^2+z^2\right)\psi_{22}^2-3y(7x^2-3y^2+2z^2)\gamma_{22}^2}{\rho^7}$
α_{eZ22}	$\frac{-30xyz\psi_{22}^2+15z(-x^2+y^2)\gamma_{22}^2}{\rho^7}$
α_{eX30}	$\frac{5C_{30}xz(3x^2+3y^2-4z^2)}{2\rho^9}$
α_{eY30}	$\frac{5C_{30}yz(3x^2+3y^2-4z^2)}{2\rho^9}$
α_{eZ30}	$\frac{C_{30}(-3x^4-3y^4-8z^4-6x^2y^2+24x^2z^2+24y^2z^2)}{2\rho^9}$
α_{eX31}	$\frac{3}{2}\cdot\frac{5xy\left(x^2+y^2-6z^2\right)\psi_{31}^1+\left(4x^4-y^4+4z^4+3x^2y^2-27x^2z^2+3y^2z^2\right)\gamma_{31}^1}{\rho^9}$
α_{eY31}	$\frac{3}{2}\cdot\frac{\left(-x^4+4y^4+4z^4+3x^2y^2+3x^2z^2-27y^2z^2\right)\psi_{31}^1+5xy(x^2+y^2-6z^2)\gamma_{31}^1}{\rho^9}$
α_{eZ31}	$\frac{15}{2}\cdot\frac{yz(3x^2+3y^2-4z^2)\psi_{31}^1+xz(3x^2+3y^2-4z^2)\gamma_{31}^2}{\rho^9}$
α_{eX32}	$\frac{15}{2}\cdot\frac{2yz(-6x^2+y^2+z^2)\psi_{32}^2+xz(-5x^2+9y^2+2z^2)\gamma_{32}^2}{\rho^9}$
α_{eY32}	$\frac{15}{2}\cdot\frac{2xz(x^2-6y^2+z^2)\psi_{32}^2-yz(9x^2-5y^2+2z^2)\gamma_{32}^2}{\rho^9}$
α_{eZ32}	$\frac{15}{2}\cdot\frac{2xy(x^2+y^2-6z^2)\psi_{32}^2-(x^2-y^2)(x^2+y^2-6z^2)\gamma_{32}^2}{\rho^9}$
α_{eX33}	$\frac{15}{2}\cdot\frac{xy(-15x^2+13y^2+6z^2)\psi_{33}^3-(4x^4+3y^4-21x^2y^2-3x^2z^2+3y^2z^2)\gamma_{33}^3}{\rho^9}$

Table 3.3: Induced acceleration by the Earth gravity attraction in inertial Cartesian coordinates (continued)

α_{eY33}	$\frac{15}{2} \cdot \frac{(3x^4 + 4x^4 - 21x^2y^2 + 3x^2z^2 - 3y^2z^2)\psi_{33}^3 - xy(13x^2 - 15y^2 + 6z^2)\gamma_{33}^3}{\rho^9}$
α_{ez33}	$\frac{105}{2} \cdot \frac{yz(-3x^2 + y^2)\psi_{33}^3 - xz(x^2 - 3y^2)\gamma_{33}^3}{\rho^9}$

$\rho = \sqrt{x^2 + y^2 + z^2}$, $\psi_{nm}^i = C_{nm}\sin(i\theta) + S_{nm}\cos(i\theta)$, $\gamma_{nm}^i = C_{nm}\cos(i\theta) - S_{nm}\sin(i\theta)$, where n and m are the degree and order of the Zonals and Tesserals.

3.1.2 Normalised Earth's Gravity Attraction

The geopotential coefficients C_{nm} and S_{nm} are affected by the Earth radius to the power of the order of n which can be seen in Eq. (3.4). For higher-order terms their magnitude varies very strong (see Table 3.1). To hold the magnitude in a narrow band, it is common to normalise the geopotential coefficients and the Legendre polynomial. Additionally, the non-normalised variant becomes unstable at around $n = 70$ and $m = 70$. For higher accuracy, only the normalised function can handle higher degree fields properly which is the standard of the NASA.
The geopotential function Eq. (3.4) can be rewritten, like in Montenbruck [18], as

$$\bar{U}(x, y, z, \theta) = \frac{\mu_\oplus}{r} \sum_{n=0}^{\infty} \sum_{m=0}^{n} \frac{R_\oplus^n}{r^n} \bar{P}_{nm}(\sin\phi)(\bar{C}_{nm}\cos(m\lambda) + \bar{S}_{nm}\sin(m\lambda)), \tag{3.11}$$

where

$$\bar{C}_{nm} = N \cdot C_{nm} \tag{3.12}$$

$$\bar{S}_{nm} = N \cdot S_{nm} \tag{3.13}$$

$$\bar{P}_{nm} = N^{-1} \cdot P_{nm} \tag{3.14}$$

with

$$N_{nm} = \left(\frac{(n+m)!}{(2 - \delta_{0m})\,(2n+1)\,(n-m)!} \right)^{1/2}. \tag{3.15}$$

The Kronecker symbol δ_{0m} is 1 for $n = m$ and 0 for $n \neq m$.
Now, the non-normalised geopotential coefficients from Table 3.1 can be normalised. Using Table 3.4, Eq. (3.14) into Eq. (3.11) and inserting the result in Eq. (3.9). This gives the normalised acceleration induced by the Earth gravity attraction.

$$\begin{bmatrix} \bar{a}_{eX} & \bar{a}_{eY} & \bar{a}_{eZ} \end{bmatrix}^T = \nabla_{xyz} \frac{\mu_\oplus}{r} \sum_{n=0}^{\infty} \sum_{m=0}^{n} \frac{R_\oplus^n}{r^n} N^{-1} P_{nm}(\sin\phi)(\bar{C}_{nm}\cos(m\lambda) + \bar{S}_{nm}\sin(m\lambda)) \tag{3.16}$$

Writing the complete sum of the normalised geopotential function, a new term of order $n = 2$ and

Table 3.2: Gravitational potential for Earth in ECI frame

U_{00}	$\dfrac{\mu_\oplus}{(x^2+y^2+z^2)^{1/2}}$
U_{20}	$\mu_\oplus R_\oplus^2 \cdot \dfrac{C_{20}(-x^2-y^2+2z^2)}{2(x^2+y^2+z^2)^{5/2}}$
U_{22}	$3\mu_\oplus R_\oplus^2 \cdot \dfrac{C_{22}\left[(x^2-y^2)\cos(2\theta)+2xy\sin(2\theta)\right]+S_{22}\left[(y^2-x^2)\sin(2\theta)+2xy\cos(2\theta)\right]}{2(x^2+y^2+z^2)^{5/2}}$
U_{30}	$\mu_\oplus R_\oplus^3 \cdot \dfrac{C_{30}z\left(-3x^2-3y^2+2z^2\right)}{2(x^2+y^2+z^2)^{7/2}}$
U_{31}	$\mu_\oplus R_\oplus^3\left(-3x^2-3y^2+12z^2\right) \cdot \dfrac{C_{31}\left(x\cos\theta+y\sin\theta\right)+S_{31}\left(y\cos\theta-x\sin\theta\right)}{2(x^2+y^2+z^2)^{7/2}}$
U_{32}	$15\mu_\oplus R_\oplus^3 z \cdot \dfrac{C_{32}\left[\left(x^2-y^2\right)\cos(2\theta)+2xy\sin(2\theta)\right]+S_{32}\left[\left(y^2-x^2\right)\sin(2\theta)+2xy\cos(2\theta)\right]}{(x^2+y^2+z^2)^{7/2}}$
U_{33}	$\dfrac{\mu_\oplus R_\oplus^3}{(x^2+y^2+z^2)^{7/2}} \cdot \begin{array}{l}\left(C_{33}\left(x\cos\theta+y\sin\theta\right)\left[\left(x^2+y^2\right)-4\left(y\cos\theta-x\sin\theta\right)^2\right]-\right.\\ \left.-S_{33}\left(y\cos\theta-x\sin\theta\right)\left[\left(x^2+y^2\right)-4\left(x\cos\theta+y\sin\theta\right)^2\right]\right)\end{array}$

of degree $m = 1$ appears. This can be explained by $\bar{C}_{21}$ and $\bar{S}_{21}$ which are non-zero unlike in the not normalised form (compare with Table 3.1). Therefore, the acceleration term is extended by an additional term α_{eX21}:

$$\begin{aligned}\bar{a}_{eX} =&\mu_\oplus(\alpha_{eX00}+R_\oplus^2N_{20}^{-1}\alpha_{eX20}+R_\oplus^2N_{21}^{-1}\alpha_{eX21}+R_\oplus^2N_{22}^{-1}\alpha_{eX22}+R_\oplus^3N_{30}^{-1}\alpha_{eX30}+\\ &R_\oplus^3N_{31}^{-1}\alpha_{eX31}+R_\oplus^3N_{32}^{-1}\alpha_{eX32}+R_\oplus^3N_{33}^{-1}\alpha_{eX33})\end{aligned} \tag{3.17}$$

$$\begin{aligned}\bar{a}_{eY} =&\mu_\oplus(\alpha_{eY00}+R_\oplus^2N_{20}^{-1}\alpha_{eY20}+R_\oplus^2N_{21}^{-1}\alpha_{eY21}+R_\oplus^2N_{22}^{-1}\alpha_{eY22}+R_\oplus^3N_{30}^{-1}\alpha_{eY30}+\\ &R_\oplus^3N_{31}^{-1}\alpha_{eY31}+R_\oplus^3N_{32}^{-1}\alpha_{eY32}+R_\oplus^3N_{33}^{-1}\alpha_{eY33})\end{aligned} \tag{3.18}$$

$$\begin{aligned}\bar{a}_{eZ} =&\mu_\oplus(\alpha_{eZ00}+R_\oplus^2N_{20}^{-1}\alpha_{eZ20}+R_\oplus^2N_{21}^{-1}\alpha_{eZ21}+R_\oplus^2N_{22}^{-1}\alpha_{eZ22}+R_\oplus^3N_{30}^{-1}\alpha_{eZ30}+\\ &R_\oplus^3N_{31}^{-1}\alpha_{eZ31}+R_\oplus^3N_{32}^{-1}\alpha_{eZ32}+R_\oplus^3N_{33}^{-1}\alpha_{eZ33}),\end{aligned} \tag{3.19}$$

where α_{nm} can be found in Table 3.3 and 3.5. Note: the used geopotential coefficients are the normalised ones, but the used Legendre polynomials are the non-normalised. Thus, the N_{nm}^{-1} term appears.

Table 3.4: Normalised geopotential coefficients up to order and degree three in units of 10^{-6}

n	m	$\bar{C}_{nm}$	$\bar{S}_{nm}$
0	0	1.00	0.00
1	0	0.00	0.00
1	1	0.00	0.00
2	0	−484.165371736	0.00
2	1	−0.000186987635955	0.00119528012031
2	2	2.43914352398	−1.40016683654
3	0	0.957254173792	0.00
3	1	2.02998882184	0.248513158716
3	2	0.904627768605	−0.619025944205
3	3	0.721072657057	1.41435626958

Table 3.5: Induced acceleration by the Earth gravity attraction in inertial Cartesian coordinates

α_{eX21}	$\dfrac{3z\left[-5xy\,\psi^1_{21} + \gamma^1_{21}(-4x^2 + y^2 + z^2)\right]}{\rho^7}$
α_{eY21}	$\dfrac{3z\left[-5xy\,\psi^1_{21} + \gamma^1_{21}(x^2 - 4y^2 + z^2)\right]}{\rho^7}$
α_{eZ21}	$\dfrac{3(x^2 + y^2 - 4z^2)(x\gamma^1_{21} + y\psi^1_{21})}{\rho^7}$

$\rho = \sqrt{x^2 + y^2 + z^2}$, $\psi^i_{nm} = C_{nm}\sin(i\theta) + S_{nm}\cos(i\theta)$, $\gamma^i_{nm} = C_{nm}\cos(i\theta) - S_{nm}\sin(i\theta)$, where n and m are the degree and order of the Zonals and Tesserals.

3.2 Gravity Attraction of Celestial Bodies

Besides the gravity attraction of Earth, a body in a geostationary orbit is affected by the gravitation of other celestial bodies – mainly the Sun and the Moon. Therefore, the two-body problem has to be increased to a n-body problem. If the model has to be very precise, other planets like Jupiter should be considered, too.
In space from the satellite's point of view other celestial bodies (according to Montenbruck [18]) can be seen as a point mass M with which Newton's law of gravity is generally given by

$$\mathbf{a}_{cb1} = GM_{cb} \cdot \frac{\mathbf{r}_{cb} - \mathbf{r}_{sc}}{|\mathbf{r}_{cb} - \mathbf{r}_{sc}|^3} = \mu_{cb} \frac{\mathbf{r}_{cb} - \mathbf{r}_{sc}}{|\mathbf{r}_{cb} - \mathbf{r}_{sc}|^3}, \tag{3.20}$$

where μ_{cb} is the gravitational coefficient of the celestial body which affects the satellite. $\mathbf{r}_{cb}$ and $\mathbf{r}_{sc}$ are the inertial Cartesian coordinates of the celestial body and the spacecraft, respectively.
It can be assumed that the spacecraft has a constant mass for a small time interval. Consequently, by Newton's second law of motion it can be explained that the satellite is affected by an additional acceleration because of the celestial body (see Sidi [21]).

$$\mathbf{a}_{cb2} = \mu_{cb} \cdot \frac{\mathbf{r}_{cb}}{|\mathbf{r}_{cb}|^3} \tag{3.21}$$

Eq. (3.20) and Eq. (3.21) are subtracted for the disturbing acceleration of the celestial body to the satellite.

$$\mathbf{a}_{cb} = \mu_{cb} \cdot \left(\frac{\mathbf{r}_{cb} - \mathbf{r}_{sc}}{|\mathbf{r}_{cb} - \mathbf{r}_{sc}|^3} - \frac{\mathbf{r}_{cb}}{|\mathbf{r}_{cb}|^3} \right) \tag{3.22}$$

The total perturbing acceleration of the spacecraft by n celestial bodies is given by

$$\mathbf{a}_{totalsc} = \sum \mathbf{a}_{cbN}, \tag{3.23}$$

where $\mathbf{a}_{cbN}$ is the acceleration of the different celestial bodies.
For geostationary satellites, only the Sun and the Moon are regarded as perturbing celestial bodies (see Fig. 3.3). The achieved accuracy of the model is sufficient for most cases

$$\mathbf{a}_{totalCB} = \mu_{\odot} \cdot \left(\frac{\mathbf{r}_{\odot} - \mathbf{r}_{sc}}{|\mathbf{r}_{\odot} - \mathbf{r}_{sc}|^3} - \frac{\mathbf{r}_{\odot}}{|\mathbf{r}_{\odot}|^3} \right) + \mu_{☽} \cdot \left(\frac{\mathbf{r}_{☽} - \mathbf{r}_{sc}}{|\mathbf{r}_{☽} - \mathbf{r}_{sc}|^3} - \frac{\mathbf{r}_{☽}}{|\mathbf{r}_{☽}|^3} \right), \tag{3.24}$$

with $\mathbf{r}_{☽}$ and $\mathbf{r}_{\odot}$ being the inertial Cartesian position of the Moon and the Sun, respectively.
In Fig. 3.4, a spacecraft is positioned in ideal geostationary orbit exactly over the equator-Greenwich meridian crossing on the 1st of July 2016 for 28 days and only the Moon induced perturbations are considered. It can be seen that the moon cycle lasts about 28 days.

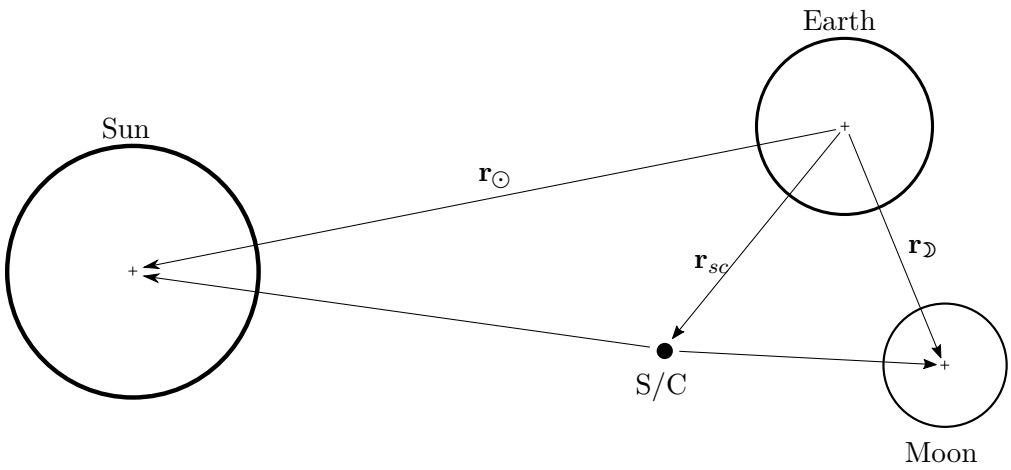

Figure 3.3: Third body disturbance of spacecraft

Table 3.6: Perturbing acceleration of Moon and Sun in inertial Cartesian coordinates

$a_{cbX\odot}$	$\frac{x_\odot - x_{sc}}{\eta_\odot^3} - \frac{x_\odot}{\rho_\odot}$	$a_{cbX☽}$	$\frac{x_☽ - x_{sc}}{\eta_☽^3} - \frac{x_☽}{\rho_☽}$
$a_{cbY\odot}$	$\frac{y_\odot - y_{sc}}{\eta_\odot^3} - \frac{y_\odot}{\rho_\odot}$	$a_{cbY☽}$	$\frac{y_☽ - y_{sc}}{\eta_☽^3} - \frac{y_☽}{\rho_☽}$
$a_{cbZ\odot}$	$\frac{z_\odot - z_{sc}}{\eta_\odot^3} - \frac{z_\odot}{\rho_\odot}$	$a_{cbZ☽}$	$\frac{z_☽ - z_{sc}}{\eta_☽^3} - \frac{z_☽}{\rho_☽}$

$\eta_i = \sqrt{(x_i - x_{sc})^2 + (y_i - y_{sc})^2 + (z_i - z_{sc})^2}$, $\rho_i = \sqrt{x_i^2 + y_i^2 + z_i^2}$ with i being the celestial body.

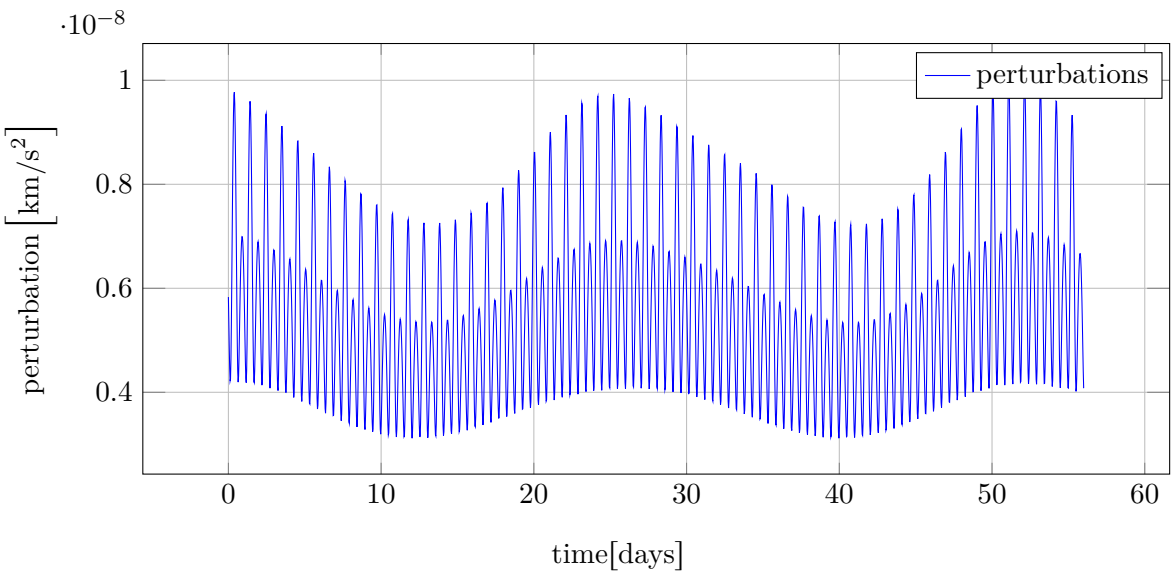

Figure 3.4: Norm of moon perturbation for geostationary spacecraft for one year at longitude of 60 deg

3.3 Solar Radiation Pressure

3.3.1 Neglection of Umbra and Penumbra

A geostationary satellite is exposed to electromagnetic waves which are radiated by the Sun. Those waves, mainly consisting of photons, interact with the surface of the spacecraft. Depending on the surface characteristics the waves get reflected ($\epsilon = 1$) or absorbed ($\epsilon = 0$), with the reflectivity coefficient ϵ. Thus, the formula for the solar radiation pressure, in opposite to the gravitational forces, depends on the surface area A, the mass m and the reflectivity coefficient. As a result of the large solar arrays of geostationary satellites this disturbance cannot be neglected and some assumptions have to be made: the reflectivity coefficient stays constant, umbra and penumbra are ignored.[20][21] The eccentricity of the Earth's orbit varies during the year, hence the solar radiation pressure changes by $\pm 3.3\,\%$. Finally, Montenbruck [18] gives the acceleration of the solar radiation pressure with the dependency of the reflectivity coefficient ϵ, mass m and the surface area A:

$$\mathbf{a}_{srp} = -P_{\odot} \frac{1AU^2}{|\mathbf{r}_{\odot} - \mathbf{r}_{sc}|^2} \frac{A}{m} \cos\theta \left[(1-\epsilon)\, \mathbf{e}_{\odot} + 2\epsilon \cos\theta \mathbf{n} \right], \tag{3.25}$$

where the normal vector of Sun-Spacecraft is described by $\mathbf{e}_{\odot}$ and the normal vector of the surface area by $\mathbf{n}$. The angle between $\mathbf{e}_{\odot}$ and $\mathbf{n}$ is described by θ. The distance between Sun and spacecraft is given by the norm of $\mathbf{r}_{\odot} - \mathbf{r}_{sc}$. 1 AU is one astronomical unit which is about $149,597,870.691\,\mathrm{km}$ [18]. The solar radiation pressure $P_{\odot}$ can be calculated with

$$P_{\odot} = \frac{\Phi}{c}, \tag{3.26}$$

with Φ being the solar flux of about $1367\,\mathrm{W/m^2}$ and c the speed of light.
Due to the assumption of $\mathbf{n}$ always pointing in the direction of $\mathbf{e}_{\odot}$, θ is zero. Accordingly, the waves are perpendicular to the surface area and the Eq. (3.25) simplifies to

$$\mathbf{a}_{srp} = -P_{\odot} C_R \frac{\mathbf{r}_{\odot}}{r_{\odot}^3} \frac{A}{m} \cdot 1\,\mathrm{AU}^2, \tag{3.27}$$

where the radiation coefficient is $C_R = 1 + \epsilon$.
The acceleration vector of the solar radiation pressure is given by

$$\mathbf{a}_{srp} = \mathbf{a}_{srpX}\mathbf{X} + \mathbf{a}_{srpY}\mathbf{Y} + \mathbf{a}_{srpZ}\mathbf{Z} \tag{3.28}$$

in the inertial Cartesian coordinate system. The single components of Eq. (3.28) can be seen in Table 3.7.

3.3.2 Umbra and Penumbra

In the previous part, the umbra and penumbra for geostationary satellite were ignored. In the following, a spherical body will be used for eclipse calculations. The shadow factor ν is according to

Table 3.7: Solar radiation pressure in inertial Cartesian frame

a_{srpX}	$-P_{\odot}C_R \cdot \frac{A}{m} \cdot 1AU^2 \cdot \frac{x_{\odot} - x_{sc}}{\eta^3}$
a_{srpY}	$-P_{\odot}C_R \cdot \frac{A}{m} \cdot 1AU^2 \cdot \frac{y_{\odot} - y_{sc}}{\eta^3}$
a_{srpZ}	$-P_{\odot}C_R \cdot \frac{A}{m} \cdot 1AU^2 \cdot \frac{z_{\odot} - z_{sc}}{\eta^3}$

$$\eta = \sqrt{(x_{\odot} - x_{sc})^2 + (y_{\odot} - y_{sc})^2 + (z_{\odot} - z_{sc})^2}.$$

Montenbruck [18]

$$\begin{aligned} \nu &= 0 && \text{if the spacecraft is in umbra,} \\ \nu &= 1 && \text{if the spacecraft is in sunlight,} \\ 0 < \nu &< 1 && \text{if the spacecraft is in penumbra} \end{aligned} \tag{3.29}$$

which improves the Eq. (3.25) of the acceleration due to the solar radiation pressure at Earth distance to

$$\mathbf{a}_{srp} = -\nu P_{\odot} \frac{1\,\mathrm{AU}^2}{\mathbf{r}_{\odot}^2} \frac{A}{m} \cos\theta \left[(1-\epsilon)\, \mathbf{e}_{\odot} + 2\epsilon \cos\theta \mathbf{n} \right]. \tag{3.30}$$

As reported in Montenbruck [18], the shadow function depends on the area A of the occulted segment of the apparent solar disk and of the apparent radius of the occulted body a (see Eq. (3.34) to (3.40)).

$$\nu = 1 - \frac{A}{\pi a^2} \tag{3.31}$$

First, the Sun vector $\mathbf{r}_{\odot}$ in the J-2000 coordinate frame, the spacecraft vector $\mathbf{r}_{sc}$ and the occulting body vector $\mathbf{r}_B$ have to be created (see Fig. 3.5) which results in a Sun – occulted body vector $\mathbf{s}_{\odot}$ and in a spacecraft-body vector $\mathbf{s}$

$$\mathbf{s}_{\odot} = \mathbf{r}_{\odot} - \mathbf{r}_B \tag{3.32}$$

$$\mathbf{s} = \mathbf{r}_{sc} - \mathbf{r}_B \tag{3.33}$$

Eq. (3.31) contains the surface area A which is described as:

$$A = a^2 \arccos\left(\frac{x}{a}\right) + b^2 \arccos\left(\frac{c-x}{b}\right) - cy \tag{3.34}$$

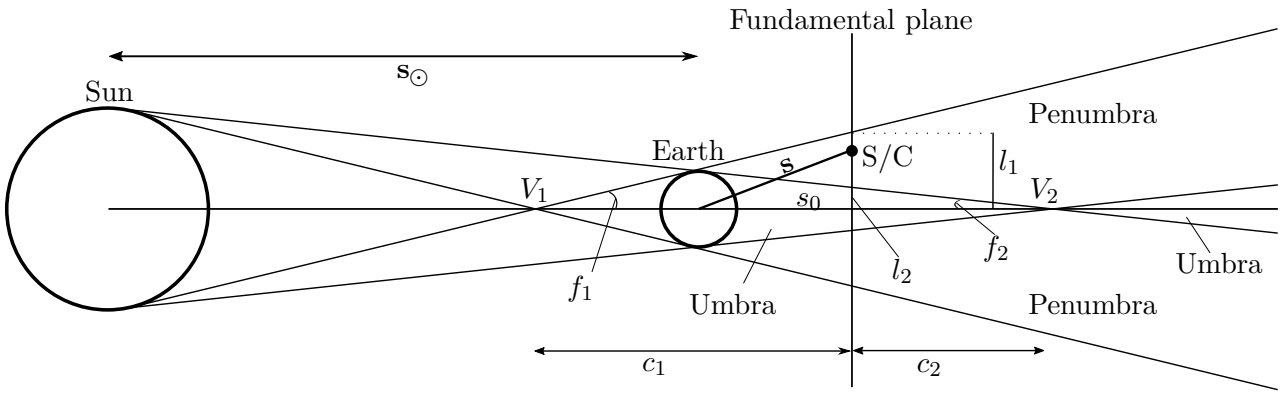

Figure 3.5: Shadow model according to Montenbruck [18]

with

$$x = \frac{a^2 - b^2 + c^2}{2c} \tag{3.35}$$

$$y = \sqrt{a^2 - x^2} \tag{3.36}$$

$$a = \arcsin\left(\frac{R_\odot}{|\mathbf{r}_\odot - \mathbf{r}_{sc}|}\right) \tag{3.37}$$

$$b = \arcsin\left(\frac{R_B}{|\mathbf{s}|}\right) \tag{3.38}$$

$$c = \arccos\left(\frac{-\mathbf{s}^T\left(\mathbf{r}_\odot - \mathbf{r}_{sc}\right)}{|\mathbf{s}| \cdot |\mathbf{r}_\odot - \mathbf{r}_{sc}|}\right) \tag{3.39}$$

$$s_0 = \frac{\mathbf{s}^T \mathbf{s}_\odot}{|\mathbf{s}_\odot|} \tag{3.40}$$

where b and c are the apparent radius of the occulting body and the apparent separation of the centre of the bodies, respectively. The position of the occulting body $\mathbf{r}_B$ is in the inertial Cartesian frame and R_B is the radius of it. $R_\odot$ is the radius of the Sun. $\mathbf{r}_\odot$ and $\mathbf{r}_{sc}$ are corresponding to the position vectors for the Sun and for the spacecraft.

This formula gives the ν for all possible positions of the spacecraft around the occulting body. Unfortunately, there are locations where the ν is not a number. Therefore, it is important to constrain the satellite position in the penumbra and the umbra. The distance of the spacecraft to the shadow axis can be found via Pythagoras:

$$l = \sqrt{|\mathbf{s}|^2 - s_0^2} \tag{3.41}$$

The half cone angles at the vertices V_1 and V_2 are expressed by:

$$\sin f_1 = \frac{R_\odot + R_B}{|\mathbf{s}_\odot|} \tag{3.42}$$

$$\sin f_2 = \frac{R_\odot - R_B}{|\mathbf{s}_\odot|} \tag{3.43}$$

The distance from the vertex V_1 and V_2 to the fundamental plane is given by c_1 and c_2.

$$c_1 = s_0 + \frac{R_B}{\sin f_1} \tag{3.44}$$

$$c_2 = s_0 - \frac{R_B}{\sin f_2} \tag{3.45}$$

Finally, if the spacecraft distance to the shadow axis l is greater than the penumbra plus umbra distance l_1, the satellite has left the eclipse and is located in the sunlight.

$$l_1 = c_1 \tan f_1 \tag{3.46}$$

$$l_2 = c_2 \tan f_2, \tag{3.47}$$

If l_2 is negative, the geostationary satellite is in the total eclipse region.
If the condition

$$|a - b| < c < (a + b) \tag{3.48}$$

is not satisfied, $(a + b) \leqslant c$ results in no occultation. For a full occultation c has to be smaller than $(b - a)$ for $a < b$. For a partial but maximum occultation, which is also called annular eclipse, $c < (a - b)$ for $a > b$.[18]
From the geostationary point of view, the Earth appears in an angle of $8.70\,^\circ$ and the Sun in an angle of $0.5\,^\circ$. Consequently, the penumbra has an opening angle of $0.5\,^\circ$. The longest eclipse duration is about 71.5 min. The total time in penumbra for the maximum eclipse is 4 min. Each season, there is a maximum penumbra duration of 4 min because of the change of the inclination of the Sun.[22]
In Fig. 3.6, a spacecraft is placed at an altitude of 1000 km above the Earth surface on the 1st of January 2014. The Sun and the Moon positions are fixed, the Earth is not rotating – just the spacecraft is positioned at different longitudes around the equator. It is easy to see that the norm of the solar radiation pressure is constant for most of the time but not between 45 deg and 157 deg. The reason for this is that the spacecraft enters the penumbra and then into the umbra of the Earth. If the solar radiation pressure acceleration is between the constant term of $2.28 \cdot 10^{-10}\,\mathrm{km/s^2}$ and $0\,\mathrm{km/s^2}$ the spacecraft is located in the penumbra (see Fig. 3.5). The time for one orbit is $T = 2\pi\sqrt{\frac{a^3}{\mu}} = 105.12\,\mathrm{min}$. Hence, the spacecraft is situated in the umbra for 31.1 % of the orbit time which is approximately 32.7 min. The satellite's total time the penumbra is about 0.2336 min which is for one orbit approximately 14.02 s.

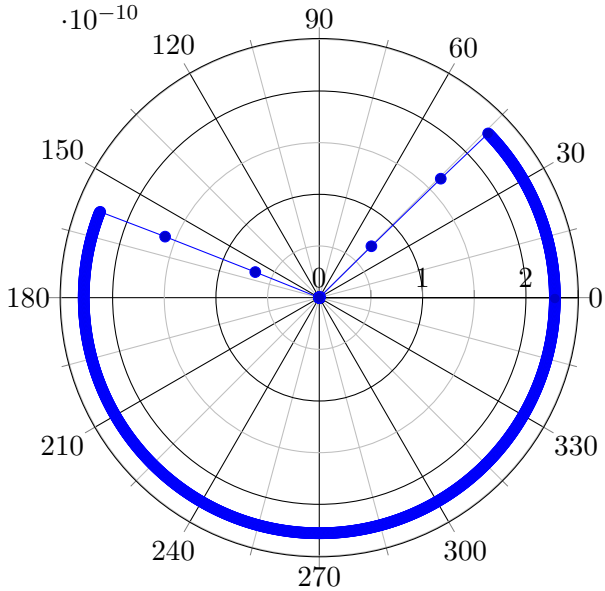

Figure 3.6: Norm of solar radiation pressure acceleration including eclipse acting on a spacecraft in height of 1000 km at the same moment with different longitude values

4 Approximate Sequence of Riccati Equations

4.1 State-dependent Riccati Equations

The possible usage of non-linearities in the system and the great flexibility due to the weighting matrices are the reason why the SDRE have become very popular [10]. For the SDRE, the non-linear system has to be brought to State-Dependent Coefficient (SDC) matrices. Then, the non-linear system has to be mathematically factorised which creates additional degrees of freedom. These can be used to tune the final system. The new quasi-linear system depends on the state vector and is used to minimise the performance index.[1, 2, 10]
In the first section of the theoretical part, the SDRE approach and its conditions are shown. Afterwards, the control structure and the influence of the factorisation are shortly described. For further information, the author recommends common literature like Cloutier [1] and Çimen [10].

4.1.1 Theory

Considering the autonomous, non-linear, full-state observable, infinite-horizon problem which is given by

$$\dot{\mathbf{x}}(t) = \mathbf{f}(\mathbf{x}) + \mathbf{B}(\mathbf{x})\mathbf{u}(t) \tag{4.1}$$

with $\mathbf{x}(0) = \mathbf{x}_0$, the state vector $\mathbf{x} \in \mathbb{R}^n$, the input vector $\mathbf{u}(t) = \mathbb{R}^m$ and the time $t \in [0, \infty)$. Furthermore, it is to mention that $\mathbf{f} : \mathbb{R}^n \to \mathbb{R}^n$, $\mathbf{B} : \mathbb{R}^n \to \mathbb{R}^{n\times m}$ and $\mathbf{B}(\mathbf{x}) \neq \mathbf{0}$. Another condition for $\mathbf{f}(\mathbf{x})$ is it has to be a continuously differentiable function of $\mathbf{x}$. An additional important assumption is $\mathbf{f}(\mathbf{0}) = \mathbf{0}$ at the uncontrolled origin $\mathbf{x} = \mathbf{0}$ which is assumed to be an equilibrium point. The performance index which will be minimised is not quadratic in $\mathbf{x}$ but in $\mathbf{u}$.[10]

$$J(\mathbf{x}(t), \mathbf{u}(t)) = 0.5 \int_0^\infty \left[\mathbf{x}^T(t)\mathbf{Q}(\mathbf{x})\mathbf{x}(t) + \mathbf{u}^T(t)\mathbf{R}(\mathbf{x})\mathbf{u}(t)\right] dt \tag{4.2}$$

The weighting matrices $\mathbf{Q}(\mathbf{x})$ and $\mathbf{R}(\mathbf{x})$ are semi-positive definite and positive definite for all $\mathbf{x}$, respectively. Usually, $\mathbf{Q}(\mathbf{x})$ and $\mathbf{R}(\mathbf{x})$ are chosen in such way that $J(\mathbf{x}(t), \mathbf{u}(t))$ converges globally.
The optimal problem to be solved is

$$\mathbf{u}(\mathbf{x}) = -\mathbf{K}(\mathbf{x})\mathbf{x} \tag{4.3}$$

with $\mathbf{u}(\mathbf{0}) = \mathbf{0}$ so that the performance index Eq. (4.2) is minimised subject to the non-linear constraints of Eq. (4.1). The matrix $\mathbf{K}$ is later described in Section 4.1. The minimisation of the cost

function and the assumed infinite-horizon of the non-linear system hold, therefore:

$$\lim_{t\to\infty} \mathbf{x}(t) = \mathbf{0} \tag{4.4}$$

Hence, the SDRE solution is suboptimal and locally asymptotically stable.[1, 2, 10, 23]

4.1.2 State-Dependent Coefficient Matrix

Factorisation or extended linearisation is used to bring the non-linear system of Eq. (4.1) with the assumptions mentioned in Section 4.1 to the SDC form:

$$\dot{\mathbf{x}}(t) = \mathbf{A}(\mathbf{x})\mathbf{x}(t) + \mathbf{B}(\mathbf{x})\mathbf{u}(t) \tag{4.5}$$

where $\mathbf{A} : \mathbb{R}^n \to \mathbb{R}^{n\times n}$ and $\mathbf{x}(\mathbf{0}) = \mathbf{x}_0$. By using mathematical factorisation of $\mathbf{f}(\mathbf{x})$ it is guaranteed that $\mathbf{f}(\mathbf{0}) = \mathbf{0}$ and $\mathbf{f}(\mathbf{x}) \in \mathfrak{C}^1$ is valid. Now, the matrices $\mathbf{A}(\mathbf{x})$ and $\mathbf{B}(\mathbf{x})$ are depending on the state and are having a linear structure. Furthermore, there are infinite ways of choosing the factorised matrices for $n > 1$, but they have to be observable and controllable for all $\mathbf{x}$.[1, 10, 23]

4.1.3 Controllability

According to Lunze [17] a system is fully controllable if it is possible to bring an arbitrary state vector $\mathbf{x}(t_0)$ with a suitable input vector $\mathbf{u}(t)$ to an arbitrary final state vector $\mathbf{x}(t_f)$ in finite time $[0, t_f]$. As reported by Kalman, a system is fully controllable if

$$\operatorname{rank}(\zeta) = \mathrm{n}, \tag{4.6}$$

where

$$\zeta = \begin{bmatrix} \mathbf{B} & \mathbf{AB} & \mathbf{A}^2\mathbf{B} & \dots & \mathbf{A}^{n-1}\mathbf{B} \end{bmatrix}. \tag{4.7}$$

Consequently, the locally reachable space of controllable systems has to be equal to the state space dimension. The original system is called, in consonance with Hammett [6] *weakly controllable* if

$$\operatorname{rank}[\Delta_c(\mathbf{x})] = \mathrm{n} \tag{4.8}$$

holds for all $\mathbf{x}$. $\Delta_c(\mathbf{x})$ can be determined via:

- $\Delta_0 = \operatorname{span}(\mathbf{B}) = \operatorname{span}(b_i)$, where b_i are the different columns of $\mathbf{B}(x)$ with $1 \leqslant i \leqslant m$ and m are the number of columns.
- $\Delta_1 = \Delta_0 + [a, b_i] + [b_j, b_i]$, where $1 \leqslant i \leqslant m$, $1 \leqslant j \leqslant m$, a is the invariant of the factorised $\mathbf{A}(x)\mathbf{x}(t)$, $[a, b_i]$ is the Lie bracket and the sum of the spans is described with the plus sign.
- $\Delta_k = \Delta_{k-1} + [a, d_j] + [b_i, d_j]$, where $1 \leqslant i \leqslant m$, $1 \leqslant j \leqslant n$ with d_j has a basis of Δ_{k-1}.
- Finish, if $\Delta_{k+1} = \Delta_k$.

Hammett [7] showed some theorems about the controllability. Just the theorems are described here – for the proofs the author refers to Hammett [6, 7].

Theorem 1 *Considering a non-linear, non-factorised system (see Eq. (4.5)) with* $\boldsymbol{A}$ *being assumed to be a* $\mathfrak{C}^1$ *function, so that the system can be factorised. Estimate the factorised* $[\boldsymbol{A}(x), \boldsymbol{B}(x)]$ *is controllable for all* $\boldsymbol{x}(t)$ *such that Eq. (4.6) holds. Then the non-linear non-factorised system does not necessarily need to be weakly controllable.*

Theorem 2 *Considering a non-linear factorised system (see Eq. (4.5)) with* $n = 2$ *and* $\boldsymbol{B}(x)$ *as being constant. Assume that* $\boldsymbol{A}(\boldsymbol{x})$ *is chosen that* $\boldsymbol{J}(\boldsymbol{x})\boldsymbol{B} = k\boldsymbol{A}(\boldsymbol{x})\boldsymbol{B}$ *for all* $\boldsymbol{x}$*, where* $k \neq 0 \in \mathbb{R}$ *and* $\boldsymbol{J}$ *is the Jacobian of* $\boldsymbol{A}(\boldsymbol{x})$*. If the factorised system is controllable for all* $\boldsymbol{x}$*, the original system is weakly controllable on an open and dense subset of* $\mathbb{R}^2$*. Vice versa, if the original system is weakly controllable on* $\mathbb{R}^2$*, then the factorised system is controllable for all* $\boldsymbol{x}$*.*

Theorem 3 *Considering the non-linear factorised system (see Eq. (4.5)) and assuming that Eq. (4.6) holds, then the original system is weakly controllable in an area around the origin.*

Theorem 4 *Considering the non-linear factorised system (see Eq. (4.5)) and let* $m \geqslant n$*, assuming* $\boldsymbol{B}(\boldsymbol{x})$ *has rank* n *for all* $\boldsymbol{x}$*, then the factorised system is controllable for all* $\boldsymbol{x}$ *and the original system is weakly controllable on* $\mathbb{R}^n$*.*

If rank$\mathbf{B}(\mathbf{x}) = n$ the system matrix $\mathbf{A}(\mathbf{x}(t))$ can be completely arbitrary for the reason that all the controllability conditions hold.[6]

4.1.4 Observability

If it is possible to get the state vector $\mathbf{x}_0$ from the input vector $\mathbf{u}(t)$ and from the controlled vector $\mathbf{y}(t)$ in a finite time interval $[0, t_f]$, the system is called to be fully observable. According to Kalman, a system is fully observable (see Lunze [17]) if

$$\text{rank}\begin{pmatrix} \mathbf{C} \\ \mathbf{CA} \\ \mathbf{CA}^2 \\ \vdots \\ \mathbf{CA}^{n-1} \end{pmatrix} = \text{n}. \tag{4.9}$$

with

$$\mathbf{C}^T(x)\mathbf{C}(x) = \mathbf{Q}(x). \tag{4.10}$$

The sufficient test for controllability (see Eq. (4.6)) can be used to check for detectability (observability). Since Eq. (4.10) holds, Eq. (4.9) can be rewritten to

$$\zeta_o = \begin{bmatrix} \mathbf{Q}^{1/2} & \mathbf{Q}^{1/2}\mathbf{A} & \mathbf{Q}^{1/2}\mathbf{A}^2 & \dots & \mathbf{Q}^{1/2}\mathbf{A}^{n-1} \end{bmatrix} \tag{4.11}$$

and has rank$\zeta_o = \text{n} \ \forall \mathbf{x} \in \mathbb{R}^n$. If $\mathbf{Q}$ is chosen in such a way that it is positive-definite for all $\mathbf{x} \in \mathbb{R}^n$ Eq. (4.11) is always guaranteed.[10]

4.1.5 Linear Quadratic Control

This section will only briefly summarise the Linear Quadratic control (LQ control), as the range of this topic exceeds the scope of this thesis. For the whole derivations the author recommends Lewis [13].
The non-linear system can be described by

$$\dot{\mathbf{x}} = \mathbf{f}(\mathbf{x}, \mathbf{u}, t) \tag{4.12}$$

with $t \geqslant t_0$ where t_0 is fixed and it is the condition to solve the minimisation problem

$$min_{\mathbf{x}(t),\mathbf{u}(t)} \int_{t_0}^{t_f} \mathbf{L}(\mathbf{x}, \mathbf{u}, t)dt, \tag{4.13}$$

where $\mathbf{L}(\mathbf{x}, \mathbf{u}, t)$ is the Lagrangian. After some calculation, this results in a solution for the Euler-Lagrange equations:

$$\begin{aligned} \dot{\mathbf{x}} &= \frac{\partial \mathbf{H}}{\partial \boldsymbol{\lambda}} \\ \dot{\boldsymbol{\lambda}} &= -\frac{\partial \mathbf{H}}{\partial \mathbf{x}} \\ 0 &= \frac{\partial \mathbf{H}}{\partial \mathbf{u}} \end{aligned} \tag{4.14}$$

where the Hamiltonian $\mathbf{H}(\mathbf{x}, \boldsymbol{\lambda}, \mathbf{u}, t) = \mathbf{L}(\mathbf{x}, \mathbf{u}, t) + \boldsymbol{\lambda}^T [\mathbf{f(x,t)} + \mathbf{g(x,t)}\ \mathbf{u}]$ and $\boldsymbol{\lambda}$ is the co-state vector. Finally, the three necessary conditions of optimality are created [28]:

$$\begin{aligned} \mathbf{Qx} + \mathbf{A}^T\boldsymbol{\lambda} &= -\dot{\boldsymbol{\lambda}} \\ \mathbf{Ru} + \mathbf{B}^T\boldsymbol{\lambda} &= 0 \\ \dot{\mathbf{x}} - \mathbf{Ax} - \mathbf{Bu} &= 0 \end{aligned} \tag{4.15}$$

The second row can be reformed to

$$\mathbf{u}(t) = -\mathbf{R}^{-1}\mathbf{B}^T\boldsymbol{\lambda} \tag{4.16}$$

The co-state $\boldsymbol{\lambda}$ is assumed to be the result of the multiplication of $\mathbf{P}(\mathbf{x})\mathbf{x}$ where $\mathbf{P}(\mathbf{x})$ is the solution of the algebraic Riccati equation (see Section 4.1).[13, 28]

4.1.6 Control Structure

Due to the factorisation it is possible to formulate the non-linear system similar to the well known Linear Quadratic Regulator (LQR) method. Therefore, it is possible to use the solution of the continuous time algebraic SDRE

$$\mathbf{P}(\mathbf{x})\mathbf{A}(\mathbf{x}) + \mathbf{A}^T(\mathbf{x})\mathbf{P}(\mathbf{x}) - \mathbf{P}(\mathbf{x})\mathbf{B}(\mathbf{x})\mathbf{R}^{-1}(\mathbf{x})\mathbf{B}^T(\mathbf{x})\mathbf{P}(\mathbf{x}) + \mathbf{Q}(\mathbf{x}) = \mathbf{0} \tag{4.17}$$

in Eq. (4.16)

$$\mathbf{u}(\mathbf{x}) = -\mathbf{R}^{-1}(\mathbf{x})\mathbf{B}^T(\mathbf{x})\mathbf{P}(\mathbf{x})\mathbf{x}. \tag{4.18}$$

It is important to mention that $\mathbf{P}$ is semi-positive definite and a function of $\mathbf{x}$. Inserting Eq. (4.18) into Eq. (4.5) leads to

$$\dot{\mathbf{x}}(t) = \left[\mathbf{A}(\mathbf{x}) - \mathbf{B}(\mathbf{x})\mathbf{R}^{-1}(\mathbf{x})\mathbf{B}^T(\mathbf{x})\mathbf{P}(\mathbf{x})\right]\mathbf{x}(t). \tag{4.19}$$

The algebraic Riccati equation (4.17) can be solved via backwards integration. Hence, a final semi-positive definite weighting matrix P_∞ is chosen in the beginning. The $\mathbf{P}_\infty$ has the index ∞ because the LQR is valid in infinite-time horizons. According to Çimen [9], these can be approximated for linear time-invariant systems with a very large final time and a constant desired output vector as $\mathbf{P}(t)$ can be seen as a steady-state solution:

$$\mathbf{P}(t) \approx \mathbf{P} \tag{4.20}$$

Eq. (4.18) can be written as

$$\mathbf{u}(\mathbf{x}) = -\mathbf{K}(x)\mathbf{x} \tag{4.21}$$

where $\mathbf{K}(x) = \mathbf{R}^{-1}(\mathbf{x})\mathbf{B}^T(\mathbf{x})\mathbf{P}(\mathbf{x})$ is called the Kalman gain which can be found in the definition in Eq. (4.3).
While knowing that the final $\mathbf{P}(\mathbf{x}_f) = \mathbf{S}$, the performance index of Eq. (4.2) can be rewritten:

$$J(\mathbf{x}(t), \mathbf{u}(t)) = 0.5\mathbf{x}^T(t_f)\mathbf{S}\mathbf{x}(t_f) + 0.5\int_0^\infty \left[\mathbf{x}^T(t)\mathbf{Q}\mathbf{x}(t) + \mathbf{u}^T(t)\mathbf{R})\mathbf{u}(t)\right] dt \tag{4.22}$$

To sum up, the solution of the SDRE is a general solution of the infinite-time LQR problem where the matrices are depending on the state instead of being constant.[10, 23]

4.1.7 Degrees of Freedom

The mathematical factorisation leads to infinite possibilities for the SDC matrices

$$\mathbf{f}(\mathbf{x}) = \mathbf{A}_1(\mathbf{x}) = \mathbf{A}_2(\mathbf{x}) \tag{4.23}$$

where $\mathbf{A}_1$ and $\mathbf{A}_2$ are two different factorisations of the same non-linear system. Then, it is possible to create a third factorisation

$$\mathbf{A}_3(\mathbf{x}, \alpha) = \alpha\mathbf{A}_1(\mathbf{x}) + (1-\alpha)\mathbf{A}_2(\mathbf{x}) \tag{4.24}$$

where $\alpha \in [0, 1]$. α provides additional degrees of freedom which "can be used to enhance performance or effect tradeoffs between performance, optimality, stability, robustness, and disturbance rejection"[10]. In addition, the new degrees of freedom are not available in classical optimal control methods. α has to be chosen that the controllability of the system $(\mathbf{A}(\mathbf{x}, \alpha), \mathbf{B}(x))$ is always guaranteed. This assures local asymptotical stability. Due to the factorisation the solution is not unique

for systems with $n > 1$.[10]
Cloutier [3] and Steinfeldt [23] proved that the global asymptotic stability of the closed-loop system $\mathbf{A}_{cl}(\mathbf{x}) = \mathbf{A}(\mathbf{x}) - \mathbf{B}(\mathbf{x})\mathbf{K}(\mathbf{x})$ is valid for any initial condition under the assumptions that $(\mathbf{A}(\mathbf{x}), \mathbf{B}(\mathbf{x}))$ and $\left(\mathbf{A}(\mathbf{x}), \sqrt{\mathbf{Q}}(\mathbf{x})\right)$ are observable and controllable. Moreover, the closed-loop system is pointwise Hurwitz stable. Additionally, all matrices which are needed to describe the SDC matrices have to be $\mathfrak{C}^1$ matrix-valued functions.[1, 10]
To conclude this chapter, the SDRE method is very simple to implement and has a great flexibility due to the factorisation which is not unique. For the reason of the different factorisation results the performance index can vary. The system is always at least local asymptotically stable (mostly if there are many equilibrium points) and in some cases even global asymptotically stable.

4.2 Approximate Squence of Riccati Equations

The ASRE method was developed by Çimen [12] in 2002 and was published in 2004. It is a method for global optimal feedback control for multi-input-multi-output non-linear systems in a finite-time horizon. Like the SDRE, this approach is using a factorised non-linear system which is in the SDC matrix form. The ASRE method calculates the Riccati equations offline until they converge. The final values are used for the online control.[8]

4.2.1 Background

The general non-linear autonomous system

$$\dot{\mathbf{x}} = \mathbf{f}(\mathbf{x}, \mathbf{u}) \tag{4.25}$$

with $\mathbf{x}(t_0) = \mathbf{x}_0$ is factorised like mentioned in Section 4.1. Furthermore, it is assumed that the origin is at an equilibrium point that $\mathbf{f}(\mathbf{0}, \mathbf{0}) = \mathbf{0}$. According to Çimen [11], many authors used this "pseudo-linear" form to solve the SDRE.

> However, the SDRE feedback provides a locally optimal control policy, which can only be applied to autonomous regulator problems. This is because the approach requires solving the infinite-time algebraic Riccati equation and, unfortunately, the theory which deals with this for the optimal tracking problem is not available. [12]

A system in the form of

$$\dot{\mathbf{x}}(t) = \mathbf{A}(\mathbf{x})\mathbf{x}(t) \tag{4.26}$$

converges in continuous time for a sequence of linear time variant approximations

$$\dot{\mathbf{x}}^{[i]}(t) = \mathbf{A}\left(\mathbf{x}^{[i-1]}(t)\right)\mathbf{x}^{[i]}(t). \tag{4.27}$$

The proof of the global stability is given by Çimen in [11, 12].

4.2.2 Linear Quadratic Optimal Control

So far the performance index had no final time, meaning the upper boundary of the integral was always infinite. This changed for the ASRE method to a finite-time horizon with a final time t_f. Thus, the performance index of Eq. (4.22) changes to

$$J(\mathbf{x}(t), \mathbf{u}(t)) = 0.5\mathbf{x}^T(t_f)\mathbf{S}\mathbf{x}(t_f) + 0.5\int_{t_0}^{t_f} \left[\mathbf{x}^T(t)\mathbf{Q}(t)\mathbf{x}(t) + \mathbf{u}^T(t)\mathbf{R}(t)\mathbf{u}(t)\right] dt \tag{4.28}$$

where t_0 is the initial time and the described state $\dot{\mathbf{x}}(t)$ is the same as in the observable state-dependent matrix of Eq. (4.5). The necessary conditions of optimality (see Eq. (4.15)) still hold. By using Eq. (4.16) to the first and third condition of optimality:

$$\begin{aligned} \dot{\mathbf{x}}(t) &= \mathbf{A}(t)\mathbf{x}(t) - \mathbf{B}(t)\mathbf{R}^{-1}(t)\mathbf{B}^T(t)\boldsymbol{\lambda}(t) \\ \dot{\boldsymbol{\lambda}}(t) &= -\mathbf{Q}(t)\mathbf{x}(t) - \mathbf{A}^T(t)\boldsymbol{\lambda}(t) \end{aligned} \tag{4.29}$$

This is a coupled two point boundary value problem with $\mathbf{x}(t_0) = \mathbf{x}_0$ and $\boldsymbol{\lambda}(t_f) = \mathbf{S}\mathbf{x}(t_f)$.
Choosing $\mathbf{P}(t_f) = \mathbf{S}$ under the assumption of $\boldsymbol{\lambda}(t) = \mathbf{P}(t)\mathbf{x}(t)$ for a positive definite matrix $\mathbf{P}(t)$. The result is an optimal solution for $\mathbf{u}(t)$.

$$\mathbf{u}(t) = -\mathbf{R}^{-1}(t)\mathbf{B}^T(t)\mathbf{P}(t)\mathbf{x}(t) \tag{4.30}$$

where $\mathbf{P}(t)$ is calculated via the differential algebraic Riccati equation

$$\dot{\mathbf{P}}(t) = -\mathbf{Q}(t) - \mathbf{P}(t)\mathbf{A}(t) - \mathbf{A}^T(t)\mathbf{P}(t) + \mathbf{P}(t)\mathbf{S}(t)\mathbf{P}(t), \tag{4.31}$$

where $\mathbf{S}(t) = \mathbf{B}(t)\mathbf{R}^{-1}(t)\mathbf{B}^T(t)$. This can be used for the ASRE method.[11]

4.2.3 Theory

The ASRE approach can be used to approximate the non-linear system including the input vector of Eq. (4.5)

$$\dot{\mathbf{x}}^{[i]}(t) = \mathbf{A}\left(\mathbf{x}^{[i-1]}(t)\right)\mathbf{x}^{[i]}(t) + \mathbf{B}\left(\mathbf{x}^{[i-1]}(t), \mathbf{u}^{[i-1]}(t)\right)\mathbf{u}^{[i]}(t). \tag{4.32}$$

The performance index of the SDRE can be rewritten as

$$\begin{aligned} J^{[i]}(\mathbf{u}) =& 0.5\mathbf{x}^{[i]T}(t_f)\mathbf{Q}\left(\mathbf{x}^{[i-1]}(t_f)\right)\mathbf{x}^{[i]}(t_f) + \\ & 0.5\int_0^{t_f}\left[\mathbf{x}^{[i]T}(t)\mathbf{Q}\left(\mathbf{x}^{[i-1]}(t)\right)\mathbf{x}^{[i]}(t) + \mathbf{u}^{[i]T}(t)\mathbf{R}\left(\mathbf{x}^{[i-1]}(t)\right)\mathbf{u}^{[i]}(t)\right] dt \end{aligned} \tag{4.33}$$

for $i \geqslant 0$. The weighting matrices $\mathbf{Q}(\mathbf{x})$ and $R(\mathbf{x})$ are semi-positive definite and positive definite for all $\mathbf{x}$, respectively.
For $i = 0$ Eq. (4.32) has to be written as

$$\dot{\mathbf{x}}^{[0]}(t) = \mathbf{A}\left(\mathbf{x}_0\right)\mathbf{x}^{[0]}(t) + \mathbf{B}\left(\mathbf{x}_0, \mathbf{0}\right)\mathbf{u}^{[0]}(t) \tag{4.34}$$

with $\mathbf{x}^{[0]} = \mathbf{x}_0$ and $\mathbf{u}^{[0]} = \mathbf{0}$. As a reason for the time-varying and linear-quadratics the control vector of Eq. (4.18) is given by

$$\mathbf{u}^{[i]}(t) = -\mathbf{R}^{-1}(\mathbf{x}^{[i-1]})\mathbf{B}^T \left(\mathbf{x}^{[i-1]}(t), \mathbf{u}^{[i-1]}(t)\right) \mathbf{P}^{[i]}(t)\mathbf{x}^{[i]}(t). \tag{4.35}$$

It is to mention that only the first approximation is not time-varying. The used $\mathbf{P}^{[i]}(t)$ can be calculated via the algebraic Riccati equation from Eq. (4.17).[11]
The executing condition for the convergence is achieved if

$$\|\mathbf{x}^{[i]}(t) - \mathbf{x}^{[i-1](t)}\|_\infty \leqslant \epsilon \tag{4.36}$$

where ϵ is the tolerance and $\| \dots \|_\infty$ is the infinity norm.[26]

4.2.4 Solving the Approximate Squence of Riccati Equations

In this section, a path of how to use the ASRE method will be described.
For solving the ASRE method, it is necessary to provide an initial state vector $\mathbf{x}_0$, the initial time t_i and the final time t_f. The weighting matrices $\mathbf{Q}$ and $\mathbf{R}$ as well as the final time solution of the Riccati equation $\mathbf{P}(t_f)$. The non-linear system has to be factorised to the system matrix $\mathbf{A}(\mathbf{x}(t))$ and the input matrix $\mathbf{B}(\mathbf{x}(t), \mathbf{u}(t))$. The error tolerance ϵ has to be defined, too.
To determine the 0th iteration of $\mathbf{u}^{[0]}(t)$ of Eq. (4.35), it is crucial to solve the discrete algebraic Riccati equation Eq. (4.31) backwards in time. This means the final time solution of $\mathbf{P}(t)$ as well as the matrices $\mathbf{A}$ and $\mathbf{B}$ with the initial state $\mathbf{x}_0$ are used to detect all solutions of the Riccati equation from t_0 until t_f. The system and input matrices as well as the weighting matrices are constant for the zeroth iteration. Now, the control and the state profiles can be calculated: via Eq. (4.35) the first $\mathbf{u}(t)$ can be determined by using $\mathbf{P}(t_0)$ and $\mathbf{x}_0$. Afterwards, this $\mathbf{u}(t_0)$ is inserted to Eq. (4.34) to calculate $\mathbf{x}_1$. This cycle starts again but always with the actual $x(t)$. This can be seen in the following pseudo code. Note: P_i changes with the time according to the solution of the backwards in time integration.

```
for i:= t_0 to t_f do
begin
{
u = - R^{-1} * B^T * P_i * x
x = A * x + B * u
}
end;
```

The next iterations $i \geqslant 1$: $\mathbf{A}^{[i]}(\mathbf{x}^{[i-1]}(t))$ and $\mathbf{B}^{[i]}(\mathbf{x}^{[i-1]}(t), \mathbf{u}^{[i-1]}(t))$ are calculated for each $\mathbf{x}(t)$ of the previous iteration. If $\mathbf{Q}$ and $\mathbf{R}$ are depending on the state, they have to be determined for each $\mathbf{x}^{[i-1]}(t)$, too. The final solution of the Riccati equation $\mathbf{P}(t_f)$, which is one of the assumptions, does not change. Hence, the differential algebraic Riccati equation can be calculated backwards in time, but the state dependent matrices, especially $\mathbf{A}^{[i]}(\mathbf{x}^{[i-1]}(t))$ and $\mathbf{B}^{[i]}(\mathbf{x}^{[i-1]}(t), \mathbf{u}^{[i-1]}(t))$, have to use their states according to the time. This means that for calculating the $\mathbf{P}(t_{f-1})$ (the state one time step before final time) $\mathbf{A}^{[i]}(\mathbf{x}(t_f))$ and so on have to be considered. Now, it is possible to determine

the control and state profile forward in time. Eq. (4.35) provides the formula to figure out the control in the first step and with Eq. (4.32) the next state vector can be determined. Then, the control and state vectors are calculated for each time step until the final time is reached. It is important to mention that the used states are always available from the previous iteration and not from the actual iteration! Furthermore, the observability and the controllability of the system has to be checked for each time step as the system and input matrices change for each $\mathbf{x}(t)$.
This procedure will go on until the stop criterion is reached: the infinity norm of the actual and the previous iteration has to be below the error tolerance ϵ (see Eq. (4.36)). As soon as the error tolerance condition is satisfied the solution of the non-linear problem is available. The control profile of the ith iteration presents the (global) optimal result for the chosen factorisation and the assumed weighting matrices.
The not-neglectable disadvantage of this solution: calculating $\mathbf{P}(\mathbf{x}(t))$ very often consumes very much computational time especially for large matrices $\mathbf{A}(\mathbf{x}(t))$ and $\mathbf{B}(\mathbf{x}(t), \mathbf{u}(t))$. To compensate this disadvantage Topputo [25] presented the ASRE method using the transition matrix.

4.3 Approximate Squence of Riccati Equations with Transition Matrix Approach

The approximate sequence of Riccati equations with transition matrix starts in the same way as the normal approximate sequence of Riccati equations (see Section 4.2). The dynamics of the non-linear system have to be factorised to the form of Eq. (4.5) and the performance index can be calculated via Eq. (4.28).
For the different iterations Eq. (4.32) and its corresponding performance index Eq. (4.33) are used. The iterations are executed until the convergence condition of Eq. (4.36) is valid. The two point boundary value problem of Eq. (4.29) has to be solved in each step. Therefore, it changes to

$$\begin{pmatrix} \dot{\mathbf{x}}^{[i]} \\ \dot{\boldsymbol{\lambda}}^{[i]} \end{pmatrix} = \begin{pmatrix} \mathbf{A}(\mathbf{x}^{[i-1]}, t) & -\mathbf{B}(\mathbf{x}^{[i-1]}, t)\mathbf{R}^{-1}(\mathbf{x}^{[i-1]})\mathbf{B}^T(\mathbf{x}^{[i-1]}, t) \\ -\mathbf{Q}(\mathbf{x}^{[i-1]}) & -\mathbf{A}^T(\mathbf{x}^{[i-1]}, t) \end{pmatrix} \begin{pmatrix} \mathbf{x}^{[i]} \\ \boldsymbol{\lambda}^{[i]} \end{pmatrix} = \mathbf{H}(\mathbf{x}^{[i-1]}, t) \begin{pmatrix} \mathbf{x}^{[i]} \\ \boldsymbol{\lambda}^{[i]} \end{pmatrix} \tag{4.37}$$

This can be used to write the general solution of the transition matrix for any iteration $i \geqslant 0$:

$$\dot{\boldsymbol{\Phi}} = \mathbf{H}\boldsymbol{\Phi} \tag{4.38}$$

with $\boldsymbol{\Phi}(\mathbf{0}) = \mathbf{I}$. The complete non-linear model is factorised to a "pseudo-linear" form. So the system can be seen as linear differential equations. In the following, the initial time t_i is shown as the index $_i$ and the final time t_f as $_f$, i.e. the state vector at initial time $\mathbf{x}(t_i)$ is described as $\mathbf{x}_i$. Thus, Eq. (4.37) can be written as

$$\begin{aligned} \mathbf{x}(t) &= \boldsymbol{\phi}_{xx}(t_i, t)\mathbf{x}_i + \boldsymbol{\phi}_{x\lambda}(t_i, t)\boldsymbol{\lambda}_i \\ \boldsymbol{\lambda}(t) &= \boldsymbol{\phi}_{\lambda x}(t_i, t)\mathbf{x}_i + \boldsymbol{\phi}_{\lambda\lambda}(t_i, t)\boldsymbol{\lambda}_i. \end{aligned} \tag{4.39}$$

with the initial state $\mathbf{x}_i$ and the initial co-state $\boldsymbol{\lambda}_i$. $\boldsymbol{\phi}_{xx}$, $\boldsymbol{\phi}_{x\lambda}$, $\boldsymbol{\phi}_{\lambda x}$ and $\boldsymbol{\phi}_{\lambda\lambda}$ can be found via integration

of Eq. (4.38)

$$\dot{\mathbf{\Phi}} = \begin{pmatrix} \dot{\boldsymbol{\phi}}_{xx} & \dot{\boldsymbol{\phi}}_{x\lambda} \\ \dot{\boldsymbol{\phi}}_{\lambda x} & \dot{\boldsymbol{\phi}}_{\lambda\lambda} \end{pmatrix} = \begin{pmatrix} \mathbf{A}(\mathbf{x},t) & -\mathbf{B}(\mathbf{x},t)\mathbf{R}^{-1}(\mathbf{x})\mathbf{B}^T(\mathbf{x},t) \\ -\mathbf{Q}(\mathbf{x},t) & -\mathbf{A}^T(\mathbf{x},t) \end{pmatrix} \begin{pmatrix} \boldsymbol{\phi}_{xx} & \boldsymbol{\phi}_{x\lambda} \\ \boldsymbol{\phi}_{\lambda x} & \boldsymbol{\phi}_{\lambda\lambda} \end{pmatrix} \tag{4.40}$$

the dependency of the initial time and actual time is omitted here for the Φ. The initial conditions for $\mathbf{\Phi}$ are $\boldsymbol{\phi}_{xx}(t_i,t_i) = \boldsymbol{\phi}_{\lambda\lambda}(t_i,t_i) = \mathbf{I}_{n\times n}$ and $\boldsymbol{\phi}_{x\lambda}(t_i,t_i) = \boldsymbol{\phi}_{\lambda x}(t_i,t_i) = \mathbf{0}_{n\times n}$.
It is possible to calculate $\mathbf{\Phi}$ for all time steps since the content of $\mathbf{H}(\mathbf{x},t)$ is given via the previous state vector $\mathbf{x}(t)$. With this and a given initial co-state $\boldsymbol{\lambda}_i$ it is possible to compute all states $\mathbf{x}(t)$ and the complete optimal control function $\mathbf{u}(t)$ (see Eq. (4.16)).[27]

4.3.1 Non-linear constrained problems

In general the initial co-state $\boldsymbol{\lambda}_i$ is not given. Thus, it has to be calculated. According to Topputo [28], it is possible to divide the problem into three different problems:

- The final state vector is fixed (hard-constrained problem) – meaning the optimal control function brings the system to the given final values.
- The final state vector is free (soft-constrained problem) – meaning the optimal control function brings the system to zero or close to zero depending on the choice of the $\mathbf{S}$ matrix.
- The final state vector is fixed and free (mixed-constrained problem) – meaning a part of the final state vector is fixed and the other part is free, i.e. the state consists of the position and the velocity. The goal could be to find a certain position while the velocity is free.

4.3.1.1 Hard-constrained Problem

In hard-constrained problems, the initial state $\mathbf{x}_i$ as well as the final state $\mathbf{x}_f$ are given. While setting the time to the final value t_f the first line of Eq. (4.39) changes from

$$\mathbf{x}(t_f) = \boldsymbol{\phi}_{xx}(t_i,t_f)\mathbf{x}_i + \boldsymbol{\phi}_{x\lambda}(t_i,t_f)\boldsymbol{\lambda}_i \tag{4.41}$$

to

$$\boldsymbol{\lambda}_i(\mathbf{x}_i,\mathbf{x}_f,t_i,t_f) = \boldsymbol{\phi}_{x\lambda}^{-1}(t_i,t_f)\left(\mathbf{x}(t_f) - \boldsymbol{\phi}_{xx}(t_i,t_f)\mathbf{x}_i\right). \tag{4.42}$$

So, if the hard constraints are given, first all $\mathbf{\Phi}$ will be first calculated and can be used to describe Eq. (4.39) which is used to get the optimal control function $\mathbf{u}(t)$ with Eq. (4.16).[28]

4.3.1.2 Soft-constrained Problem

In soft-constrained problems, the final state $\mathbf{x}_f$ is not given but the matrix $\mathbf{S}$ which describes the weighting of the free states. The $\boldsymbol{\lambda}$ of Eq. (4.16) at the final time and $\mathbf{P}(\mathbf{x}_f) = \mathbf{S}$ leads to

$$\boldsymbol{\lambda}(t_f) = \mathbf{S}\mathbf{x}(t_f) \tag{4.43}$$

This can now be inserted to Eq. (4.39) at final time.

$$\begin{aligned}\mathbf{x}(t_f) &= \boldsymbol{\phi}_{xx}(t_i,t_f)\mathbf{x}_i + \boldsymbol{\phi}_{x\lambda}(t_i,t_f)\boldsymbol{\lambda}_i \\ \mathbf{S}\mathbf{x}(t_f) &= \boldsymbol{\phi}_{\lambda x}(t_i,t_f)\mathbf{x}_i + \boldsymbol{\phi}_{\lambda\lambda}(t_i,t_f)\boldsymbol{\lambda}_i.\end{aligned} \tag{4.44}$$

The first line can be substituted to the second line and formulated as

$$\boldsymbol{\lambda}_i(\mathbf{x}_i,t_i,t_f) = \left(\boldsymbol{\phi}_{\lambda\lambda}(t_i,t_f) - \mathbf{S}\boldsymbol{\phi}_{x\lambda}(t_i,t_f)\right)^{-1}\left(\mathbf{S}\boldsymbol{\phi}_{xx}(t_i,t_f) - \boldsymbol{\phi}_{\lambda x}(t_i,t_f)\right)\mathbf{x}_i \tag{4.45}$$

Finally, with a given initial state, matrix $\mathbf{S}$ and all the calculated $\boldsymbol{\Phi}$ the state vector $x(t)$ can be calculated for each time in the time interval $[t_0, t_f]$ and thus the optimal control function $\mathbf{u}(t)$.[28]

4.3.1.3 Mixed-constrained Problem

For non-linear systems with hard and soft constraints the entries of the state vector $\mathbf{x}$ are divided in the hard constraints (fixed at final time) named as $\mathbf{y}$ and in the soft constraints (free at final time) $\mathbf{z}$. Additionally, a $n \times n$ matrix $\mathbf{S}$ where n is the number of rows of z has to be given. The co-state vector $\boldsymbol{\lambda}$ is splitted to $\boldsymbol{\epsilon}$ and $\boldsymbol{\eta}$ which are the co-states of the hard and soft constraints, respectively. Eq. (4.39) can be rewritten in matrix form with mixed constraints as

$$\begin{pmatrix}\mathbf{y}(t)\\ \mathbf{z}(t)\\ \boldsymbol{\epsilon}(t)\\ \boldsymbol{\eta}(t)\end{pmatrix} = \boldsymbol{\Phi}(t_i,t)\begin{pmatrix}\mathbf{y}(t_i)\\ \mathbf{z}(t_i)\\ \boldsymbol{\epsilon}(t_i)\\ \boldsymbol{\eta}(t_i)\end{pmatrix}. \tag{4.46}$$

At the final t_f Eq. (4.46) changes to

$$\begin{pmatrix}\mathbf{y}(t_f)\\ \mathbf{z}(t_f)\\ \boldsymbol{\epsilon}(t_f)\\ \boldsymbol{\eta}(t_f)\end{pmatrix} = \begin{pmatrix}\boldsymbol{\phi}_{yy} & \boldsymbol{\phi}_{yz} & \boldsymbol{\phi}_{y\epsilon} & \boldsymbol{\phi}_{y\eta}\\ \boldsymbol{\phi}_{zy} & \boldsymbol{\phi}_{zz} & \boldsymbol{\phi}_{z\epsilon} & \boldsymbol{\phi}_{z\eta}\\ \boldsymbol{\phi}_{\epsilon y} & \boldsymbol{\phi}_{\epsilon z} & \boldsymbol{\phi}_{\epsilon\epsilon} & \boldsymbol{\phi}_{\epsilon\eta}\\ \boldsymbol{\phi}_{\eta y} & \boldsymbol{\phi}_{\eta z} & \boldsymbol{\phi}_{\eta\epsilon} & \boldsymbol{\phi}_{\eta\eta}\end{pmatrix}\begin{pmatrix}\mathbf{y}(t_i)\\ \mathbf{z}(t_i)\\ \boldsymbol{\epsilon}(t_i)\\ \boldsymbol{\eta}(t_i)\end{pmatrix} \tag{4.47}$$

From here until Eq. (4.56) the dependency of $\boldsymbol{\phi}$ to t_i, t_f is omitted due to visibility reasons. Rewriting the first row and solve for $\boldsymbol{\epsilon}_i$ leads to

$$\boldsymbol{\epsilon}_i = \boldsymbol{\phi}_{y\epsilon}^{-1}\left(\mathbf{y}_f - \boldsymbol{\phi}_{yy}\mathbf{y}_i - \boldsymbol{\phi}_{yz}\mathbf{z}_i - \boldsymbol{\phi}_{y\eta}\boldsymbol{\eta}_i\right), \tag{4.48}$$

where the only unknown element on the right hand-side is $\boldsymbol{\eta}_i$ which is the initial co-state of the soft constraints. Using Eq. (4.43) with the actual nomenclature for the soft constraints and inserting to the forth row of Eq. (4.47):

$$\mathbf{S}\mathbf{z}_f = \boldsymbol{\phi}_{\eta y}\mathbf{y}_i + \boldsymbol{\phi}_{\eta z}\mathbf{z}_i + \boldsymbol{\phi}_{\eta\epsilon}\boldsymbol{\epsilon}_i + \boldsymbol{\phi}_{\eta\eta}\boldsymbol{\eta}_i \tag{4.49}$$

Substitute the second row of Eq. (4.47) into Eq. (4.49):

$$\mathbf{S}\left(\boldsymbol{\phi}_{zy}\mathbf{y}_i + \boldsymbol{\phi}_{zz}\mathbf{z}_i\right) + \mathbf{S}\boldsymbol{\phi}_{z\epsilon}\boldsymbol{\epsilon}_i + \mathbf{S}\boldsymbol{\phi}_{z\eta}\boldsymbol{\eta}_i = \boldsymbol{\phi}_{\eta y}\mathbf{y}_i + \boldsymbol{\phi}_{\eta z}\mathbf{z}_i + \boldsymbol{\phi}_{\eta\epsilon}\boldsymbol{\epsilon}_i + \boldsymbol{\phi}_{\eta\eta}\boldsymbol{\eta}_i \tag{4.50}$$

Inserting Eq. (4.48) on the left hand-side:

$$\mathbf{SE} + \mathbf{S}\boldsymbol{\phi}_{z\epsilon}\boldsymbol{\phi}_{y\epsilon}^{-1}\left(\mathbf{y}_f - \boldsymbol{\phi}_{yy}\mathbf{y}_i - \boldsymbol{\phi}_{yz}\mathbf{z}_i\right) - \mathbf{S}\boldsymbol{\phi}_{z\epsilon}\boldsymbol{\phi}_{y\epsilon}^{-1}\boldsymbol{\phi}_{y\eta}\boldsymbol{\eta}_i + \mathbf{S}\boldsymbol{\phi}_{z\eta}\boldsymbol{\eta}_i = \mathbf{F} + \boldsymbol{\phi}_{\eta\epsilon}\boldsymbol{\epsilon}_i + \boldsymbol{\phi}_{\eta\eta}\boldsymbol{\eta}_i \tag{4.51}$$

Finally, inserting Eq. (4.48) on the right hand-side:

$$\mathbf{SE} + \mathbf{S}\boldsymbol{\phi}_{z\epsilon}\boldsymbol{\phi}_{y\epsilon}^{-1}\mathbf{G} - \mathbf{F} - \boldsymbol{\phi}_{\eta\epsilon}\boldsymbol{\phi}_{y\epsilon}^{-1}\mathbf{G} = \mathbf{H}\boldsymbol{\eta}_i \tag{4.52}$$

where

$$\begin{aligned}
\mathbf{E} &= \boldsymbol{\phi}_{zy}\mathbf{y}_i + \boldsymbol{\phi}_{zz}\mathbf{z}_i \\
\mathbf{F} &= \boldsymbol{\phi}_{\eta y}\mathbf{y}_i + \boldsymbol{\phi}_{\eta z}\mathbf{z}_i \\
\mathbf{G} &= \mathbf{y}_f - \boldsymbol{\phi}_{yy}\mathbf{y}_i - \boldsymbol{\phi}_{yz}\mathbf{z}_i \\
\mathbf{H} &= \mathbf{S}\boldsymbol{\phi}_{z\epsilon}\boldsymbol{\phi}_{y\epsilon}^{-1}\boldsymbol{\phi}_{y\eta} - \mathbf{S}\boldsymbol{\phi}_{z\eta} + \boldsymbol{\phi}_{\eta\eta} - \boldsymbol{\phi}_{\eta\epsilon}\boldsymbol{\phi}_{y\epsilon}^{-1}\boldsymbol{\phi}_{y\eta}.
\end{aligned} \tag{4.53}$$

Solving Eq. (4.52) for $\boldsymbol{\eta}_i$:

$$\mathbf{H}^{-1}\mathbf{K} = \boldsymbol{\eta}_i \tag{4.54}$$

where

$$\mathbf{K} = \mathbf{SE} + \mathbf{S}\boldsymbol{\phi}_{z\epsilon}\boldsymbol{\phi}_{y\epsilon}^{-1}\mathbf{G} - \mathbf{F} - \boldsymbol{\phi}_{\eta\epsilon}\boldsymbol{\phi}_{y\epsilon}^{-1}\mathbf{G} \tag{4.55}$$

$\mathbf{K}$ results with clever restructuring in

$$\begin{aligned}
\mathbf{K} = &\left(\mathbf{S}\boldsymbol{\phi}_{zy} - \mathbf{S}\boldsymbol{\phi}_{z\epsilon}\boldsymbol{\phi}_{y\epsilon}^{-1}\boldsymbol{\phi}_{yy} + \boldsymbol{\phi}_{\eta\epsilon}\boldsymbol{\phi}_{y\epsilon}^{-1}\boldsymbol{\phi}_{yy} - \boldsymbol{\phi}_{\eta y}\right)\mathbf{y}_i + \\
&\left(\mathbf{S}\boldsymbol{\phi}_{zz} - \mathbf{S}\boldsymbol{\phi}_{z\epsilon}\boldsymbol{\phi}_{y\epsilon}^{-1}\boldsymbol{\phi}_{yz} + \boldsymbol{\phi}_{\eta\epsilon}\boldsymbol{\phi}_{y\epsilon}^{-1}\boldsymbol{\phi}_{yz} - \boldsymbol{\phi}_{\eta z}\right)\mathbf{z}_i + \\
&\left(\mathbf{S}\boldsymbol{\phi}_{z\epsilon}\boldsymbol{\phi}_{y\epsilon}^{-1} - \boldsymbol{\phi}_{\eta\epsilon}\boldsymbol{\phi}_{y\epsilon}^{-1}\right)\mathbf{y}_f.
\end{aligned} \tag{4.56}$$

Calculating $\boldsymbol{\Phi}$ at the final time via integration of Eq. (4.57) (which is the same as Eq. (4.40), but for mixed constraints) and the given vectors $\mathbf{y}_i$, $\mathbf{z}_i$ and $\mathbf{y}_f$ can be used to determine the free co-state vector $\boldsymbol{\eta}_i$. Now, the co-state vector $\boldsymbol{\epsilon}_i$ of the fixed constrained problem can be calculated via Eq. (4.48).

$$\begin{pmatrix} \dot{\boldsymbol{\phi}}_{yy} & \dot{\boldsymbol{\phi}}_{yz} & \dot{\boldsymbol{\phi}}_{y\epsilon} & \dot{\boldsymbol{\phi}}_{y\eta} \\ \dot{\boldsymbol{\phi}}_{zy} & \dot{\boldsymbol{\phi}}_{zz} & \dot{\boldsymbol{\phi}}_{z\epsilon} & \dot{\boldsymbol{\phi}}_{z\eta} \\ \dot{\boldsymbol{\phi}}_{\epsilon y} & \dot{\boldsymbol{\phi}}_{\epsilon z} & \dot{\boldsymbol{\phi}}_{\epsilon\epsilon} & \dot{\boldsymbol{\phi}}_{\epsilon\eta} \\ \dot{\boldsymbol{\phi}}_{\eta y} & \dot{\boldsymbol{\phi}}_{\eta z} & \dot{\boldsymbol{\phi}}_{\eta\epsilon} & \dot{\boldsymbol{\phi}}_{\eta\eta} \end{pmatrix} = \begin{pmatrix} \mathbf{A}(\mathbf{x},t) & -\mathbf{B}(\mathbf{x},t)\mathbf{R}^{-1}(\mathbf{x})\mathbf{B}^T(\mathbf{x},t) \\ -\mathbf{Q}(\mathbf{x},t) & -\mathbf{A}^T(\mathbf{x},t) \end{pmatrix} \begin{pmatrix} \boldsymbol{\phi}_{yy} & \boldsymbol{\phi}_{yz} & \boldsymbol{\phi}_{y\epsilon} & \boldsymbol{\phi}_{y\eta} \\ \boldsymbol{\phi}_{zy} & \boldsymbol{\phi}_{zz} & \boldsymbol{\phi}_{z\epsilon} & \boldsymbol{\phi}_{z\eta} \\ \boldsymbol{\phi}_{\epsilon y} & \boldsymbol{\phi}_{\epsilon z} & \boldsymbol{\phi}_{\epsilon\epsilon} & \boldsymbol{\phi}_{\epsilon\eta} \\ \boldsymbol{\phi}_{\eta y} & \boldsymbol{\phi}_{\eta z} & \boldsymbol{\phi}_{\eta\epsilon} & \boldsymbol{\phi}_{\eta\eta} \end{pmatrix} \tag{4.57}$$

Note: The ϕ of Eq. (4.57) are depending on t_i, t and at initial time $\phi(t_i, t_i)$ the diagonal elements are identity matrices and the non-diagonal elements are zero matrices.
To summarise the mixed-constrained problem: an initial state vector $\mathbf{x}$ with fixed and soft constraints is given. Thus, the co-state vector can be detected with determining $\boldsymbol{\Phi}$ at the final time t_f. It is

important to mention that the single free and fixed co-state vectors have to be merged to

$$\boldsymbol{\lambda}_i = \begin{bmatrix} \boldsymbol{\epsilon}_i & \boldsymbol{\eta}_i \end{bmatrix}^T . \tag{4.58}$$

This can be used in Eq. (4.39) to solve for each $\mathbf{x}$ and $\boldsymbol{\lambda}$ at each time in the interval $[t_i, t_f]$. Finally, the optimal control function $\mathbf{u}(t)$ can be found with Eq. (4.16).[28]

4.3.2 Implementation of the Approximate Sequence of Riccati Equations with Transition Matrix Approach

Per definition the ASRE method converges to the optimal solution of the non-linear system within a certain amount of iterations. Can this be used for the ASRE method with transition matrix?
First, the non-linear system and the performance index have to be factorised like mentioned in Section 4.1 such that Eq. (4.1), (4.5) and the performance index of Eq. (4.33) can be used.
For the first iteration $i = 0$ the matrices $\mathbf{A}^{[0]}(\mathbf{x}_i, t)$, $\mathbf{B}^{[0]}(\mathbf{x}_i, t)$, $\mathbf{Q}^{[0]}(\mathbf{x}_i, t)$ and $\mathbf{R}^{[0]}(\mathbf{x}_i, t)$ are defined via the initial state vector $\mathbf{x}_i$. Note: $\mathbf{Q}$ and $\mathbf{R}$ do not have to be depending on the state vector, thus they can be constant for each iteration.
Afterwards, these constant matrices are used to calculate the state transition matrix $\boldsymbol{\Phi}$ for each time step in the time interval $[t_i, t_f]$ with Eq. (4.40). The integration term has to be solved with time forward integration.
Depending on the constraints, the initial co-state $\boldsymbol{\lambda}_i$ is determined via Eq. (4.42) for hard constraints, for soft-constrained problems Eq. (4.45) and for mixed constraints Eq. (4.58). The $\phi(t_i, t_f)$-terms are always the $\boldsymbol{\Phi}$ at final time.
Then, the state vector $\mathbf{x}(t)$ and the co-state vector $\boldsymbol{\lambda}(t)$ are calculated with Eq. (4.39). This time, the $\phi(t, t_f)$-terms are all the previous calculated ϕ starting at t_i until t_f. For each time step the state and co-state vector are determined. Thus, the only changing terms on the right hand side of those two equations are the ϕ-terms. The solutions of $\mathbf{x}(t)$ and $\boldsymbol{\lambda}(t)$ are used to calculate the optimal control function $\mathbf{u}(t)$ with Eq. (4.16).
The next iterations $i \geqslant 1$ start with updating the matrices $\mathbf{A}^{[i]}(\mathbf{x}^{[i-1]}, t)$, $\mathbf{B}^{[i]}(\mathbf{x}^{[i-1]}, t)$, $\mathbf{Q}^{[i]}(\mathbf{x}^{[i-1]}, t)$ and $\mathbf{R}^{[i]}(\mathbf{x}^{[i-1]}, t)$. These are created for each time step with all the, in the previous iteration calculated, $\mathbf{x}(t)$. Now, $\boldsymbol{\Phi}(t_i, t)$ is generated via Eq. (4.40) from initial time until final time by forward integration. Important is the matrix $\mathbf{H}$ is not constant anymore, it changes with each time step because of $\mathbf{x}^{[i-1]}(t)$. It is essential to notice that the state vector $\mathbf{x}(t)$ exists for each time step. Thus, it is possible to imagine it is a row vector

$$\begin{bmatrix} \mathbf{x}(t_0) & \mathbf{x}(t_1) & \dots & \mathbf{x}(t_f) \end{bmatrix}, \tag{4.59}$$

where each column represents the state vector at the given time. Now, for example the matrix $\mathbf{A}^{[i]}(\mathbf{x}^{[i-1]}, t)$ can be calculated for each time step with different states. Hence, the state vectors from the previous iteration (see Eq. (4.59)) are used to describe the actual system matrix $\mathbf{A}$ for each time step.
Afterwards, $\boldsymbol{\lambda}_i$, $\mathbf{x}(t)$, $\boldsymbol{\lambda}(t)$ and $\mathbf{u}(t)$ of the i-th iteration are built in the same way as in the zeroth iteration.
If the infinity norm is smaller than the error tolerance ϵ there will be no further iterations (see

Eq. (4.36)). The final state vector $\mathbf{x}(t) = \mathbf{x}^{[i]}(t)$, the co-state vector $\boldsymbol{\lambda}(t) = \boldsymbol{\lambda}^{[i]}(t)$ and the control vector $\mathbf{u}(t) = \mathbf{u}^{[i]}(t)$ describe the optimal solution of the non-linear problem.

4.3.3 Example of Approximate Sequence of Riccati Equations

An example is demonstrating the ASRE approach and the dependency of the factorisation to the result of the used method to minimise the performance index. The example is presented by Hammett [7].
Considering a system:

$$\begin{aligned} \dot{x}_1 &= x_1 x_2 + x_2 \\ \dot{x}_2 &= u \end{aligned} \tag{4.60}$$

After bringing the system to SDC matrix form it is obvious that the rank of the input matrix $\mathbf{B} = \begin{bmatrix} 0 & 1 \end{bmatrix}^T$ is equal to 1. Thus, Theorem 1 and Theorem 2 have to hold. If the rank of $\mathbf{B}$ would be equal to the number of rows, then the system matrix $\mathbf{A}(\mathbf{x}(t))$ could be arbitrary. However, as the rank of the input matrix is not equal to 2, the system matrix is not allowed to be arbitrary – the factorised matrix has to hold the controllability conditions (see Theorem 1 until Theorem 4).
A mathematical factorisation of the non-linear system is chosen – remember there are infinite possibilities:

$$\mathbf{A}_1 = \begin{bmatrix} 0.5x_2 & 0.5x_1 + 1 \\ 0 & 0 \end{bmatrix} \tag{4.61}$$

The rank of the controllability matrix is:

$$\text{rank}\boldsymbol{\zeta}_1 = \text{rank} \begin{bmatrix} 0 & 0.5x_1 + 1 \\ 1 & 0 \end{bmatrix} = 2, \tag{4.62}$$

If $x_1 \neq -2$, the system is controllable. Nevertheless, it is not fully controllable in the closed loop form. Using Theorem 2 shows that the first factorisation of $\mathbf{A}$ is not *weakly* controllable, too:

$$\begin{bmatrix} x_1 + 1 \\ 0 \end{bmatrix} \neq k \cdot \begin{bmatrix} 0.5x_1 + 1 \\ 0 \end{bmatrix} \tag{4.63}$$

for any $k \neq 0 \in \mathbb{R}^2$.
As long as $\mathbf{A}_1$ is neither fully controllable nor *weakly* controllable, another factorisation has to be chosen:

$$\mathbf{A}_2 = \begin{bmatrix} 0 & x_1 + 1 \\ 0 & 0 \end{bmatrix} \tag{4.64}$$

If $x_1 = -1$, the rank of the controllability matrix is unequal to the number of rows. Therefore, full controllability according to Theorem 1 is not given. However, it is possible to verify that this

factorisation is *weakly* controllable via Theorem 2:

$$\begin{bmatrix} x_1 + 1 \\ 0 \end{bmatrix} = k \cdot \begin{bmatrix} x_1 + 1 \\ 0 \end{bmatrix}, \tag{4.65}$$

which is valid for $k = 1$. Hence, the factorisation $\mathbf{A}_2$ is not fully controllable but *weakly*. Theorem 2 says if an original system is weak controllable, the factorised system is fully controllable for all states. Thus, $\mathbf{A}_2$ is a valid factorisation of the non-linear system.
A system with full controllability and *weakly* controllability should have a better behaviour and a better performance index:

$$\mathbf{A}_3 = \begin{bmatrix} x_2 & 1 \\ 0 & 0 \end{bmatrix} \tag{4.66}$$

$\mathbf{A}_3$ is fully controllable for all $\mathbf{x}(t)$ without any restrictions according to Theorem 1. However Theorem 2 does not hold:

$$\begin{bmatrix} x_1 + 1 \\ 0 \end{bmatrix} \neq k \cdot \begin{bmatrix} 1 \\ 0 \end{bmatrix}, \tag{4.67}$$

for any k. So, the factorisation of $\mathbf{A}_3$ is fully controllable but not *weakly* controllable. Now, Theorem 3 can be used to verify the controllability in a small area around the origin. Choosing

$$\dot{x}_1 = x_1 x_2 + a x_2 \tag{4.68}$$

guarantees *weakly* controllability next to the origin for a small a. Thus, $\mathbf{A}_3$ is fully and *weakly* controllable for, for example, $a = 10$. In the following evaluation $\mathbf{A}_2$ and $\mathbf{A}_3$ are used to show that different factorisations lead to different solutions of the problem. For a further discussion of the factorisation Eq. (4.24) provides other factorisations.

$$\mathbf{A}_\alpha(\mathbf{x}, \alpha) = \alpha \mathbf{A}_2(\mathbf{x}) + (1 - \alpha)\mathbf{A}_3(\mathbf{x}) \tag{4.69}$$

The factor α is chosen to be $\alpha_1 = 0.75$, $\alpha_2 = 0.5$ and $\alpha_3 = 0.25$.
For the ASRE method the time is chosen with $t_i = 0\,\mathrm{s}$, $t_f = 5\,\mathrm{s}$ and the step size is $0.01\,\mathrm{s}$. The weighting matrices are $\mathbf{Q} = \mathbf{I}_{2\times 2}$ and $\mathbf{R} = 1$. The initial state vector x_i will be at $\begin{bmatrix} 2 & 1 \end{bmatrix}^T$ and $x_f = \begin{bmatrix} 3 & 3 \end{bmatrix}^T$. The error tolerance ϵ will be at 10^{-6}. The problem will be shown as a hard-constrained one and as a second example a soft-constrained problem.

Example 1: Hard-constrained Problem

As a first example, the mentioned parameters like initial and final time as well as the weighting matrices are given. For matrix $\mathbf{A}_3$ (see Eq. (4.66)) the 1 is replaced with a variable to cover the weak controllability. The gain is chosen to be 10 – as mentioned in Eq. (4.68).
Different $\mathbf{A}$ factorisations result in different cost functions and need a diverse number of iterations (see Table 4.2). For example, the second factorisation of $\mathbf{A}$ from Eq. (4.64) converges within 19 iterations to a tolerance error ϵ of under 10^{-6} with the cost of approximately 20.146. The used cost

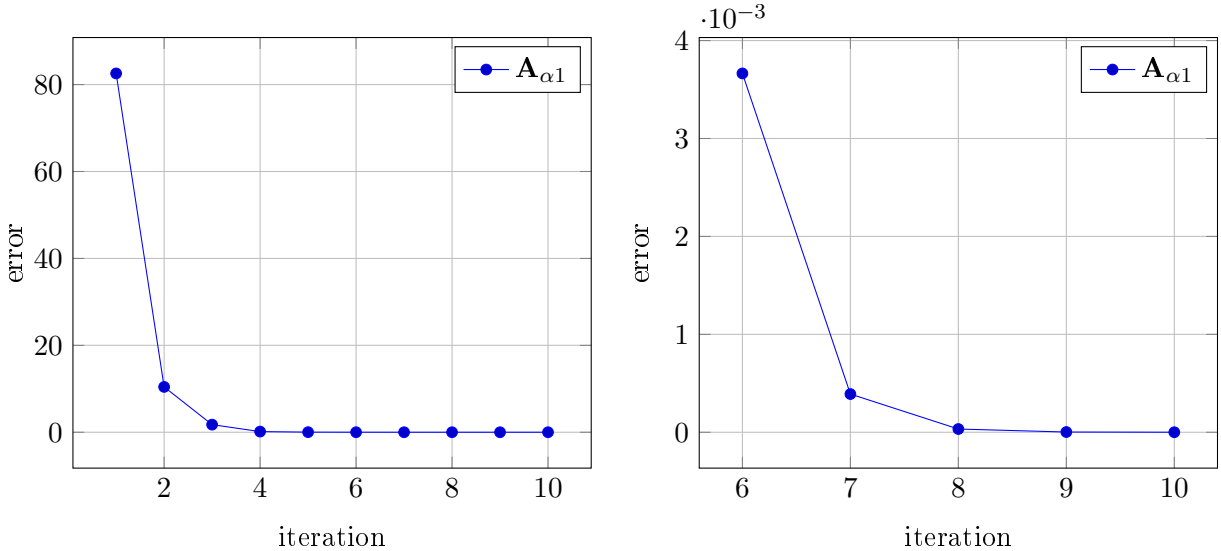

(a) All iterations **(b)** Zoomed in to the last five iterations

Figure 4.1: Error behaviour of factorisation $\mathbf{A}_{\alpha 1}$ in a hard constrained non-linear problem

function can be found in Eq. (4.33). In contrast, $\mathbf{A}_{\alpha 1}$ needs only 10 iterations, but the cost function is the highest with approximately 21.67. It has to be mentioned that the cost function is calculated in this thesis via trapezoideal numerical integration.

In Fig. 4.2a and Fig. 4.2b, the x and y profiles over the time are shown. It is easy to see that both have the same initial and final conditions, but they have different trajectories. The factorisation of $\mathbf{A}_3$ has some changes of the direction in contrast to $\mathbf{A}_2$ which has one and two changes for y and x, respectively. The according control profiles (see Fig. 4.2c and Fig. 4.2d) show a similar behaviour as both start with a control input of approximately -5. Factorisation $\mathbf{A}_3$ is in the positive half plane after 0.5 s and it decreases its control input down to zero. In second 3 to 4 it is again in the negative plane and its final value is around 10. Contrary, $\mathbf{A}_2$ crosses the zero control line at about 1 s and increases in a kind of exponential manner to a control input at final time t_f of approximately 4. In Fig. 4.2e, the x-y plane describes the behaviour of both factorisations. $\mathbf{A}_2$ is one curve while $\mathbf{A}_3$ goes from the initial starting point to the origin where a small circle is shown. Afterwards, it heads in a wild curve towards the final point.

In Fig. 4.3a, the trajectory of all five mentioned factorisations are shown. Since the factorisations $\mathbf{A}_\alpha$ are defined via Eq. (4.69). They have to lie between $\mathbf{A}_2$ and $\mathbf{A}_3$. Those two do not have to be the most optimal of all five. Indeed, the optimal in terms of a minimal amount of iterations is $\mathbf{A}_{\alpha 1}$. However, the most important criterion is the minimisation of the cost function. In this example, the factorisation with the best effort is $\mathbf{A}_2$ (see Table 4.2).

It can be seen that the control input has a huge impact on the cost function (see Eq. (4.33)) due to its quadratic influence. Consequently, the control profiles of all five factorisations are compared. It can be seen that $\mathbf{A}_3$ needs the most control input at the final time while $\mathbf{A}_2$ needs the lowest. The other factorisations are between $\mathbf{A}_2$ and $\mathbf{A}_3$ which can be expected. Taking into account these control profiles, the results can be verified with Table 4.2.

In Fig. 4.1, the infinity norm of the different iterations with its previous iteration is shown. Fig. 4.1b displays a kind of decreasing exponential function. So, the non-linear system converges very fast

Table 4.1: Error progress of the infinity norm of the actual iteration compared with the previous iteration of factorisation $\mathbf{A}_{\alpha 1}$ in a hard constrained non-linear problem

iterations	error
1	82.56803737833987
2	10.43119303962681
3	1.747328132134665
4	0.149650636017087
5	0.019704478764051
6	0.003664528782459
7	3.900612699274664E-4
8	3.300278887519159E-5
9	2.229813719334395E-6
10	1.674776269888767E-7

towards its global optimum until the error tolerance is fulfilled. In Table 4.1, the values for the error behaviour are given. Assuming that the error tolerance is $\epsilon = 1 \cdot 10^{-6}$ then the 10th iteration is the optimal one as the error is smaller than the ϵ. The convergence towards the global optimum is described in Fig. 4.4. The initial iteration has an abrupt change of its trajectory next to the origin. In the next iteration this spike is optimised and a smoother trajectory can be found. Additionally, the optimal difference between the initial and the first iteration is quite huge. However, from the first to the final iteration, it is more or less the same trajectory.

Example 2: Soft-constrained Problem

Now, the previous example will be repeated but with soft constraints. As a solution of the Riccati equation at final time, it is assumed: $\mathbf{P}(t_f) = \mathbf{S} = 100\,\mathbf{I}_{2\times 2}$
The ASRE approach for soft constraints will bring the system from its initial conditions to a final state which does not have to be defined in the beginning. The optimisation will always bring the system towards zero in all states depending on the weighting matrix $\mathbf{S}$.
In Fig. 4.5a and Fig. 4.5b, the smallest y-value of factorisation $\mathbf{A}_2$ has a larger absolute value than the smallest y of $\mathbf{A}_3$. For the greatest x-value, the factorisations are switched. Factorisation $\mathbf{A}_3$ converges to zero within 2.5 s for x and y. The converging of $\mathbf{A}_2$ needs about 4 s. This can be seen in the control profile plots (see Fig. 4.5c and Fig. 4.5c), too. $\mathbf{A}_3$ can converge faster because the control input in the first second is larger than the input of $\mathbf{A}_2$, but $\mathbf{A}_3$ has a larger overshot. In comparison of both trajectories in the x-y plane, $\mathbf{A}_2$ and $\mathbf{A}_3$ have a similar behaviour – except that $\mathbf{A}_3$ does not go straight towards the origin but with a small curve next to it.
Plotting all five factorisations, it is possible to see that the $\mathbf{A}_\alpha$ are depending on the factor of Eq. (4.69). The closer a factorisation is at one of the main factorisations, the stronger is the depen-

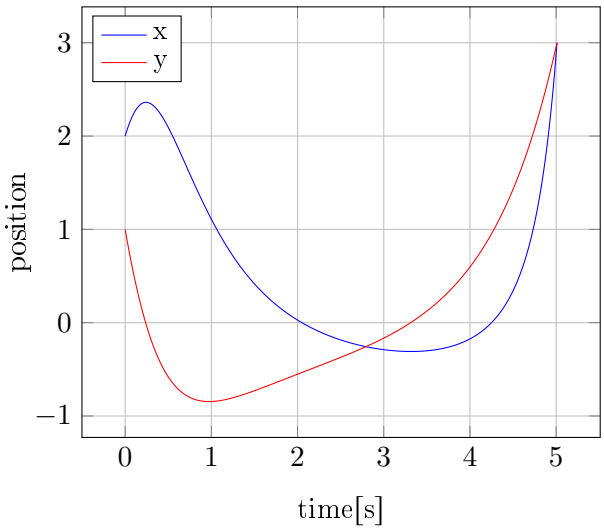

(a) Position vs. time of factorisation $\mathbf{A}_2$

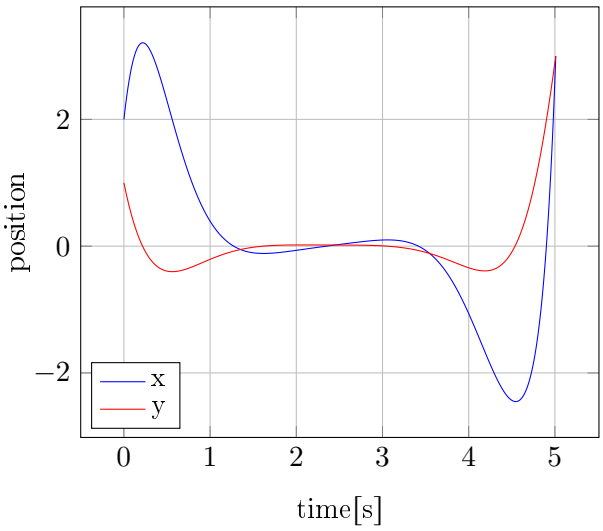

(b) Position vs. time of factorisation $\mathbf{A}_3$

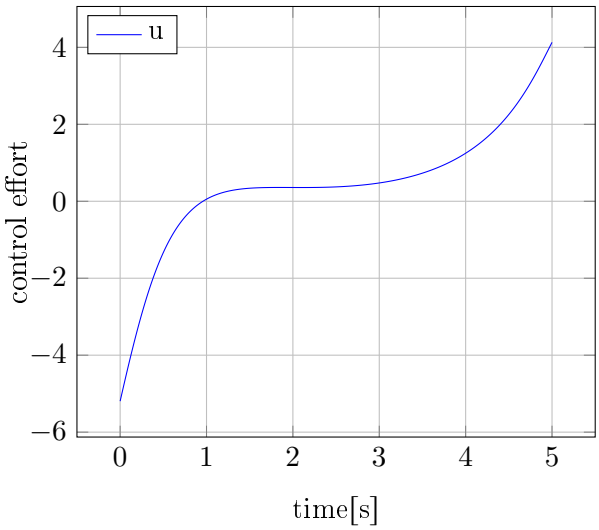

(c) Control profile of factorisation $\mathbf{A}_2$

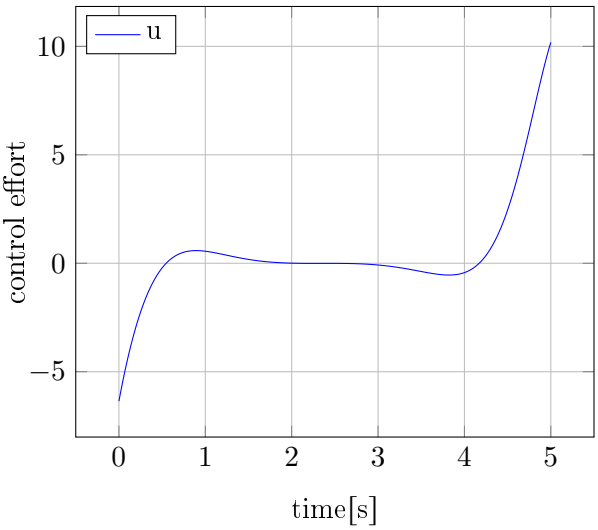

(d) Control profile of factorisation $\mathbf{A}_3$

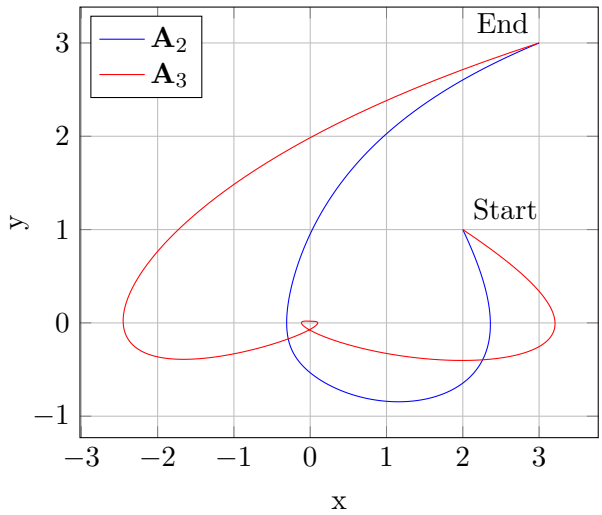

(e) x-y plane of factorisation $\mathbf{A}_2$ and $\mathbf{A}_3$

Figure 4.2: Hard constraints of factorisation $\mathbf{A}_2$ and $\mathbf{A}_3$

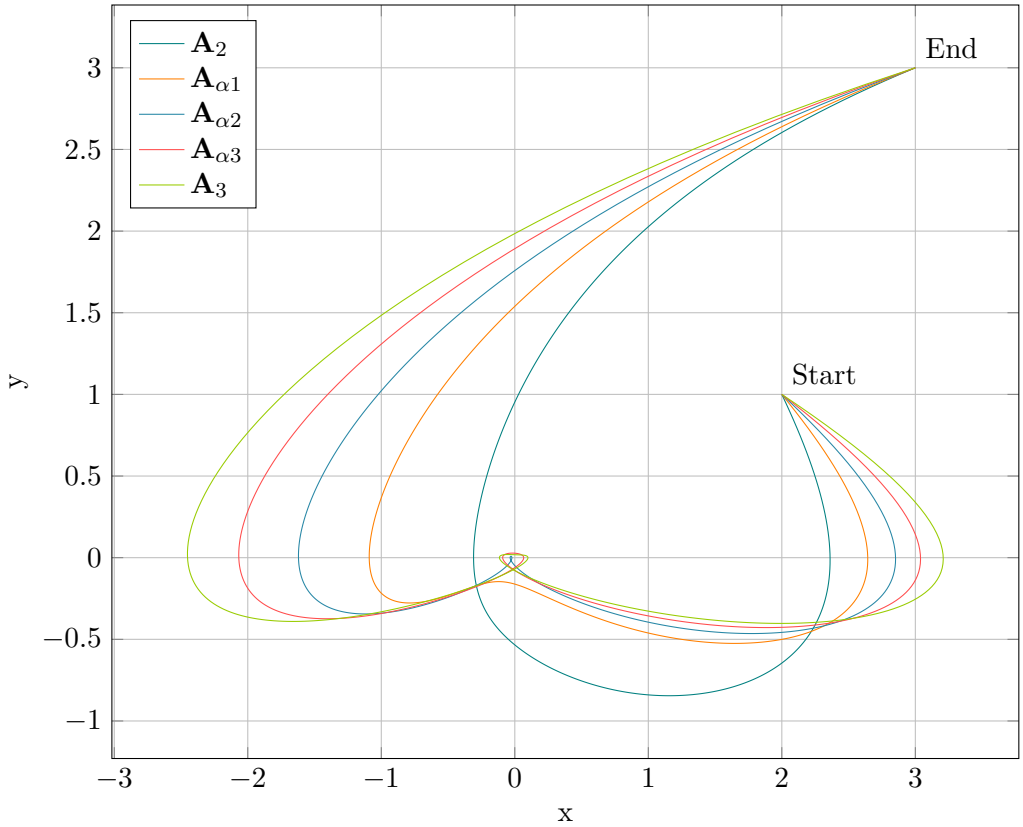

(a) x-y plane

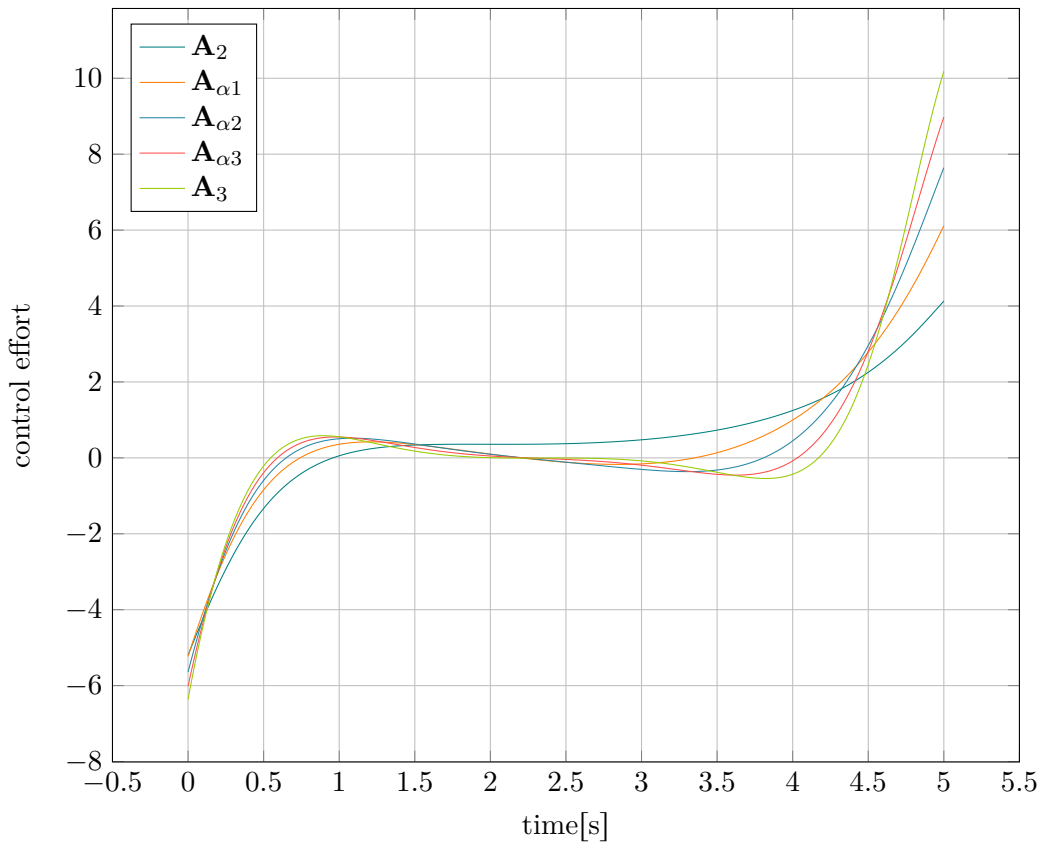

(b) Control profile

Figure 4.3: Hard constrained problem solved by different factorisations

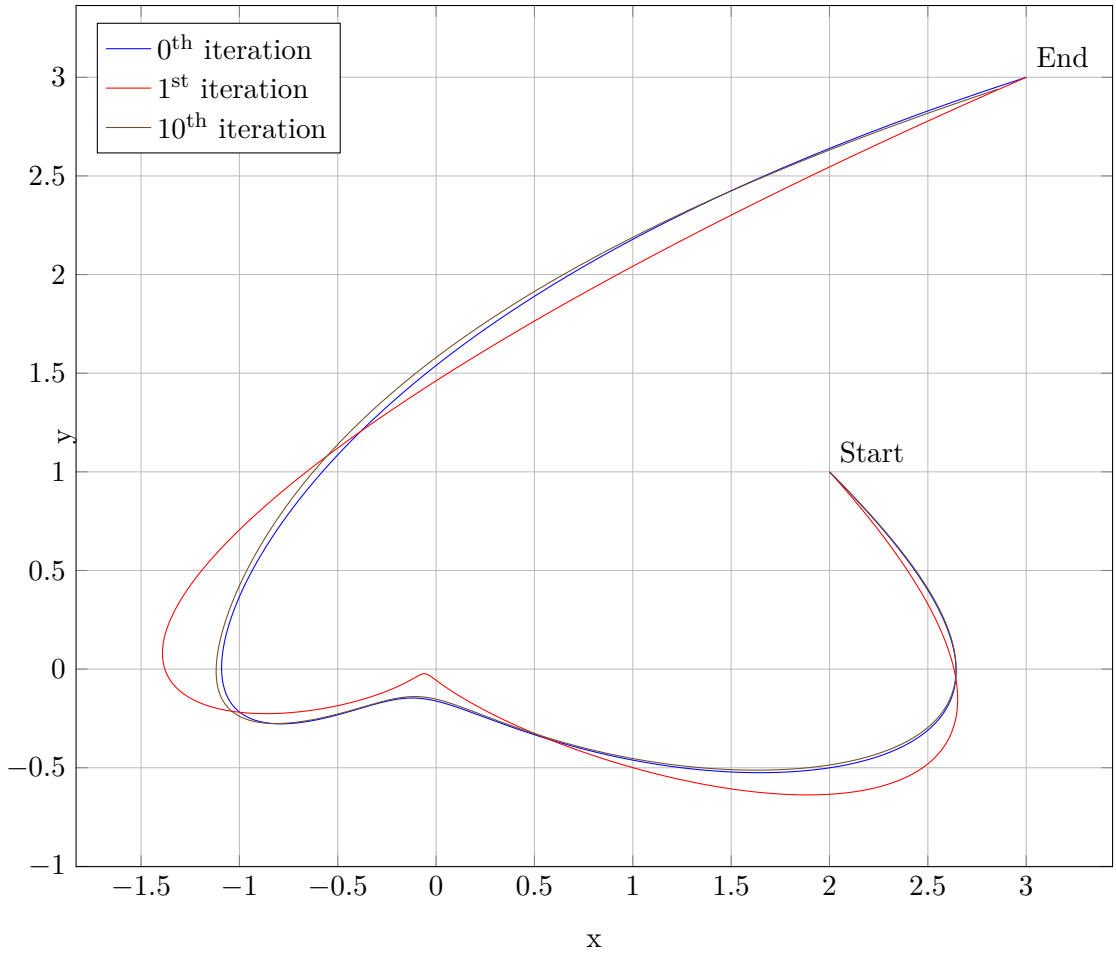

Figure 4.4: Hard constraints of factorisation $\mathbf{A}_{\alpha 1}$ for different iterations

Table 4.2: Number of iterations and cost function of different factorisations for hard-constrained problem

A	iterations	J
$\mathbf{A}_2$	19	20.143518514337885
$\mathbf{A}_{\alpha_1}$	10	21.673534512540463
$\mathbf{A}_{\alpha_2}$	11	23.888050817871353
$\mathbf{A}_{\alpha_3}$	12	25.96220974185447
$\mathbf{A}_3$	13	27.90027315593501

dency of the original one. Thus, the $\mathbf{A}_\alpha$ factorisations follow the behaviour of mainly $\mathbf{A}_3$ at the final part. The influence of $\mathbf{A}_2$ is very limited there, because $\mathbf{A}_3$ is in the region around the origin for a longer time (see Fig. 4.6a).
The control input behaves as expected. It starts with quite large values and converges towards zero. The faster it converges, the larger is the overshoot. At the final time, the control input is zero. The reason is: no external disturbance acts on the system and the state is exactly on target.
The performance index which is the criterion to be minimised shows that the most optimal solution of all five factorisation is $\mathbf{A}_{\alpha 1}$ with a cost function of approximately 4.889 and with only 9 iterations. In contrast to this, the factorisation $\mathbf{A}_2$ needs 14 iterations and achieves only a cost function of about 5.227 which can be found in Table 4.3.

Summary of the examples

In this chapter, the ASRE method was shown on a simple example. The importance of using probably good factorisations was described. Factorisations which are created without the use of Theorem 3 return a better performance index (see $\mathbf{A}_2$ in Table 4.2). If it is possible to find a factorisation which is right in the beginning fully and *weakly* controllable (without any usage of theorems) under normal conditions the according cost function has a lower minimum than a factorisation which uses one or more theorems. In Table 4.3, the best cost function is not $\mathbf{A}_2$, but the best one is close to $\mathbf{A}_{\alpha 1}$. Furthermore, it was named that hard constrained problems head towards the chosen final states. On the other side, the soft constraints bring all states of the non-linear system to zero. The soft constrained problem often has a smaller cost function because the final states should converge to zero, but they do not have to reach the zero in final time. Thus, the soft constraints are more flexible. Also, the result depends on the weighting of the final state via the $\mathbf{S}$ matrix. In addition, the error behaviour between the previous and the actual iteration was shown. It was possible to see that it decreases until the error tolerance ϵ is greater than the infinity norm of the actual and previous iteration.
It is important to mention that the initial (zeroth) iteration is not taken into account for Table 4.2 and Table 4.3. The initial iteration is never the final solution because the result cannot be compared

Table 4.3: Number of iterations and cost function of different factorisations in soft constrained problem

$\mathbf{A}$	iterations	J
$\mathbf{A}_2$	14	5.227312196557898
$\mathbf{A}_{\alpha_1}$	9	4.889200718949835
$\mathbf{A}_{\alpha_2}$	11	4.913917988072871
$\mathbf{A}_{\alpha_3}$	12	5.007855495921995
$\mathbf{A}_3$	13	5.122534326564574

with the previous iteration. Hence, it is always handled as a special case.

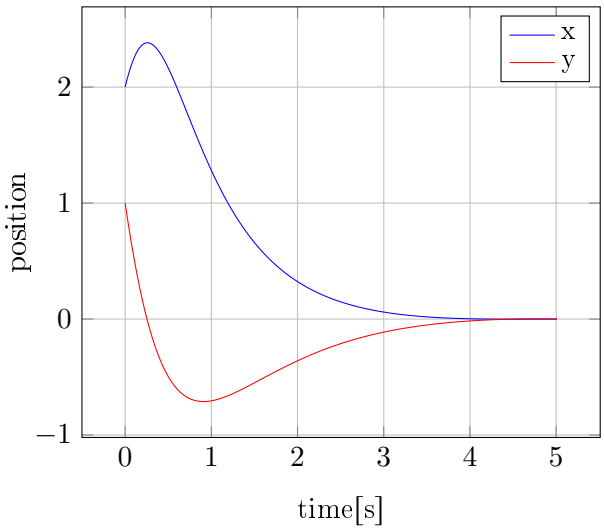

(a) Position over time of factorisation $\mathbf{A}_2$

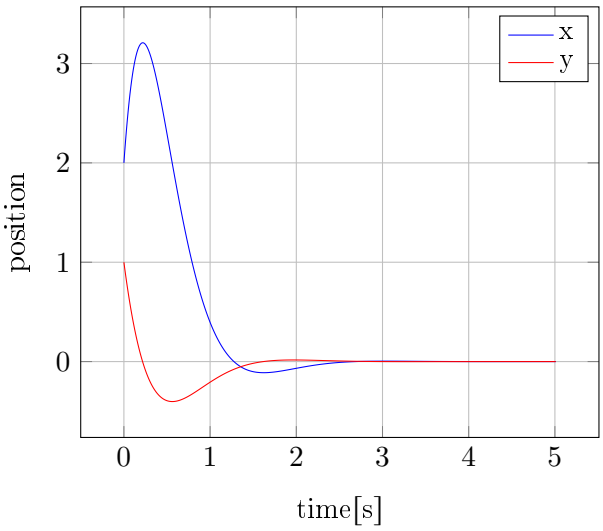

(b) Position over time of factorisation $\mathbf{A}_3$

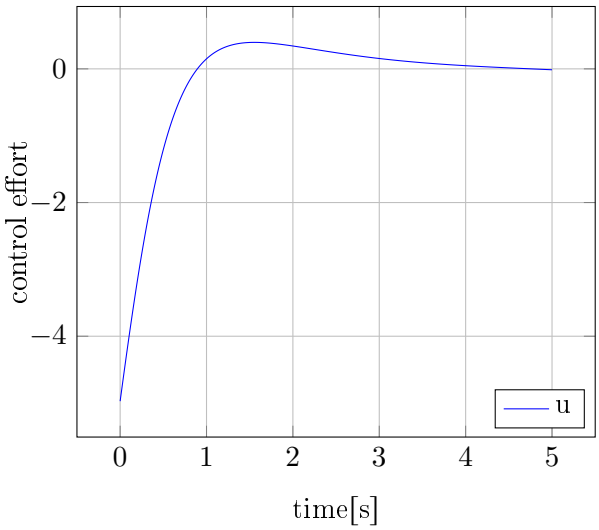

(c) Control profile of factorisation $\mathbf{A}_2$

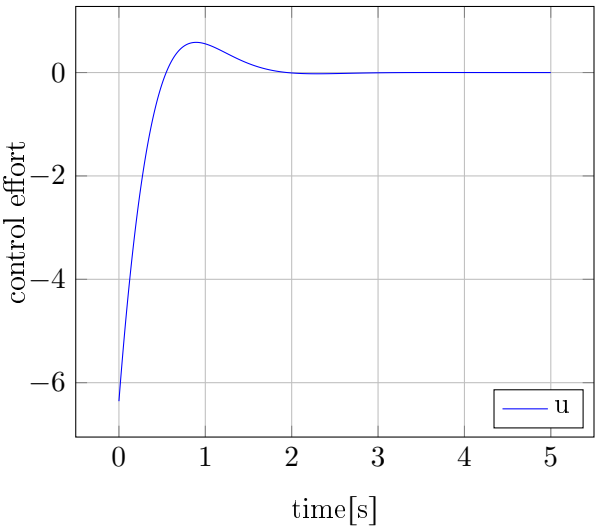

(d) Control profile of factorisation $\mathbf{A}_3$

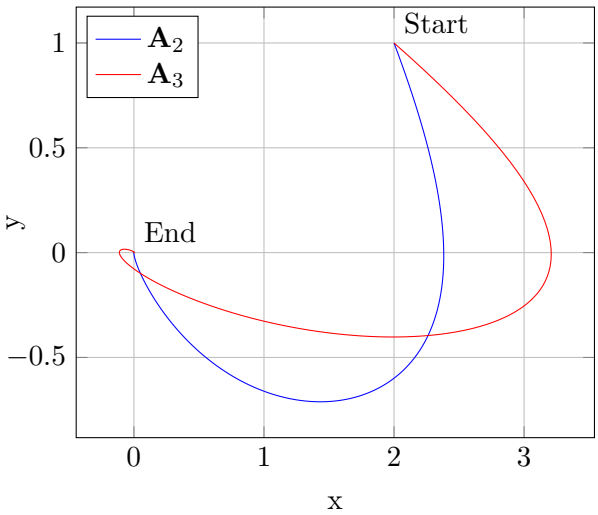

(e) x-y plane of factorisation $\mathbf{A}_2$ and $\mathbf{A}_3$

Figure 4.5: Soft constraints of factorisation $\mathbf{A}_2$ and $\mathbf{A}_3$

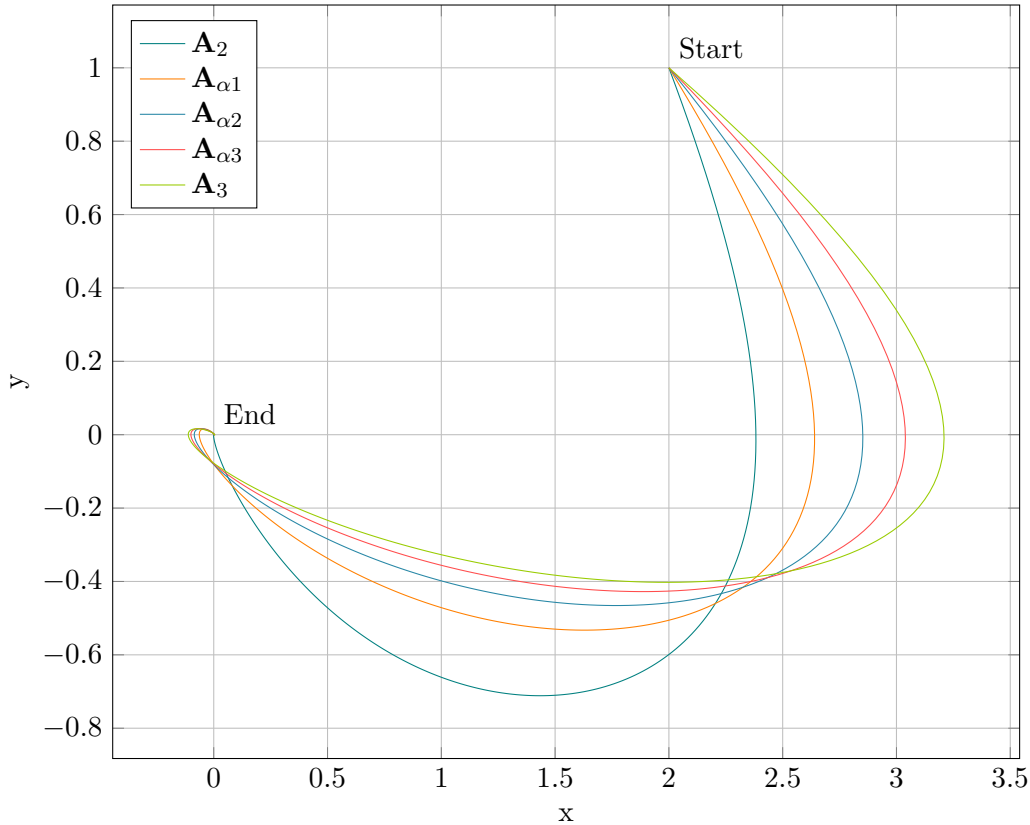

(a) x-y plane of different factorisations

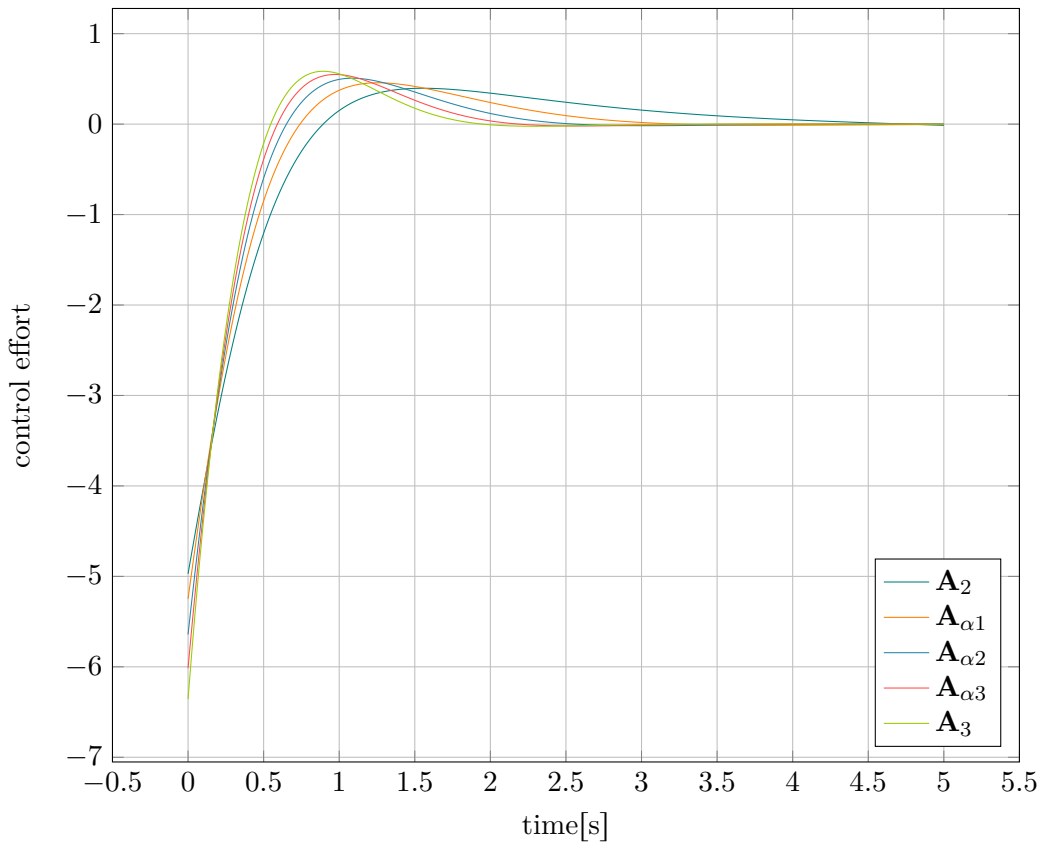

(b) Control profile of different factorisations

Figure 4.6: Soft constraints of different factorisations

5 Spacecraft Dynamics

Geostationary satellites are traditionally places in control boxes to increase the total amount of satellites with zero latitude. Normally, modern control boxes are approximately $0.1 \times 0.1\,\text{deg}$ for longitude and latitude – seen from the Earth's surface. To guarantee the position of the satellite, thrusters have to be used to hold the spacecraft in its foreseen control box. The natural drift of the spacecraft can be divided in North/South and East/West station keeping. In this thesis, these drifts are not seen as two separate control problems but as one large non-linear problem which is a relative new approach (compare with Topputo [25]).
The dynamics of these spacecrafts are well known and will be derived in the following. The dependency of the time of, for example, the state vector is omitted as for reasons of clarity.

5.1 Dynamic Equation of Motion in Spherical Coordinates

The unit vector $\mathbf{e}$ in the RTN reference frame (see Section 2.2) is given by a rotation matrix

$$\mathbf{R}_{ECI,RTN} = \begin{bmatrix} \cos\theta\cos\phi & \sin\theta\cos\phi & \sin\phi \\ -\sin\theta & \cos\theta & 0 \\ -\cos\theta\sin\phi & -\sin\theta\sin\phi & \cos\phi \end{bmatrix} \tag{5.1}$$

from the ECI to the RTN reference frame of the ECI unit vector $[i \quad j \quad k]^T$.

$$\mathbf{e} = \mathbf{R}_{ECI,RTN} \cdot \begin{bmatrix} i \\ j \\ k \end{bmatrix} \tag{5.2}$$

The derivation of Eq. (5.2) comes to

$$\begin{bmatrix} \dot{\mathbf{e}}_r \\ \dot{\mathbf{e}}_\theta \\ \dot{\mathbf{e}}_\phi \end{bmatrix} = \begin{bmatrix} 0 & \dot{\theta}\cos\phi & \dot{\phi} \\ -\dot{\theta}\cos\phi & 0 & \dot{\theta}\sin\phi \\ -\dot{\theta} & -\dot{\theta}\sin\phi & 0 \end{bmatrix} \cdot \begin{bmatrix} \mathbf{e}_r \\ \mathbf{e}_\theta \\ \mathbf{e}_\phi \end{bmatrix} \tag{5.3}$$

(see Widnall [31]). Hence, the kinematics of the satellite can be described by

$$\mathbf{r} = r \cdot \mathbf{e}_r, \tag{5.4}$$

$$\mathbf{v} = \frac{\partial}{\partial t}(r \cdot \mathbf{e}_r) = \left(\frac{\partial}{\partial t}\, r\right) \cdot \mathbf{e}_r + r\left(\frac{\partial}{\partial t}\, \mathbf{e}_r\right) = \dot{r} \cdot \mathbf{e}_r + r\dot{\theta}\cos\phi \cdot \mathbf{e}_\theta + r\dot{\phi} \cdot \mathbf{e}_\phi \tag{5.5}$$

and

$$\begin{aligned}\mathbf{a} = &\left(\ddot{r} - r\dot{\theta}^2\cos^2\phi - r\dot{\phi}^2\right)\cdot\mathbf{e}_r + \\ &\left(2\dot{r}\dot{\theta}\cos\phi + r\ddot{\theta}\cos\phi - 2r\dot{\theta}\dot{\phi}\sin\phi\right)\cdot\mathbf{e}_\theta + \\ &\left(2\dot{r}\dot{\theta} + r\dot{\theta}^2\sin\phi\cos\phi + r\ddot{\phi}\right)\cdot\mathbf{e}_\phi.\end{aligned} \tag{5.6}$$

Considering Newton's second law $F = m \cdot a$ the equations of motion in spherical coordinates in the RTN reference frame leads with

$$\mathbf{F} = F_r \cdot \mathbf{e}_r + F_\theta \cdot \mathbf{e}_\theta + F_\phi \cdot \mathbf{e}_\phi \tag{5.7}$$

and

$$\mathbf{a} = a_r \cdot \mathbf{e}_r + a_\theta \cdot \mathbf{e}_\theta + a_\phi \cdot \mathbf{e}_\phi \tag{5.8}$$

to

$$\mathbf{F} = \begin{bmatrix} F_r \\ F_\theta \\ F_\phi \end{bmatrix} = m \cdot \begin{bmatrix} a_r \\ a_\theta \\ a_\phi \end{bmatrix} = m \cdot \begin{bmatrix} \ddot{r} - r\dot{\theta}^2\cos^2\phi - r\dot{\phi}^2 \\ 2\dot{r}\dot{\theta}\cos\phi + r\ddot{\theta}\cos\phi - 2r\dot{\theta}\dot{\phi}\sin\phi \\ 2\dot{r}\dot{\theta} + r\dot{\theta}^2\sin\phi\cos\phi + r\ddot{\phi} \end{bmatrix}, \tag{5.9}$$

where the unit vectors are already cancelled. The Earth will be regarded as a point mass. So, in the RTN reference frame the satellite will only be attracted along the radial-axis (see Fig. 2.4). Therefore, the acceleration along the tangential- and the normal-axis is zero: $a_\theta = a_\phi = 0$.
The acceleration due to the point mass can be derived via Newton's laws:
The gravitational force acting on a satellite is

$$F = G\frac{m_1 m_2}{r^2}, \tag{5.10}$$

where G is the gravitational parameter, m_1 is the mass of the celestial body, m_2 is the mass of the spacecraft and r is the distance between the celestial body and the satellite. This can be combined with Newton's second law of motion:

$$F = m_2 \cdot a = G\frac{m_1 m_2}{r^2} \tag{5.11}$$

Thus, the acceleration acting on the satellite can be described with

$$a = G\frac{m_1}{r^2} = \frac{\mu}{r^2}. \tag{5.12}$$

Since the Earth is seen as a point mass and the radial-axis is not pointing towards the Earth, the radial acceleration is defined as $a_r = -\frac{\mu_\oplus}{r^2}$. Using this and solving for the second derivatives of

Eq. (5.9) leads to

$$\begin{bmatrix} \ddot{r} \\ \ddot{\theta} \\ \ddot{\phi} \end{bmatrix} = \begin{bmatrix} -\frac{\mu_\oplus}{r^2} + r\dot{\theta}^2\cos^2\phi + r\dot{\phi}^2 \\ \left(-2\dot{r}\dot{\theta}\cos\phi + 2r\dot{\theta}\dot{\phi}\sin\phi\right)\cdot\frac{1}{r\cos\phi} \\ \left(-2\dot{r}\dot{\theta} - r\dot{\theta}^2\sin\phi\cos\phi\right)\cdot\frac{1}{r} \end{bmatrix}. \tag{5.13}$$

5.2 Unperturbed and Uncontrolled Nominal Dynamics

The state vector $\mathbf{x}(t)$ is assumed to be

$$\dot{\mathbf{x}} = \begin{bmatrix} \dot{r} & \dot{\theta} & \dot{\phi} & \ddot{r} & \ddot{\theta} & \ddot{\phi} \end{bmatrix}^T. \tag{5.14}$$

Using the acceleration in spherical coordinates of Eq. (5.13) and inserting to the state vector $\mathbf{x}(t)$:

$$\dot{\mathbf{x}} = \begin{bmatrix} \dot{r} \\ \dot{\theta} \\ \dot{\phi} \\ \ddot{r} \\ \ddot{\theta} \\ \ddot{\phi} \end{bmatrix} = \begin{bmatrix} \dot{r} \\ \dot{\theta} \\ \dot{\phi} \\ -\frac{\mu_\oplus}{r^2} + r\dot{\theta}^2\cos^2\phi + r\dot{\phi}^2 \\ \left(-2\dot{r}\dot{\theta}\cos\phi + 2r\dot{\theta}\dot{\phi}\sin\phi\right)\cdot\frac{1}{r\cos\phi} \\ \left(-2\dot{r}\dot{\phi} - r\dot{\theta}^2\sin\phi\cos\phi\right)\cdot\frac{1}{r} \end{bmatrix}. \tag{5.15}$$

The drift of the angle θ has to be rewritten as $\theta = \lambda + \omega$, where ω is defined as the Earth rotational velocity as a reason of a rotating reference frame. The RTN reference frame for geostationary orbits has a deviation of the Greenwich meridian which is called nominal angle λ_n. The satellite will have an offset ϵ in the RTN frame due to the perturbations. In Eq. (5.15), the derivative of θ is used. Thus, $\dot{\lambda} = \dot{\epsilon}$ because the nominal longitude is constant.
Finally, the state vector for unperturbed and uncontrolled satellite dynamics in a rotating frame in spherical coordinates can be written as

$$\dot{\mathbf{x}} = \begin{bmatrix} \dot{x}_1 \\ \dot{x}_2 \\ \dot{x}_3 \\ \dot{x}_4 \\ \dot{x}_5 \\ \dot{x}_6 \end{bmatrix} = \begin{bmatrix} \dot{r} \\ \dot{\epsilon} \\ \dot{\phi} \\ \ddot{r} \\ \ddot{\epsilon} \\ \ddot{\phi} \end{bmatrix} = \begin{bmatrix} \dot{r} \\ \dot{\epsilon} \\ \dot{\phi} \\ -\frac{\mu_\oplus}{r^2} + r\left(\dot{\epsilon}+\omega\right)^2\cos^2\phi + r\dot{\phi}^2 \\ \left(-2\dot{r}\left(\dot{\epsilon}+\omega\right)\cos\phi + 2r\left(\dot{\epsilon}+\omega\right)\dot{\phi}\sin\phi\right)\cdot\frac{1}{r\cos\phi} \\ \left(-2\dot{r}\dot{\phi} - r\left(\dot{\epsilon}+\omega\right)^2\sin\phi\cos\phi\right)\cdot\frac{1}{r} \end{bmatrix}. \tag{5.16}$$

5.3 Perturbed and Uncontrolled Nominal Dynamics

In Section 5.2 only the two body problem is considered. However in reality many different forces act on the satellite (see Chapter 3). Thus, they have to be used in the satellite dynamics model to achieve a high accuracy. It is important to mention the perturbations described in Chapter 3 are in

an inertial reference system in Cartesian coordinates. However, the applied dynamics are with respect to the rotating frame in spherical coordinates. Thus, rotations around the z-axis under consideration of the GHA and the nominal longitude and transformations from spherical to Cartesians are needed.

$$\dot{\mathbf{x}} = \begin{bmatrix} \dot{r} \\ \dot{\epsilon} \\ \dot{\phi} \\ -\frac{\mu_{\oplus}}{r^2} + r\left(\dot{\epsilon}+\omega\right)^2 \cos^2\phi + r\dot{\phi}^2 + a_{pr}\left(r,\lambda,\phi\right) \\ \left(-2\dot{r}\left(\dot{\epsilon}+\omega\right)\cos\phi + 2r\left(\dot{\epsilon}+\omega\right)\dot{\phi}\sin\phi + a_{p\lambda}\left(r,\lambda,\phi\right)\right)\cdot\frac{1}{r\cos\phi} \\ \left(-2\dot{r}\dot{\phi} - r\left(\dot{\epsilon}+\omega\right)^2\sin\phi\cos\phi + a_{p\phi}\left(r,\lambda,\phi\right)\right)\cdot\frac{1}{r} \end{bmatrix} \tag{5.17}$$

a_{pr}, $a_{p\lambda}$ and $a_{p\phi}$ are the perturbations acting on a satellite.

5.4 Factorisation of the System Matrix

In the optimisation, the satellite dynamics are playing an important role – they will describe the system matrix $\mathbf{A}$. According to Section 4.1, the system matrix has to be brought in factorised form to use it later in the ASRE method. The factorisation has infinite possible solutions if the number of rows and columns are higher than 1. One possible form of the factorisation of the satellite dynamics with perturbations (see Eq. (5.17)) will be shown in the following:

$$\dot{\mathbf{x}} = \mathbf{A}\mathbf{x} = \begin{bmatrix} 0 & 0 & 0 & 1 & 0 & 0 \\ 0 & 0 & 0 & 0 & 1 & 0 \\ 0 & 0 & 0 & 0 & 0 & 1 \\ \mathbf{A}_{30} & 0 & 0 & 0 & 0 & 0 \\ \mathbf{A}_{40} & 0 & 0 & \mathbf{A}_{43} & \mathbf{A}_{44} & \mathbf{A}_{45} \\ \mathbf{A}_{50} & 0 & 0 & 0 & \mathbf{A}_{54} & \mathbf{A}_{55} \end{bmatrix} \cdot \mathbf{x} \tag{5.18}$$

The content of the system matrix $\mathbf{A}$ can be found in Table 5.1.
The degrees of freedom of the satellite dynamics can be increased if another factorisation is created and with the method already shown in Section 4.1 the performance of the chosen factorisation can be increased. According to the mathematical factorisation, there are only non-unique solutions for systems with $n > 1$.

Table 5.1: Factorisation of satellite dynamics

$\mathbf{A}_{30}$	$-\frac{\mu}{x_1^3} + x_6^2 + \left(x_5^2 + 2x_5\omega + \omega^2\right)\cos^2 x_3 + \frac{a_{pr}\left(r,\lambda,\phi\right)}{x_1}$
$\mathbf{A}_{40}$	$\frac{a_{p\lambda}\left(r,\lambda,\phi\right)}{x_1^2\cos x_3}$
$\mathbf{A}_{43}$	$-\frac{2\left(\omega + x_5\right)}{x_1}$
$\mathbf{A}_{44}$	$2x_6\tan x_3$
$\mathbf{A}_{45}$	$2\omega\tan x_3$
$\mathbf{A}_{50}$	$\frac{a_{p\phi}\left(r,\lambda,\phi\right)}{x_1^2} - \frac{\omega^2\sin x_3\cos x_3}{x_1}$
$\mathbf{A}_{54}$	$-\left(x_5 + 2\omega\right)\sin x_3\cos x_3$
$\mathbf{A}_{55}$	$-\frac{2x_4}{x_1}$

5.5 Perturbed and Controlled Nominal Dynamics

Due to the natural drift of spacecrafts in a geostationary orbit, they need a possibility to hold their position in space. Therefore, they are equipped with thrusters which are firing at certain time spots to hold the satellites in their control boxes. This control can be described in formulas as well. Hence, in Eq. (4.5) the input vector $\mathbf{u}(t)$ is the applied thrust. The input matrix $\mathbf{B}(\mathbf{x}(t))$ describes the influence of the input vector to the non-linear system.
The control input acceleration has to be divided by the same factors as the perturbation acceleration of Eq. (5.17). Those fractions will be placed in the input matrix $\mathbf{B}$:

$$\mathbf{B} = \begin{bmatrix} 0 & 0 & 0 \\ 0 & 0 & 0 \\ 0 & 0 & 0 \\ 1 & 0 & 0 \\ 0 & \frac{1}{r\cos\phi} & 0 \\ 0 & 0 & \frac{1}{r} \end{bmatrix} \tag{5.19}$$

The final factorised, non-linear, perturbed and controlled dynamics of a geostationary spacecraft in state-depended matrix form can be written as:

$$\dot{\mathbf{x}} = \begin{bmatrix} 0 & 0 & 0 & 1 & 0 & 0 \\ 0 & 0 & 0 & 0 & 1 & 0 \\ 0 & 0 & 0 & 0 & 0 & 1 \\ \mathbf{A}_{30} & 0 & 0 & 0 & 0 & 0 \\ \mathbf{A}_{40} & 0 & 0 & \mathbf{A}_{43} & \mathbf{A}_{44} & \mathbf{A}_{45} \\ \mathbf{A}_{50} & 0 & 0 & 0 & \mathbf{A}_{54} & \mathbf{A}_{55} \end{bmatrix} \cdot \begin{bmatrix} \dot{r} \\ \dot{\epsilon} \\ \dot{\phi} \\ \ddot{r} \\ \ddot{\epsilon} \\ \ddot{\phi} \end{bmatrix} + \begin{bmatrix} 0 & 0 & 0 \\ 0 & 0 & 0 \\ 0 & 0 & 0 \\ 1 & 0 & 0 \\ 0 & \frac{1}{r\cos\phi} & 0 \\ 0 & 0 & \frac{1}{r} \end{bmatrix} \cdot \begin{bmatrix} u_r \\ u_\lambda \\ u_\phi \end{bmatrix}, \tag{5.20}$$

where the entries of the system matrix $\mathbf{A}$ can be found in Table 5.1.

6 Valdiation and Results

For the evaluation of the capability of the ASRE method for the station keeping of geostationary satellites, a given spacecraft will be exposed to the free drift and will be controlled afterwards. For the free drift, the perturbations of Chapter 3 will be used to simulate the natural forces acting on a satellite. Therefore, a model with three Zonal terms and three Tesseral terms will be used to achieve a good accuracy of the perturbation of the Earth. The most important celestial bodies – the Sun and the Moon – are regarded as point masses. Moreover, the solar radiation pressure is taken into account as well as the effect of the Earth shadow. The control profile of the satellite will be optimised with the ASRE approach towards its global optimum depending on the used factorisation.
This chapter shows different steps to get one of the optimal solutions for the station keeping problem of geostationary satellites with electrical propulsion systems. First, the perturbation model of the satellite is verified. For this, the spacecraft is placed at a random geostationary position and it will not be controlled. The simulation of the forces acting on a geostationary spacecraft is written in Java and includes all the previous mentions perturbations as well as their restrictions. Also, this model is verified via common literature like Soop [22] and via FreeFlyer which is software for space mission design, analysis and operations.
Afterwards, the spacecraft will be commanded to a specific position. Therefore, the spacecraft dynamics are included to the simulation, but the perturbations are set to zero.
Then, the spacecraft will drift for some time and is controlled back to a certain position, where it will start to drift again. The interaction between the perturbation model and the satellites dynamic is verified. Here, the weighting matrices are not optimised which is why they have to be optimised. The weighting matrix of the input $\mathbf{R}$ will not be optimised, because the weighting of it depends on the used thrusters for the real application. With the optimal weighting matrices an optimal solution of the used factorisation will be shown. Due to the infinite amount of different factorisations, this chapter will conclude with the comparison of different factorisations and a short comparison with the result of common literature (see Losa [14]).
The different stages until the final optimisation will be at different dates and with different spacecraft masses, absorbing solar radiation area and radiation pressure parameters. This is done to show that the ASRE approach is not fixed to some specific date or parameters. The following parameters will stay the same if not reported otherwise:

- Ideal geostationary semi-major axis: $r = 42164.140100123965\,\mathrm{km}$
- Nominal longitude: $\lambda_n = 60\,\mathrm{deg}$
- Longitude deviation: $\epsilon = -0.04\,\mathrm{deg}$
- Latitude: $\phi = 0\,\mathrm{deg}$

The initial velocity is zero in all three axes. The deadband of the control box is chosen to be $2\lambda_{max} = 2\phi_{max} = 0.1\,\text{deg}$. Thus, the maximal deviation of the control box centre in one direction is at 0.05 deg. For the ASRE approach, the co-state vector has to be given in hard, soft or mixed constraints and is set according to the specific task.
The distance always has to be a hard constraint. If, for example, the distance would be a soft constrained state, the controller would try to bring the distance to zero which would result in an impact of the spacecraft on the Earth's surface. Also, it is important to mention that more hard constraints result in a higher performance index (compare with the example in Chapter 4) because the restrictions on the system are harder.
For the calculation of the total propellant mass, Eq. (2.11) will be used. Therefore, the specific impulse I_{sp} is assumed to be 3000 s.

6.1 Free Drift

To verify the free drift of the geostationary satellite, the perturbations of Earth with three Zonals and three Tesserals, the Sun and the Moon as well as the solar radiation pressure will be considered. The free drift will be shown for 14 days with a step size of 600 s. The spacecraft is placed at zero degree deviation of the nominal longitude. The starting date is chosen to be on the 1st of January 2010 at midnight. The satellite mass is set to 4500 kg, the absorbing solar radiation surface area to 300 m^2 and the radiation pressure parameter to 0.3.
In Fig. 6.1 to Fig. 6.4, it can be seen that after a while the influence of the perturbations acting on the spacecraft pushes it away from its initial position. In the beginning, the satellite was in a perfect circular orbit around the Earth, but the perturbations start to push it towards the stable points (see Fig. 3.2). The acceleration acting on the satellite will result in the distance to the Earth not being constant anymore. The orbit is going to be an elliptic orbit.
The free drift behaves as expected. Due to the perturbations, the perfect circular geostationary orbit cannot be hold and the latitude starts to oscillate around the equator.

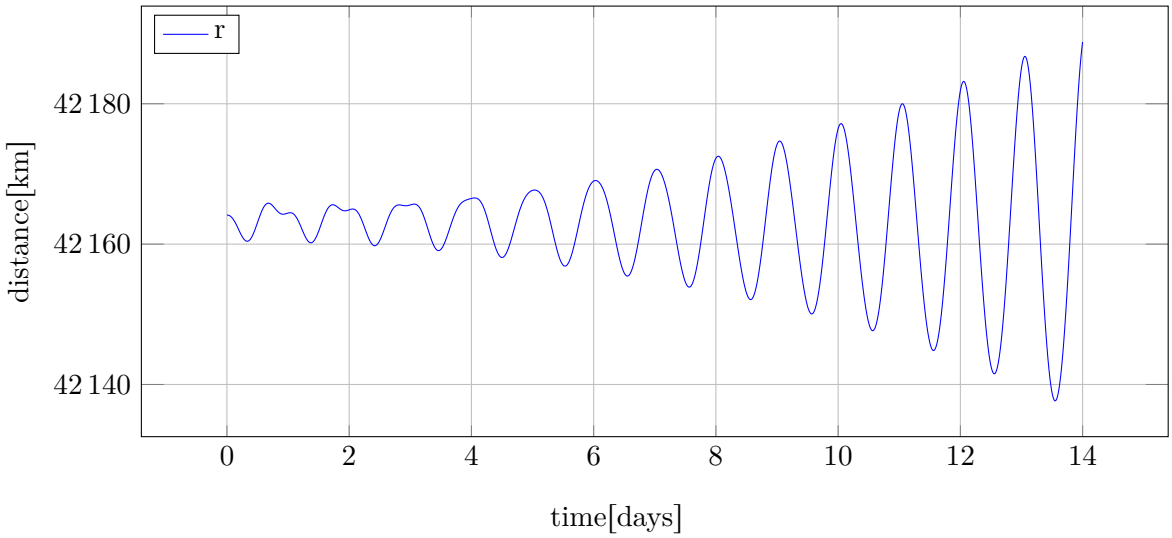

Figure 6.1: Free Drift of spacecraft in two weeks with Euler integration (600 s): distance to Earth over time

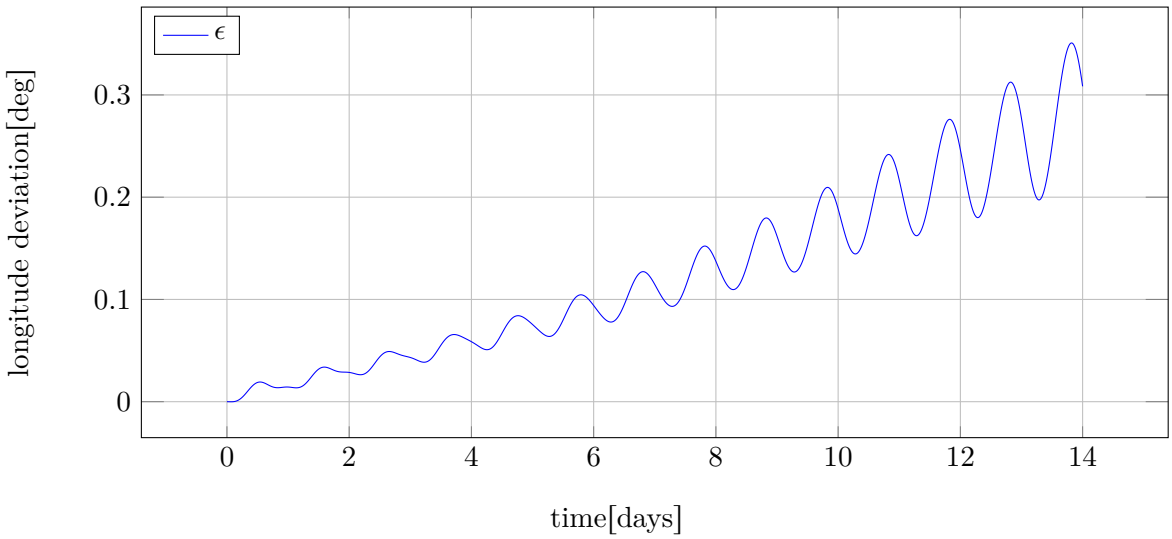

Figure 6.2: Free Drift of spacecraft in two weeks with Euler integration (600 s): longitude over time

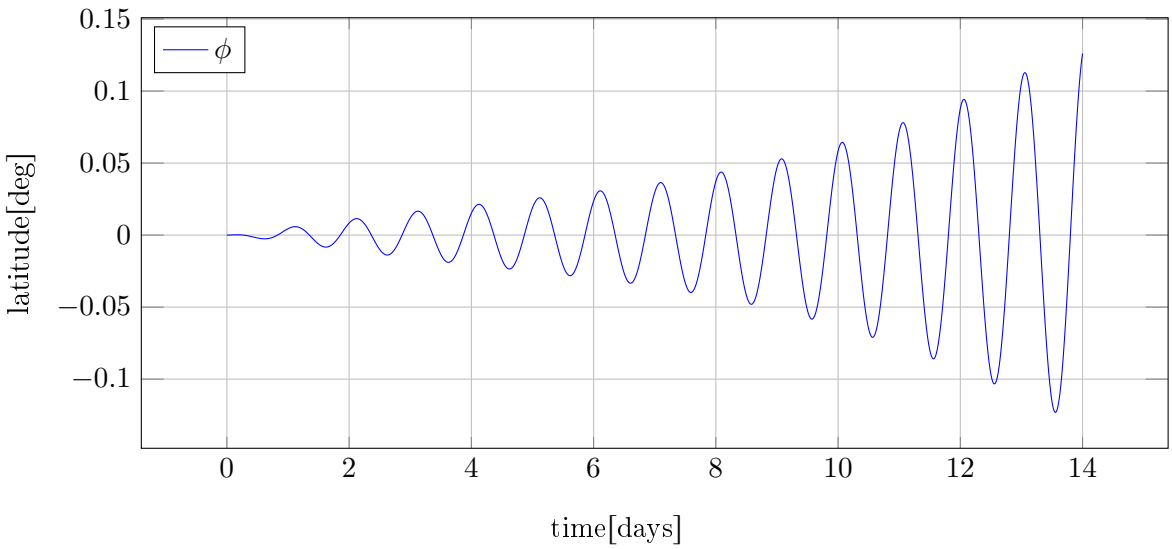

Figure 6.3: Free Drift of spacecraft in two weeks with Euler integration (600 s): latitude over time

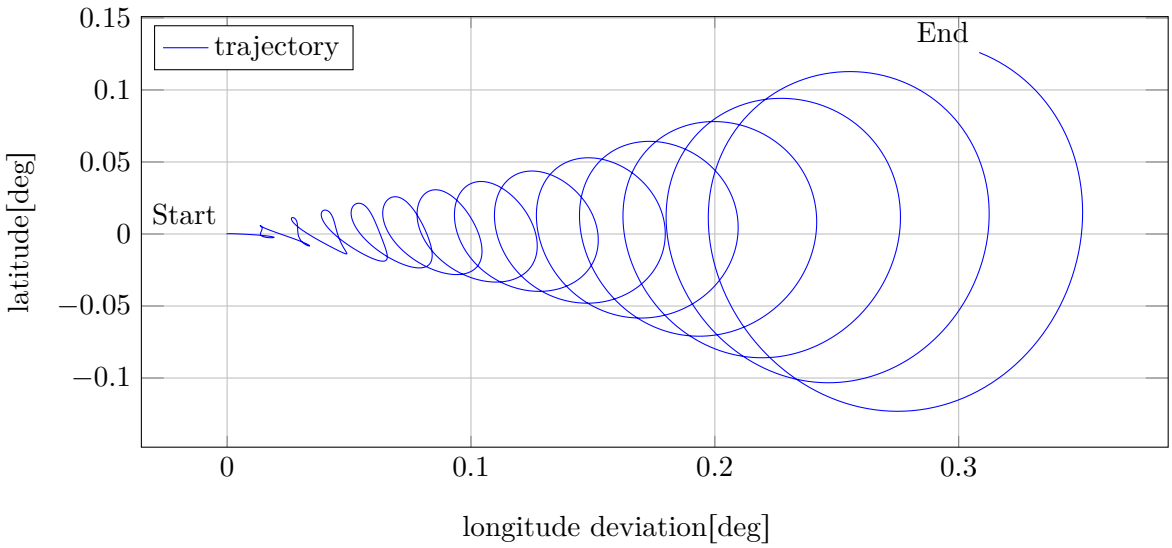

Figure 6.4: Free Drift of spacecraft in two weeks with Euler integration (600 s): longitude vs latitude

6.2 Control

For the verification of the control, the spacecraft is placed with an initial longitude deviation of +0.05 deg and an initial latitude of +0.04 deg. The distance to the Earth and the longitude deviation are considered to be hard constraints which means that they will be at their final positions at the ideal geostationary radius and at -0.04 deg, respectively. The remaining states are regarded as soft constraints which brings the total non-linear problem to a mixed constrained ASRE optimisation. The spacecraft mass is considered to be 4500 kg, the surface area 300 m^2 and the radiation parameter 0.3. The initial date for the control cycle of 12 hours is on the 1st of January 2010 with a step size of 60 s. The optimisation will keep going until the infinity norm of the actual and the previous iteration is below the error tolerance of 10^{-6}. If the non-linear system would converge to a smaller error tolerance, this would result in a smaller amount of Δv. The weighting matrices are chosen as follows:

$$\mathbf{Q} = 0 \cdot \mathbf{I}_{6\times 6}$$

$$\mathbf{R} = 1 \cdot 10^8 \cdot \mathrm{diag}\left(\mathbf{I}_{3\times 3}\right)$$

$$\mathbf{S} = 10 \cdot \mathrm{diag}\left(\mathbf{I}_{4\times 4}\right)$$

In Fig. 6.5 and Fig. 6.6, the satellite in the control box reference frame is exactly at the chosen position after the control cycle of 12 hours. The soft constraints, like the drift velocities along the axes of the RTN reference frame, are shown in Fig. 6.7 to Fig. 6.11. Due to the soft constraints, the tangential and normal velocities are not zero when the spacecraft is at its final position. Choosing the weighting matrix $\mathbf{S}$ in a better way can result in a final state closer to zero. The control profile describes the used thrust to navigate the satellite. It can be seen that the needed acceleration along the radial axis is the largest, while the tangential and normal acceleration is close to zero when the spacecraft is at the final position. The total Δv is about 0.0022 km/s which can be used to calculate the total amount of propellant which is needed for this manoeuvre. According to Eq. (2.11), the total amount of fuel is about 0.34 kg under the assumption that the specific impulse of the propellant is 3000 s. By using optimised weighting matrices as well as another factorisation, it is possible to decrease the Δv even more.

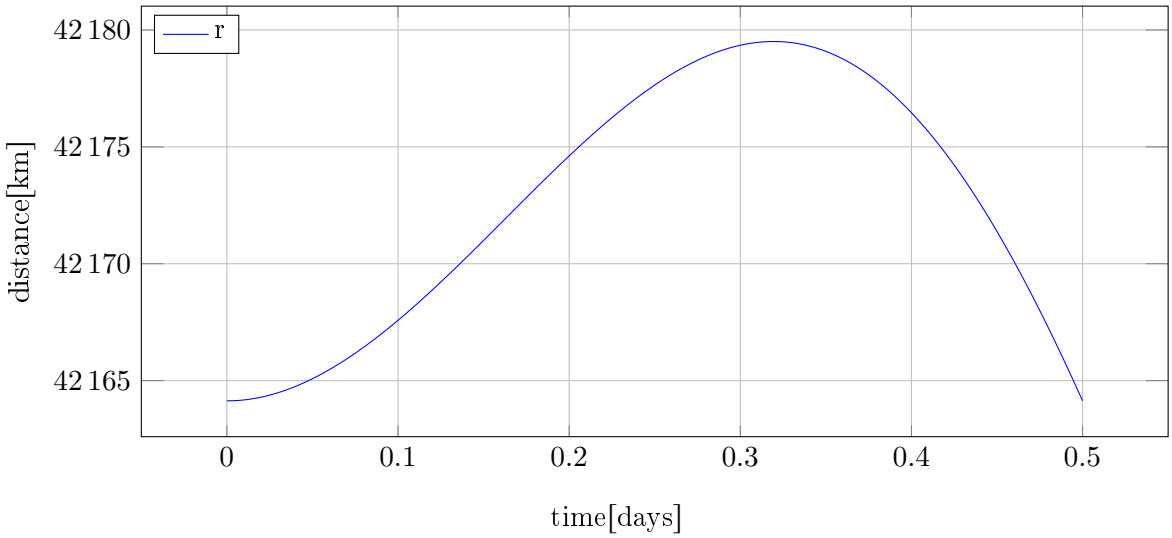

Figure 6.5: Position of spacecraft with two hard constraints (r, ϵ) with Euler integration (60 s): distance to Earth over time

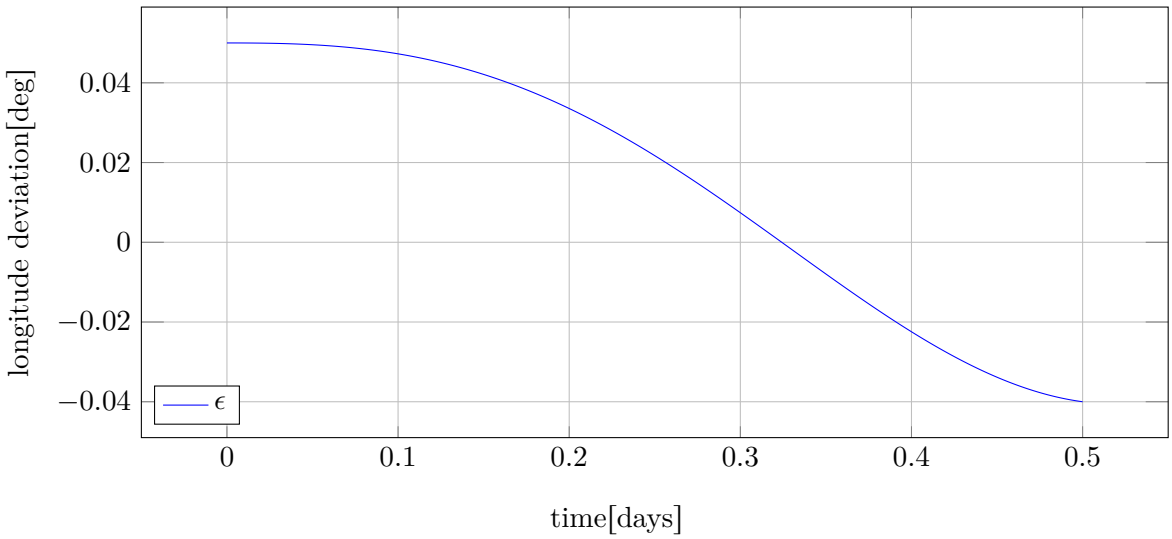

Figure 6.6: Position of spacecraft with two hard constraints (r, ϵ) with Euler integration (60 s): longitude deviation over time

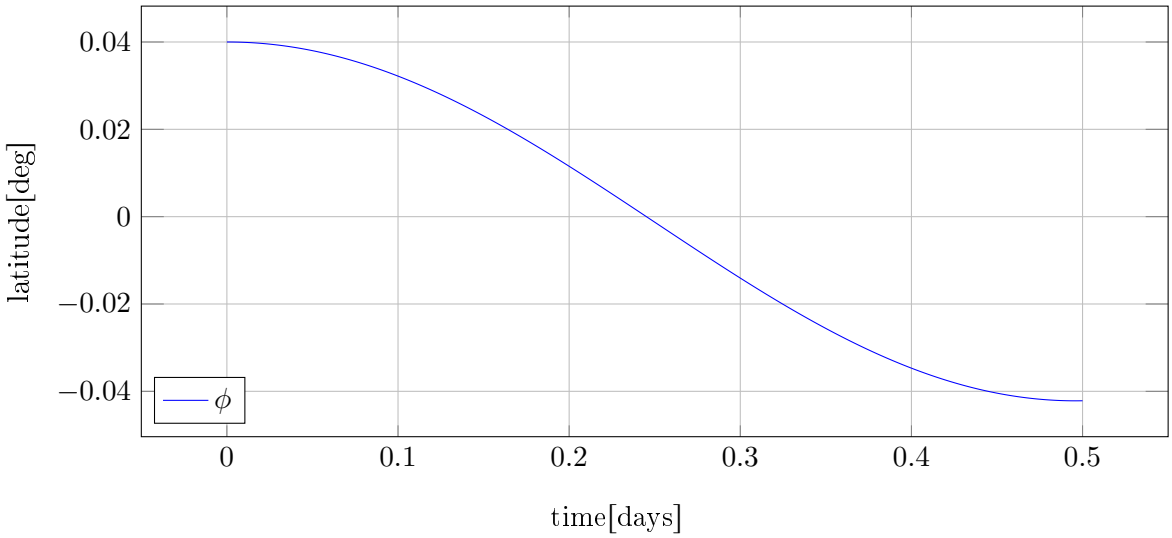

Figure 6.7: Position of spacecraft with two hard constraints (r, ϵ) with Euler integration (60 s): latitude over time

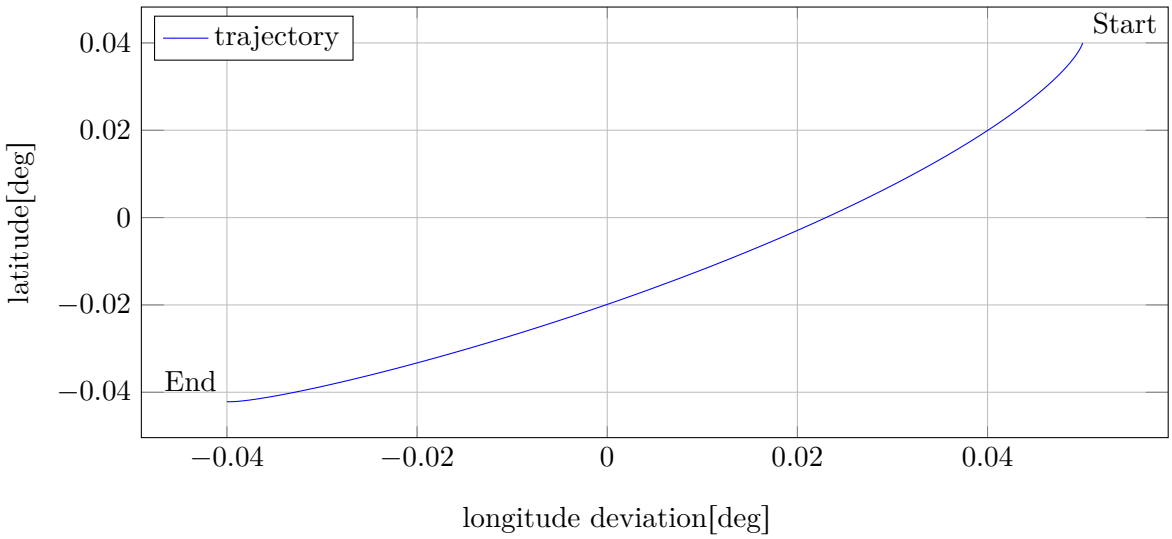

Figure 6.8: Position of spacecraft with two hard constraints (r, ϵ) with Euler integration (60 s): latitude over longitude deviation

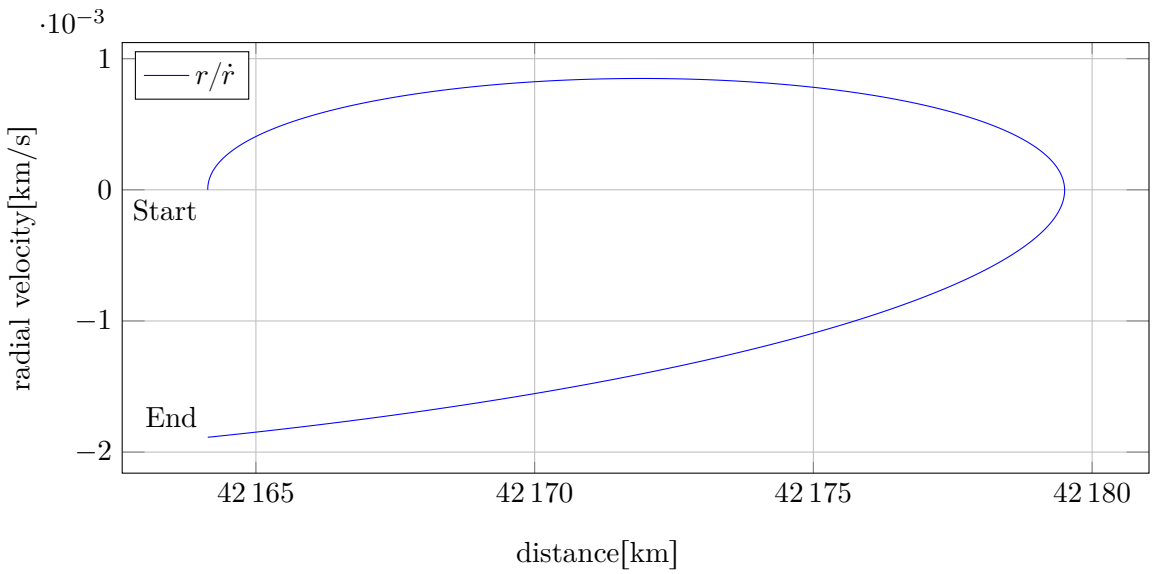

Figure 6.9: Velocity of spacecraft with two hard constraints (r, ϵ) with Euler integration (60 s): radial velocity over distance to Earth

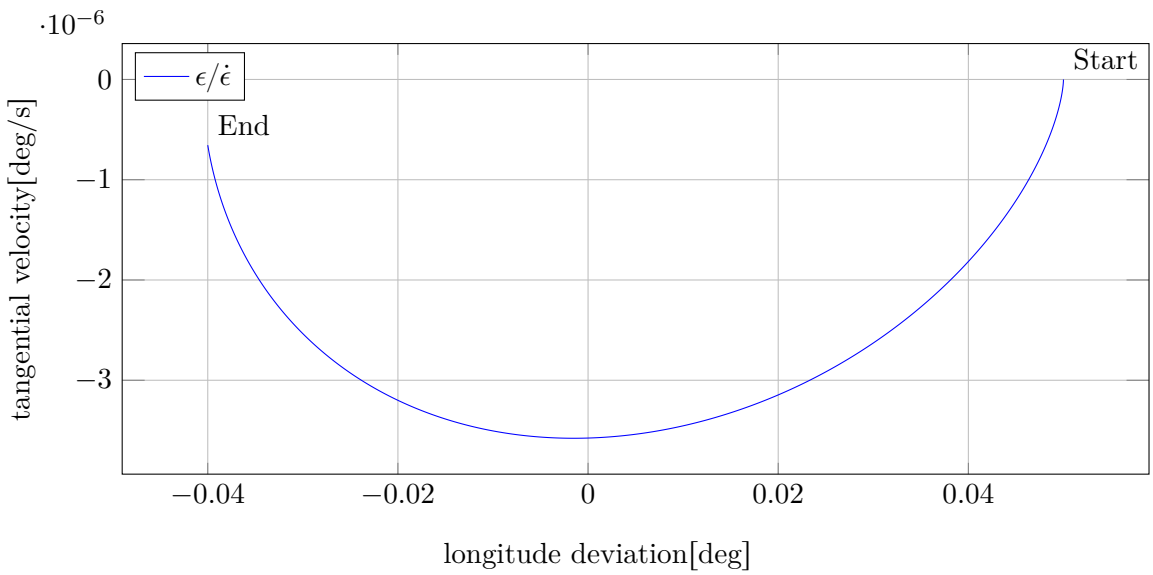

Figure 6.10: Velocity of spacecraft with two hard constraints (r, ϵ) with Euler integration (60 s): tangential velocity over longitude deviation

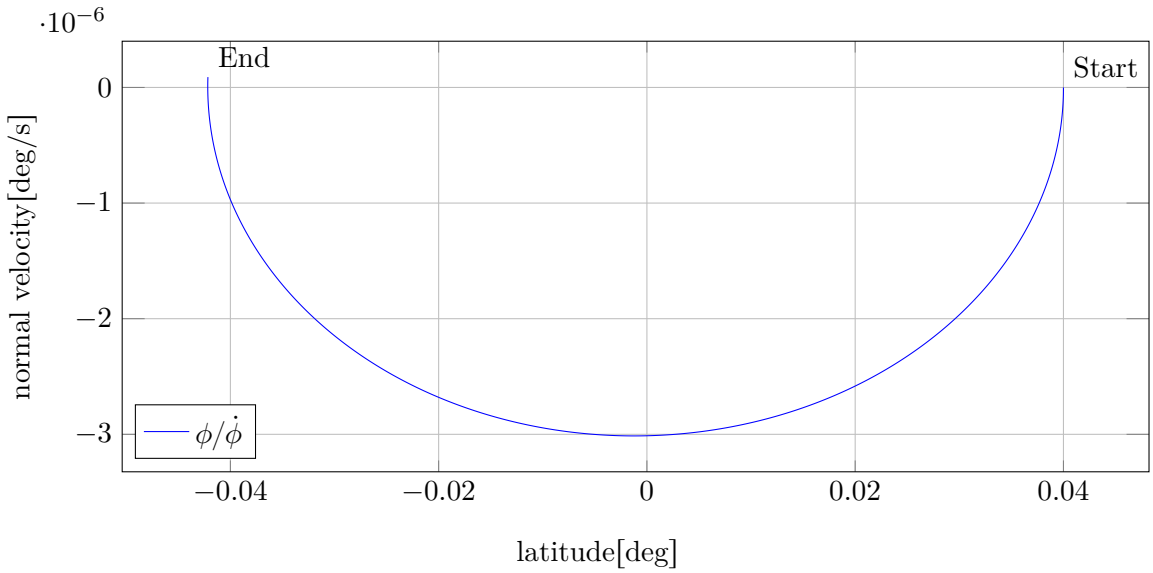

Figure 6.11: Velocity of spacecraft with two hard constraints (r, ϵ) with Euler integration (60 s): normal velocity over latitude

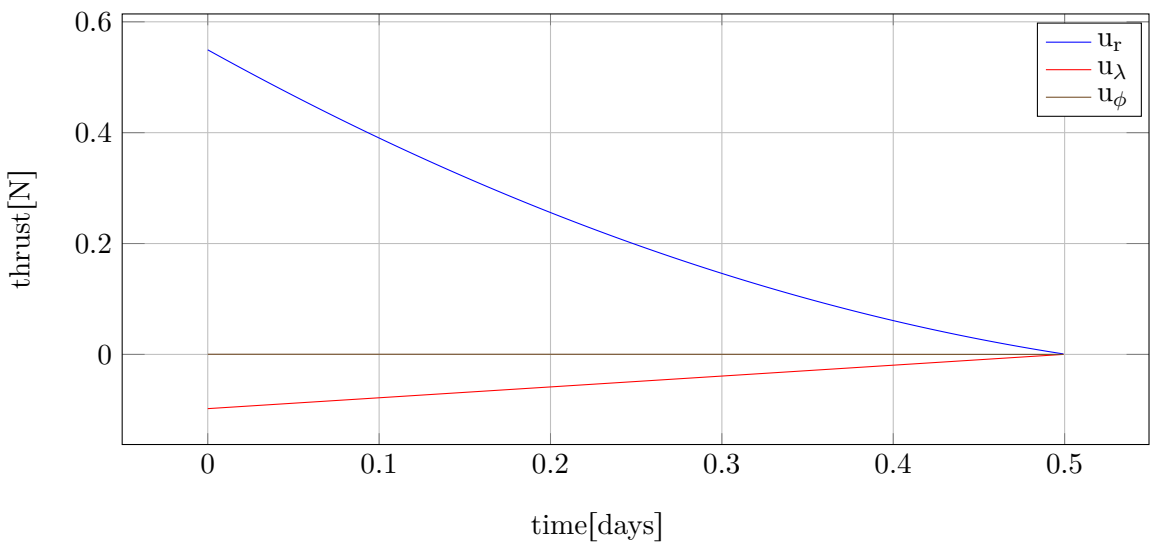

Figure 6.12: Thrust control profile of non-linear system with two hard constraints (r, ϵ) with Euler integration (60 s)

6.3 Free Drift and Control

After showing that the spacecraft can drift freely and can be controlled, a combination of both will be used to simulate ten days in orbit with the according control cycles. For this, the spacecraft is positioned at -0.04 deg for the initial longitude deviation and 0 deg latitude. The final state after each control cycle should be at the ideal geostationary orbit radius, longitude deviation of -0.04 deg, latitude of 0 deg and zero velocity along the RTN reference frame axes. The number of fixed constraints is considered to be six which results in a complete hard constrained non-linear problem. The initial date is on the 10th of July 2010 at midnight. The free drift will be 1.5 days and the control cycle 12 hours and a step size of 600 s. The error tolerance of the ASRE optimisation is assumed to be 10^{-9}. In contrast to only free drift and only control, the spacecraft mass is considered to be 3000 kg, the radiation absorption area is 100 m^2 and the radiation parameter is 0.5. The weighting matrix $\mathbf{Q}$ is assumed to be a zero matrix and $\mathbf{R}$ to be an identity matrix.
In Fig. 6.13 to Fig. 6.17, it can be seen that the geostationary satellite has a free drift of 1.5 days and is controlled afterwards to the final state conditions. The different shapes of the free drift in the distance to Earth, longitude deviation as well as in the latitude can be explained with the perturbations acting on the spacecraft – for different time points the accelerations have different magnitudes. The satellite always stays in its control box (see Fig. 6.16). It is possible to see the manoeuvres which are the straighter lines towards the final longitude deviation and latitude. The straighter the lines, the more fuel is needed. In Fig. 6.17, the thrust profile can be found. The thrust magnitude along the different axes can be compared to the position of the spacecraft. For example, the magnitude along the radial axis is in the beginning small because the magnitude of the deviation to the ideal geostationary semi-major axis is small, too. While the deviation of the latitude is large, the used thrust in nominal direction is significant as well. The total Δv for all five manoeuvres is about 33.0045 m/s which results in a total amount of propellant of 3.3625 kg according to Eq. (2.11).

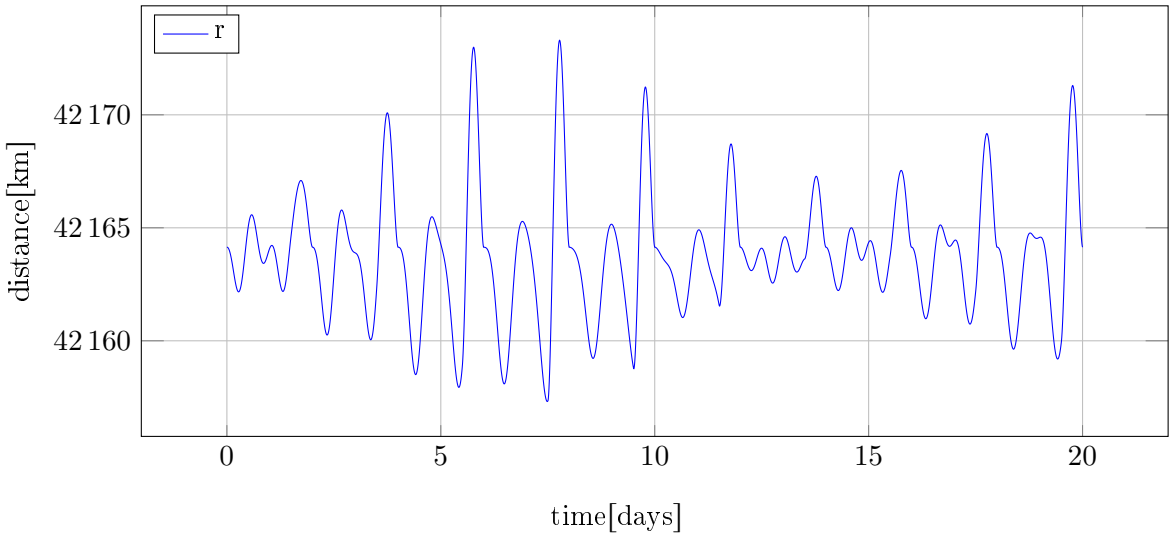

Figure 6.13: Spherical position of spacecraft after free drifts and controlled manoeuvres with only hard constraints and Euler integration (600 s): distance to Earth over time

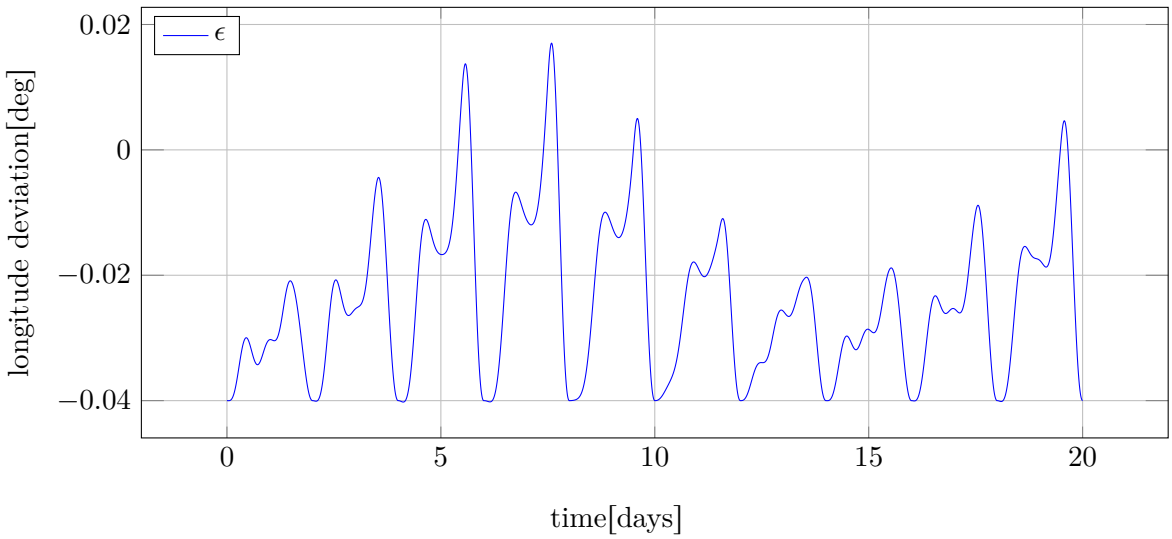

Figure 6.14: Spherical position of spacecraft after free drifts and controlled manoeuvres with only hard constraints and Euler integration (600 s): longitude deviation over time

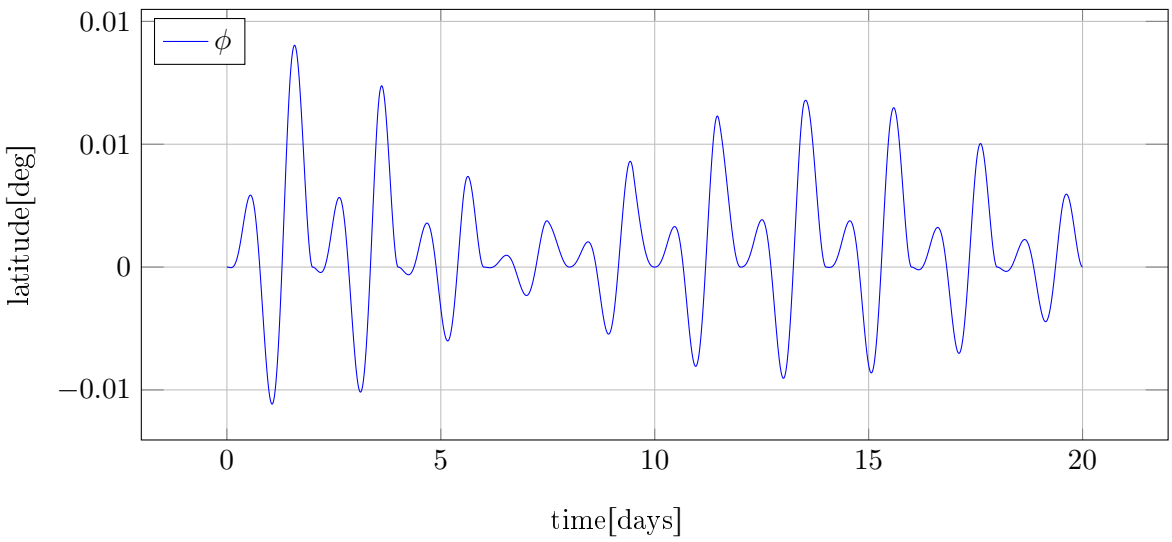

Figure 6.15: Spherical position of spacecraft after free drifts and control manoeuvres with only hard constraints and Euler integration (600 s): latitude over time

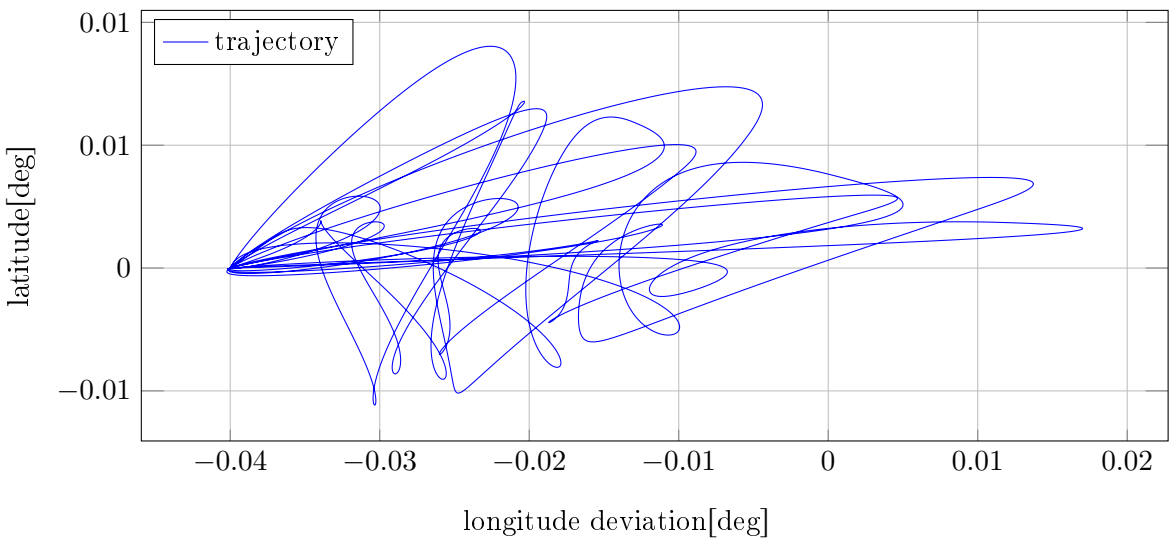

Figure 6.16: Spherical position of spacecraft after free drifts and control manoeuvres with only hard constraints and Euler integration (600 s): latitude over longitude deviation

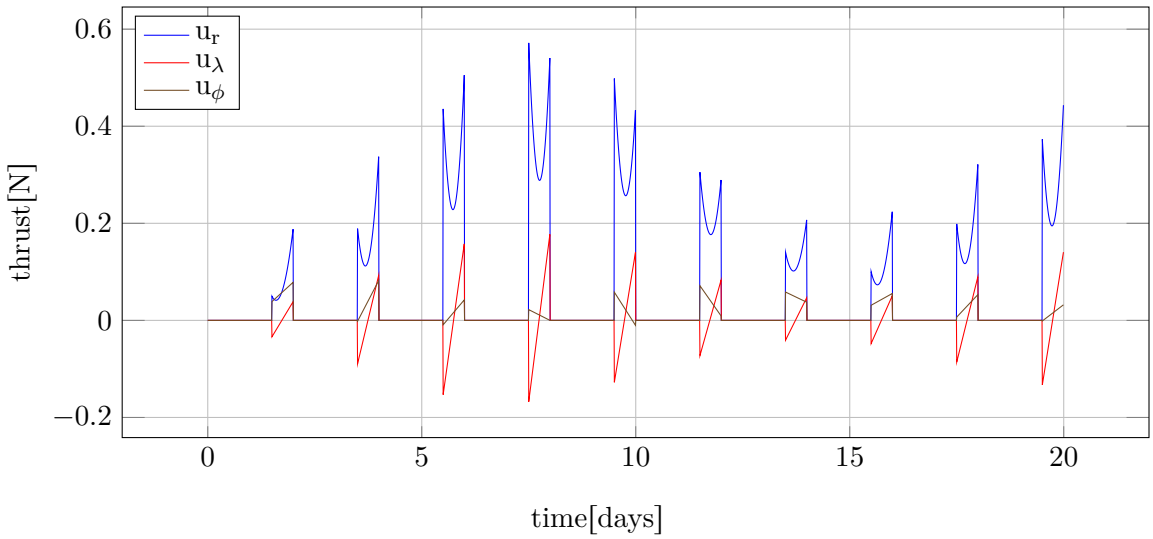

Figure 6.17: Spacecraft after free drifts and control manoeuvres with only hard constraints and Euler integration (600 s): thrust control profile

6.4 Optimisation of Weighting Matrices

Up to now, the weighting matrices have always been considered as **Q** being a zero matrix, **R** a diagonal matrix with ones in the diagonal elements and **S** as a diagonal matrix with 10 in the diagonal elements. Due to the fact that the weighting matrices influence the result, it is important to optimise them.

The non-linear system is defined in such a way that there is only one hard constraint: the distance to the Earth. The remaining states are seen as soft constraints and their final values for different diagonal values of the weighting matrices are shown. The free drift time is set to 1.5 days and the control cycle will be finished after 0.5 days with a step size of 600 s. Just one cycle of free drift and control is regarded. The initial date is on the 10th of July 2010 at midnight and the error tolerance is 10^{-9}.

In Fig. 6.18 and Fig. 6.19, it can be seen that the longitude and the latitude deviation goes to zero for the corresponding elements in the matrix **S** which is having diagonal elements of 100. According to Fig. 6.18 to Fig. 6.24, a possible final weighting matrix **S** is

$$\mathbf{S} = \begin{bmatrix} 10^2 & 0 & 0 & 0 & 0 \\ 0 & 10^2 & 0 & 0 & 0 \\ 0 & 0 & 10^2 & 0 & 0 \\ 0 & 0 & 0 & 10^7 & 0 \\ 0 & 0 & 0 & 0 & 10^6 \end{bmatrix}. \tag{6.1}$$

It is obvious that increasing the values of **S** results in more thrust which leads to a higher amount of fuel consumption(see Fig. 6.24). Thus, the values of **S** should be as small as possible, but they still have to fulfil the requirements to bring the final state very close to zero.

The behaviour of the weighting matrix **Q** is done in the same way as it was done for **S**. Fig. A.1a to Fig. A.3b (see Appendix A) display that the smaller the values for **Q**, the smaller the deviation from zero. However, small values lead to a high amount of propulsion (see Fig. A.3b). By definition, the

smallest value for $\mathbf{Q}$ is zero (see Chapter 4). Therefore, a zero $\mathbf{Q}$ matrix describes the best behaviour – the needed thrust is at about 2.7827 N and the mass of needed fuel at about 0.2836 kg.
$\mathbf{R}$ will not be optimised because the specifications of the thrusters are not known. Nevertheless, if they were known, they could be optimised in the same way.

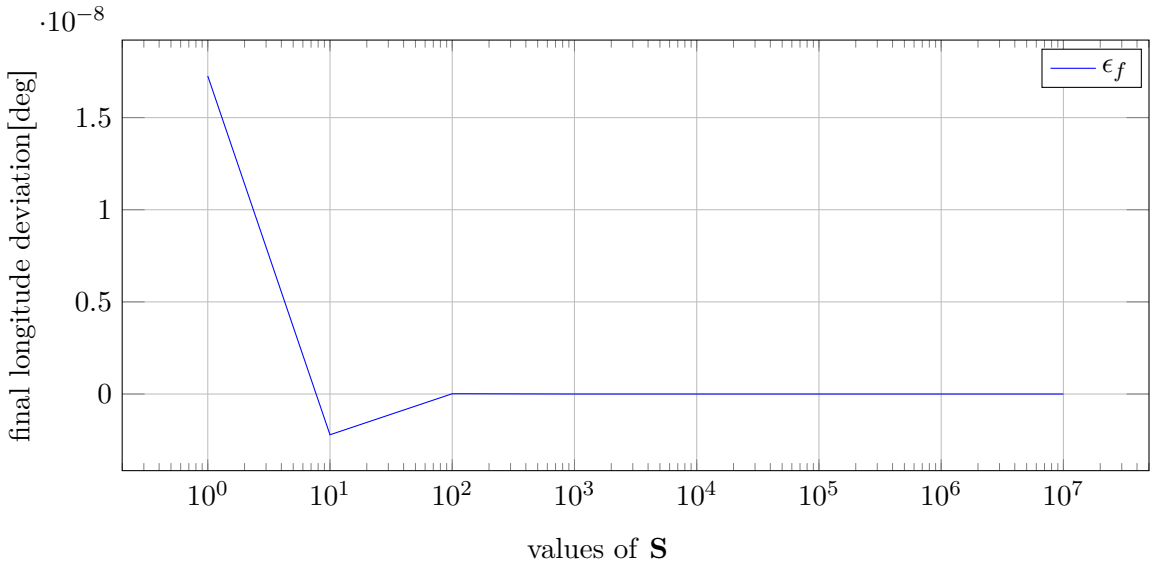

Figure 6.18: Optimisation of weighting matrix **S** with one hard constraint (r) and Euler integration (600 s): final longitude deviation values

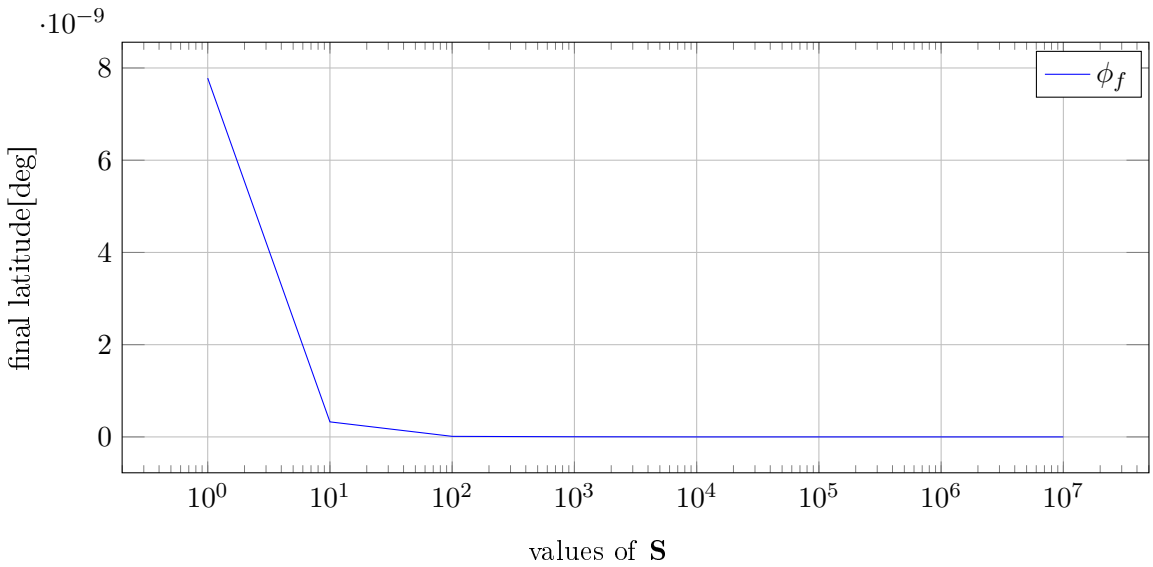

Figure 6.19: Optimisation of weighting matrix **S** with one hard constraint (r) and Euler integration (600 s): final latitude values

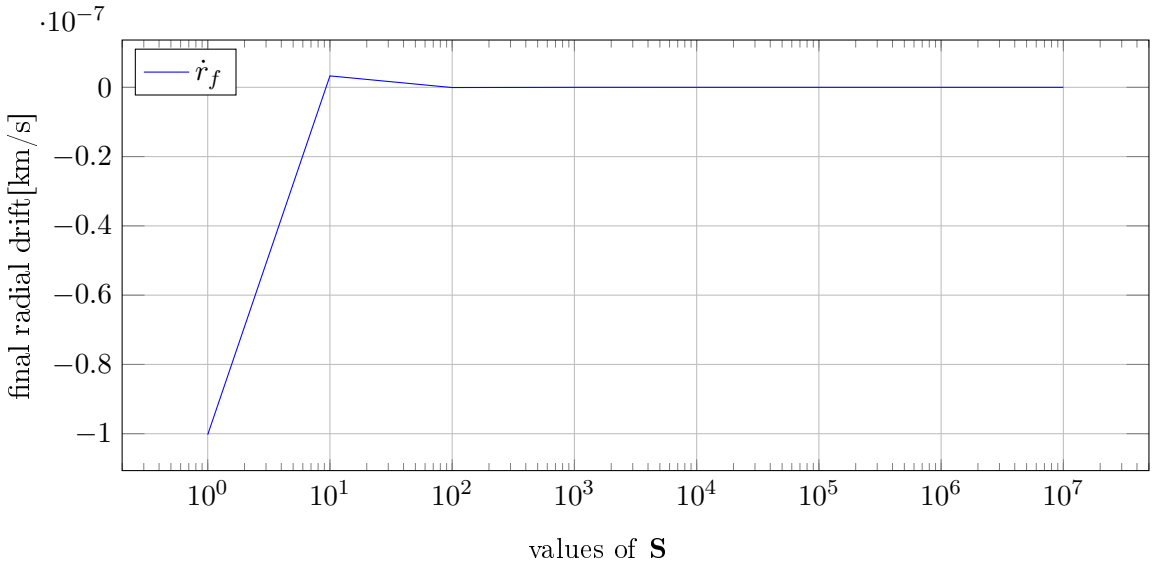

Figure 6.20: Optimisation of weighting matrix **S** with one hard constraint (r) and Euler integration (600 s): final radial drift values

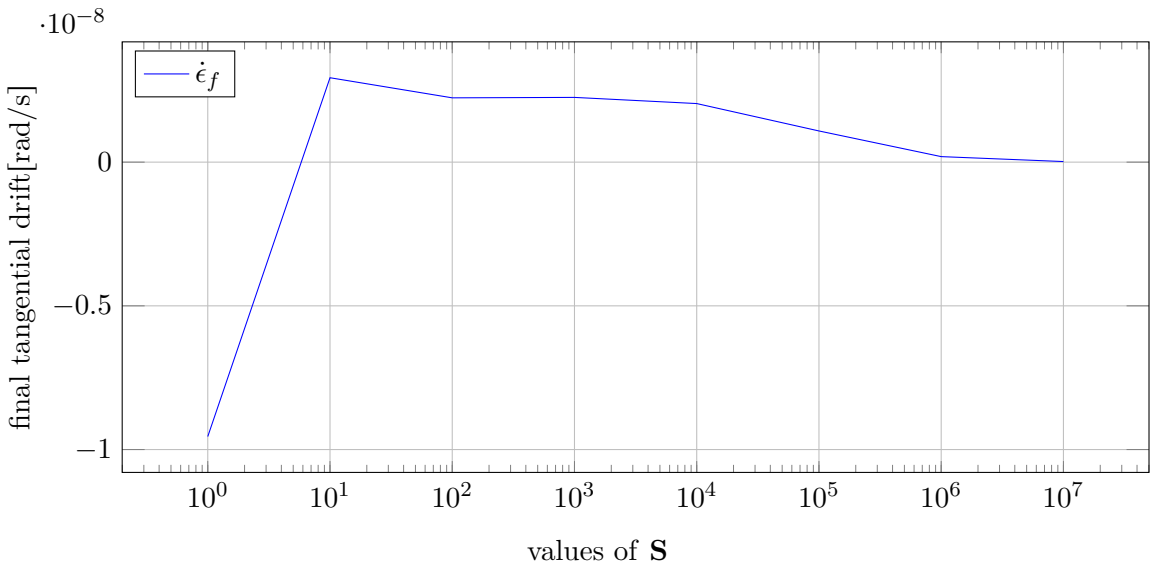

Figure 6.21: Optimisation of weighting matrix **S** with one hard constraint (r) and Euler integration (600 s): final tangential drift values

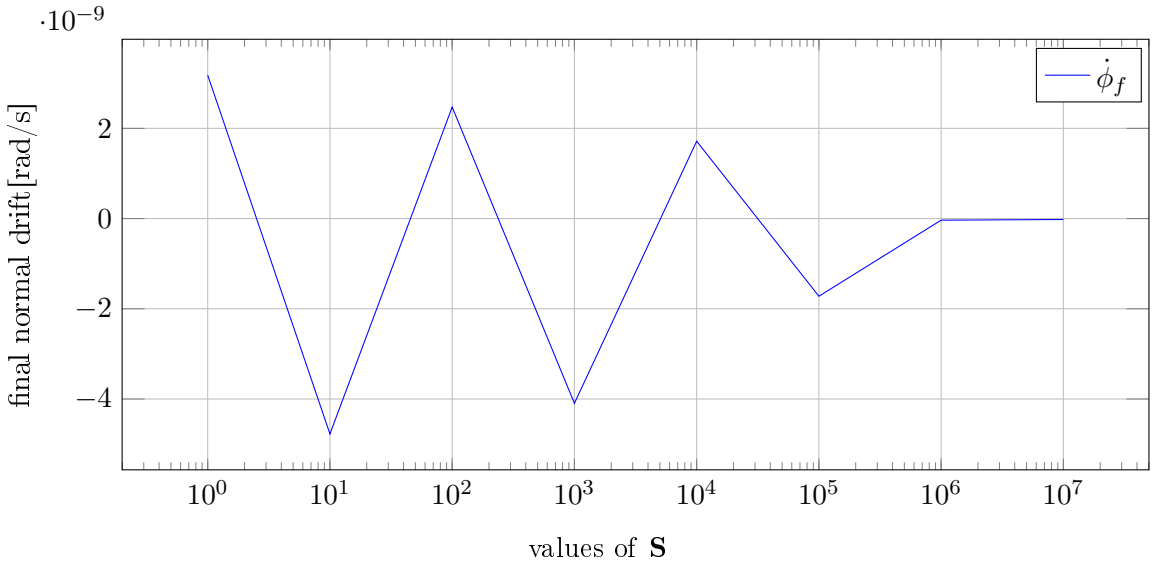

Figure 6.22: Optimisation of weighting matrix **S** with one hard constraint (r) and Euler integration (600 s): final normal drift values

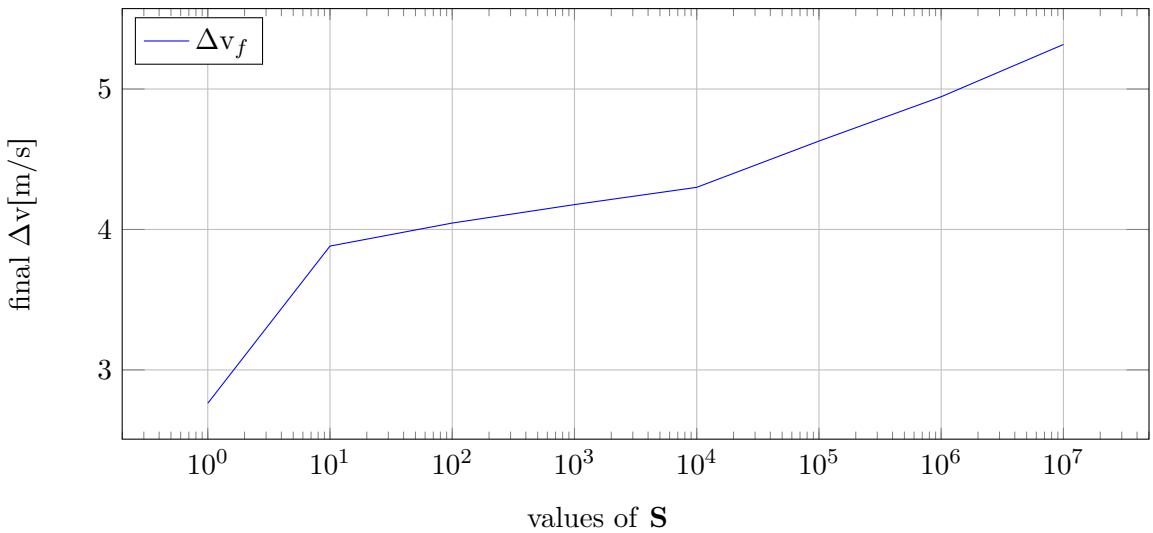

Figure 6.23: Optimisation of weighting matrix **S** with one hard constraint (r) and Euler integration (600 s): Δv

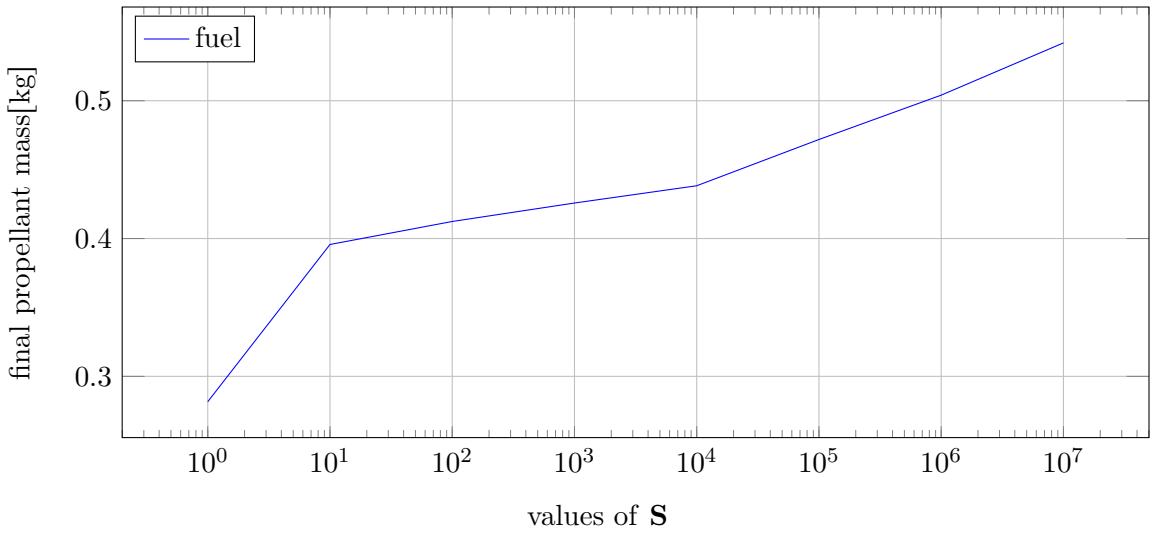

Figure 6.24: Optimisation of weighting matrix **S** with one hard constraint (r) and Euler integration (600 s): mass of used fuel

6.5 Optimised Control

The factorisation of the system matrix **A** of Eq. (5.18) is used to determine the behaviour of the geostationary spacecraft for 15 days with a free drift time of 2.5 days and a control of 0.5 days. The initial date is on the 10th of July 2016 at midnight with a step size of 600 s. The initial and final state vector $\mathbf{x}_i = \mathbf{x}_f = \begin{bmatrix} 42164.1401 & -0.04 & 0 & 0 & 0 & 0 \end{bmatrix}^T$ define the non-linear system with two hard constraints and an error tolerance of 10^{-9}. The spacecraft parameters like the mass and the radiation parameter are the same as in Section 6.4 because the optimised weighting matrices are used. **Q** is a zero six by six matrix, **R** is an identity three by three matrix and **S** is equal to $\begin{bmatrix} 10^2 & 10^2 & 10^7 & 10^6 \end{bmatrix}^T$. As the perturbation model, the full model including three Tesserals and three Zonals, Sun and Moon as well as the solar radiation pressure including the penumbra and the umbra. The satellite stays within the geostationary orbit which can be found in Fig. 6.25. In Fig. 6.26 to Fig. 6.28, it can be seen that the spacecraft stays in its control box. The control profile can be found in Fig. 6.29. The total Δv is about 21.1661 m/s. Thus, the used propellant is about 2.1567 kg which is slightly more than in the example without any optimisation of the weighting matrices (compare with Section 6.3). However in Section 6.3, the whole example corresponds for only ten days and here the example is for 15 days. Therefore, increasing the total time by 50 % results in approximately the same fuel consumption for a better choice of the weighting matrices.

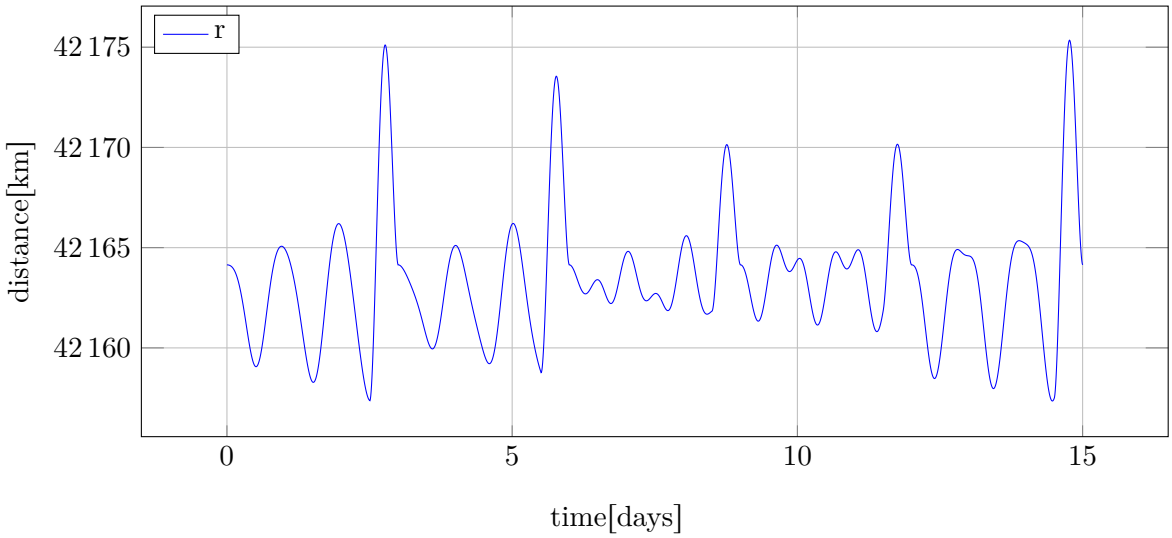

Figure 6.25: Free Drift and control of spacecraft with optimised weighting matrices with only hard constraints and Euler integration (600 s): distance to Earth vs. time

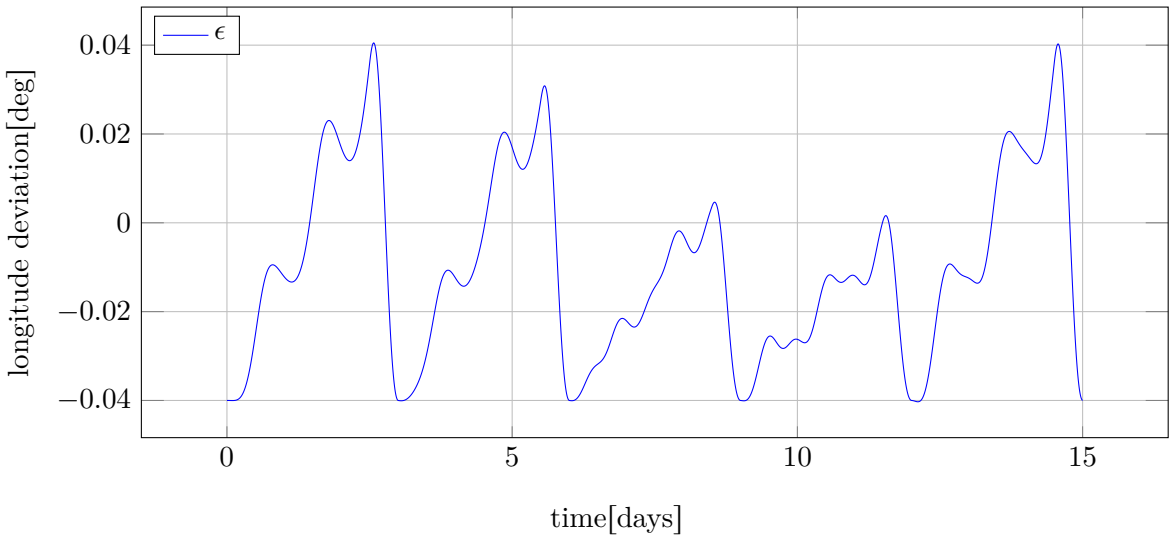

Figure 6.26: Free Drift and control of spacecraft with optimised weighting matrices with only hard constraints and Euler integration (600 s): longitude deviation vs. time

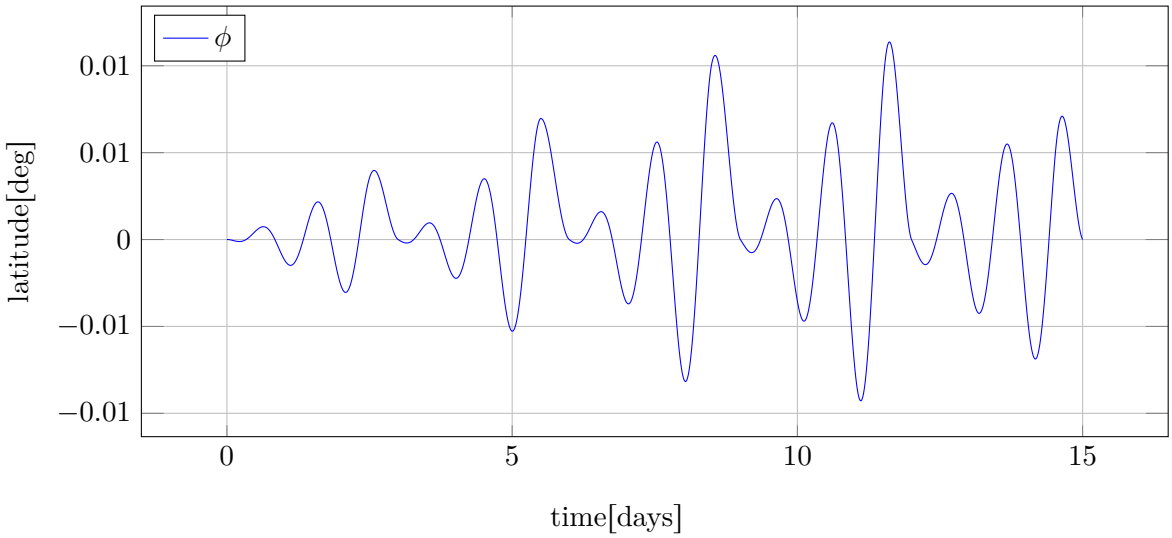

Figure 6.27: Free Drift and control of spacecraft with optimised weighting matrices with only hard constraints and Euler integration (600 s): latitude vs. time

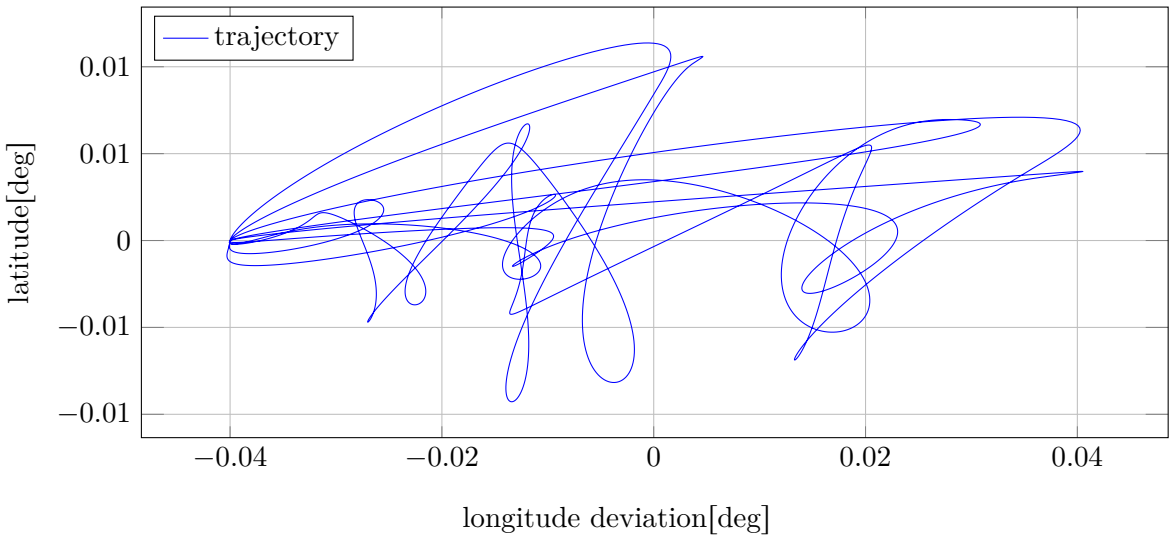

Figure 6.28: Free Drift and control of spacecraft with optimised weighting matrices with only hard constraints and Euler integration (600 s): latitude vs. longitude deviation

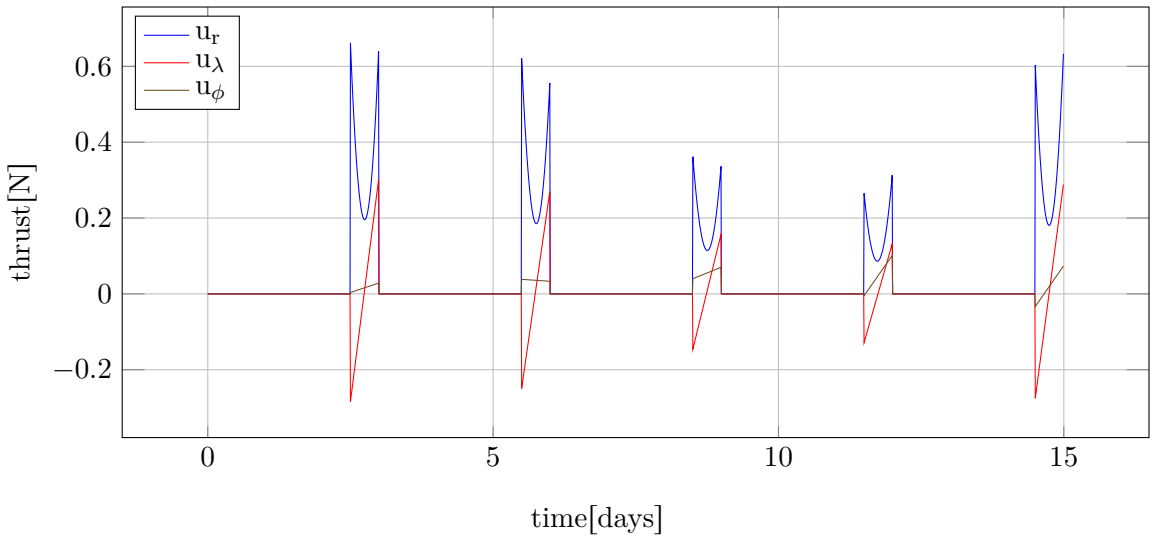

Figure 6.29: Free Drift and control of spacecraft with optimised weighting matrices with only hard constraints and Euler integration (600 s): thrust control profile

6.6 Different Factorisations

As already mentioned in Chapter 4, changing the factorisation will result in a different solution of the non-linear problem. Due to the fact that there are infinite, valid possibilities to factorise a non-linear problem with $n > 1$ it is a hard challenge to find one of the best results. Therefore, the station keeping problem for geostationary satellites with electric propulsion will be used to demonstrate the large effect of different factorisations.

In this section, the free drift plus control cycle will be calculated for one month and a second factorisation will be introduced. The velocity states of the system can be factorised to:

$$
\begin{aligned}
\dot{\mathbf{x}}_4 =& x_1 \cdot \left[-\frac{\mu}{x_1^3} + \alpha_1 x_6^2 + \alpha_2 x_5^2 \cos^2 x_3 + 2\alpha_3 x_5 \cos^2 x_3 + \omega^2 \cos^2 x_3 + \frac{a_r(r,\lambda,\phi)}{x_1} \right] + \\
& x_5 \cdot \left[x_1 x_5 \left(1-\alpha_2\right) \cos^2 x_3 + \left(1-\alpha_3\right) 2 x_1 \omega \cos^2 x_3 \right] + \\
& x_6 \cdot \left[\left(1-\alpha_1\right) x_1 x_6 \right] \\
\dot{\mathbf{x}}_5 =& x_1 \cdot \left[-\frac{2\beta_1 x_4 \omega}{x_1^2} + \frac{a_\lambda}{x_1^2 \cos x_3} \right] + \\
& x_4 \cdot \left[\frac{2\left(1-\beta_1\right)\omega}{x_1} - \frac{2\beta_2 x_5}{x_1} \right] + \\
& x_5 \cdot \left[-\frac{2\left(1-\beta_2\right) x_4}{x_1} + 2 x_6 \beta_3 \tan x_3 \right] + \\
& x_6 \cdot \left[2\left(1-\beta_3\right) x_5 \tan x_3 + 2\omega \tan x_3 \right] \\
\dot{\mathbf{x}}_5 =& x_1 \cdot \left[-\frac{\omega^2 \sin x_3 \cos x_3}{x_1} + \frac{a_\phi(r,\lambda,\phi)}{x_1^2} \right] + \\
& x_4 \cdot \left[-\frac{2\gamma x_6}{x_1} \right] + \\
& x_5 \cdot \left[-x_5 \sin x_3 \cos x_3 - 2\omega \sin x_3 \cos x_3 \right] + \\
& x_6 \cdot \left[-\frac{2\left(1-\gamma\right) x_4}{x_1} \right]
\end{aligned}
\tag{6.2}
$$

where the parameters α, β and γ are used for products which contain more than two different states. This can be done by rewriting Eq. (4.24):

$$
f_3(x) = \alpha f_1(x) + (1-\alpha) f_2(x) \tag{6.3}
$$

For the demonstration of the strong influence of the chosen factorisation, the spacecraft is simulated to be in space for 30 days while it is 1.5 days in free drift and 12 hours in the control cycle. The propagation starts on the first of July 2016 with a step size of 600 s. The weighting matrix $\mathbf{Q}$ is still a zero matrix and $\mathbf{R}$ an identity one. The number of fixed constraints is set to six. The mass of the spacecraft is assumed to be 4500 kg, the surface area to absorb radiation is 300 m^2 and the radiation parameter is 0.5.

In Fig. 6.30, the factorisation of Eq. (5.18) is used. A Δv of about 53.099 m/s is needed which is roughly a fuel consumption of 8.11 kg. In comparison, Eq. (6.2) is used with the same parameters. It is assumed that α, β and γ are equal to 1 (see Fig. 6.31). This results in an approximate Δv of 84.60 m/s and an amount of fuel of 12.92 kg which is an increase of 59.31 %.

If the factorisation of Eq. (6.2) is used with different random parameters:

$$
\begin{aligned}
\alpha_1 &= 0.7177385582720581 \\
\alpha_2 &= 0.7135013437484139 \\
\alpha_3 &= 0.1036348458357986 \\
\beta_1 &= 0.4106932641017714 \\
\beta_2 &= 0.5247763812724352 \\
\beta_3 &= 0.1734900105055931 \\
\gamma &= 0.8536348872292496
\end{aligned}
\tag{6.4}
$$

The final solution will change the Δv to a value of about 25.50 m/s and an approximate fuel mass of 3.90 kg (see Fig. 6.32). By just changing the values of α, β and γ, the new factorisation solves the same non-linear problem by using only 30.42 % of the Δv. Consequently, looking for a better factorisation should be one of the most important goals to reduce the fuel consumption for the geostationary station keeping with electrical thrusters while using the ASRE method.

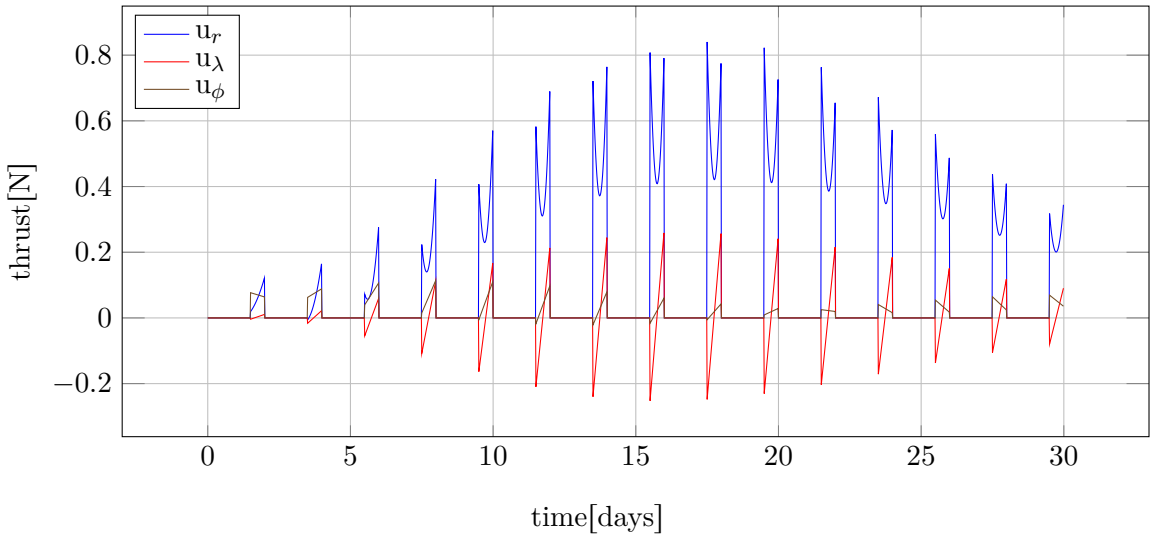

Figure 6.30: Free Drift and control of a spacecraft via factorisation $\mathbf{A}_1$ for one month with only hard constraints and Euler integration (600 s)

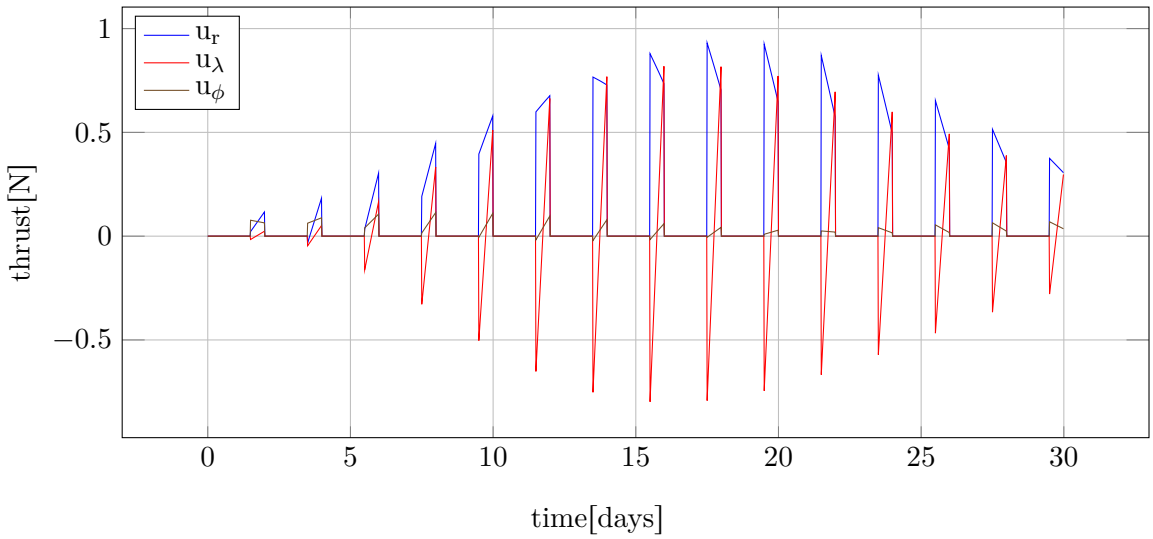

Figure 6.31: Free Drift and control of a spacecraft with ones in the parameter factorisation for one month with only hard constraints and Euler integration (600 s)

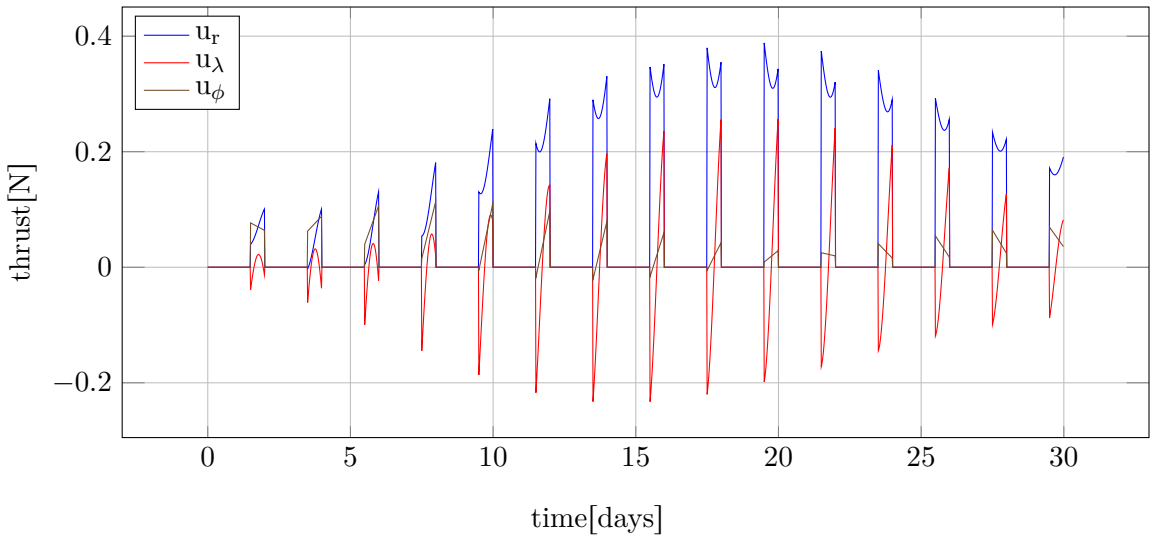

Figure 6.32: Free Drift and control of a spacecraft with random parameter factorisation for one month with only hard constraints and Euler integration (600 s)

6.7 Comparison

For the validation of the ASRE method, a comparison with common literature has to be done. The geostationary spacecraft is positioned at the ideal geostationary semi-major axis, at zero latitude and 60 deg nominal longitude. According to Losa [14], the spacecraft mass is considered to be 4500 kg, the surface area 300 m^2 and the mean reflectivity coefficient 0.3. The simulation will start at first of January 2010 and last 365 days. The factorisation of Eq. (6.2) with the parameters of Eq. (6.4) is used. This comparison only takes into account the fixed horizon approach of Losa because the ASRE method has the most commonalities with the fixed horizon approach – both calculates their optimal control input for a certain amount of time which is fixed after the calculation.

In Fig. 6.33 and Fig. 6.34, it can be seen that the spacecraft stays in its control box of $2\lambda = 2\phi =$ 0.1 deg while drifting free for 1.5 days and using its thrusters for 0.5 days. Note: the step size of those figures are at 1200 s, but only each seventh measurement point is shown.

The used thrust in all directions for the whole simulation time can be found in Fig. 6.35 to Fig. 6.37 – only each tenth measurement point is shown. The total Δv of that is at approximately 316.32 m/s which is a fuel consumption of about 48.11 kg.

In Losa [14], it is shown that the Δv of a deadband of 0.1 deg for a fixed horizon optimisation is 180.48 m/s. Via Eq. (2.11) and a specific impulse of 3000 s, the used propellant has a mass of about 27.51 kg which is approximately 57.18 % of the ASRE method.

The factorisation of Losa is improved and optimised to its perfect result. However the factorisation of Eq. (6.2) can further be improved. For example, the weighting matrices can be optimised and a better integration solver can be used. The free drift time can be optimised by using larger values – the spacecraft has still to be in the control box – or by an intelligent dynamic calculator, the maximum free drift time can be determined after each control cycle. All of these improvements will decrease the amount of propellant which is needed to hold the satellite in its control box.

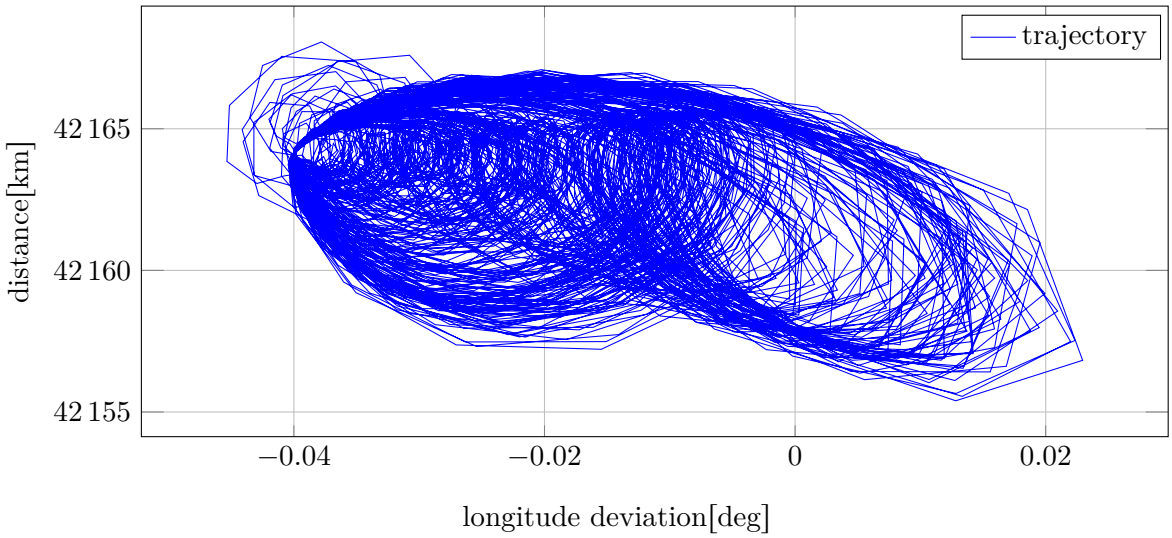

Figure 6.33: Distance to Earth over longitude for one year for a geostationary satellite with the random parameter factorisation with only hard constraints and Euler integration (1200 s)

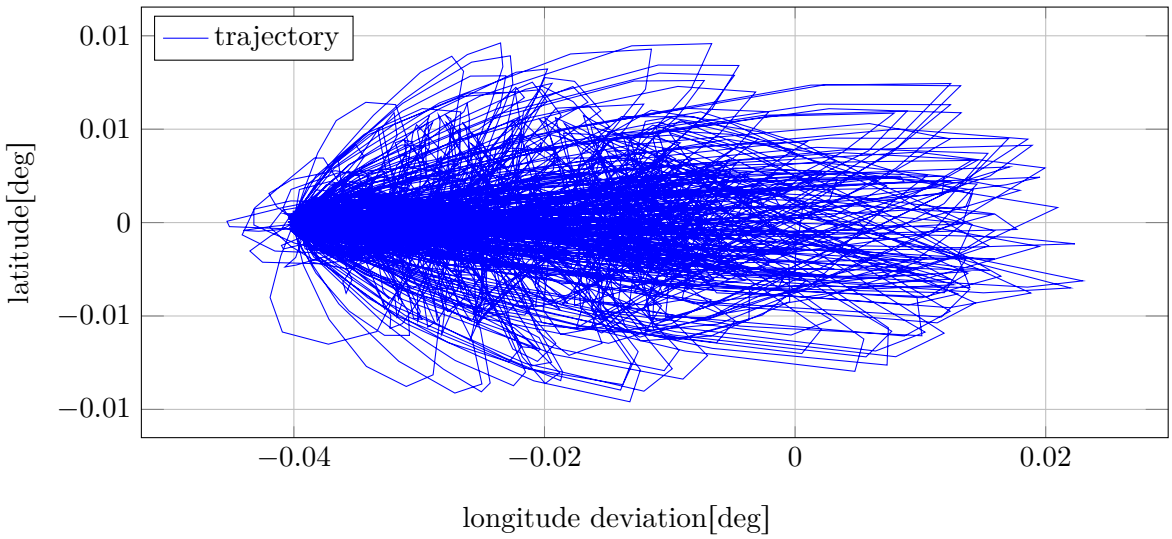

Figure 6.34: Latitude over longitude deviations for one year for a geostationary satellite with the random parameter factorisation with only hard constraints and Euler integration (1200 s)

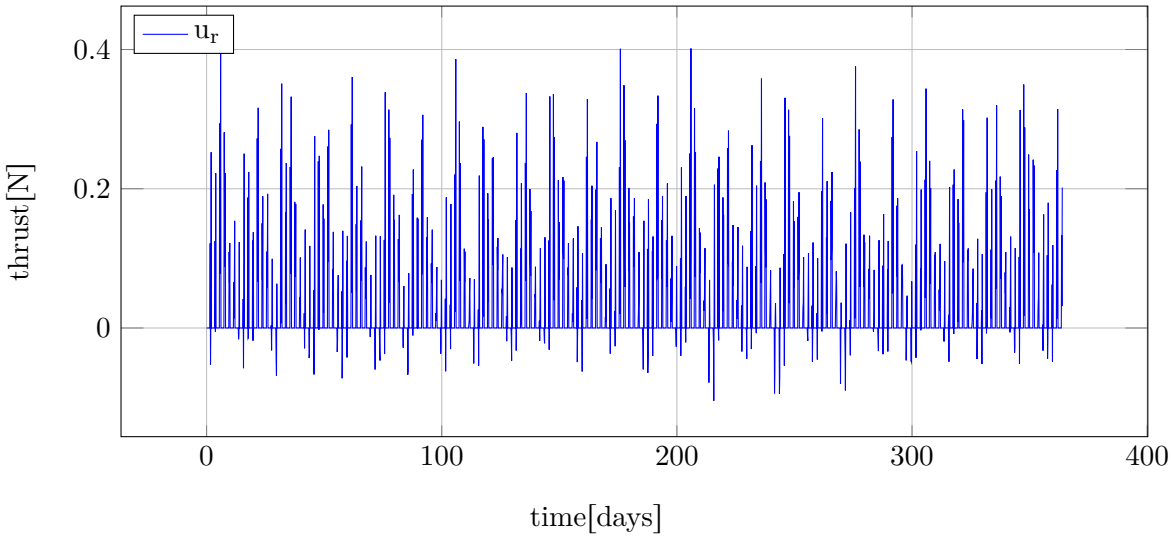

Figure 6.35: Thrust in radial direction for one year for a geostationary satellite with the random parameter factorisation with only hard constraints and Euler integration (1200 s)

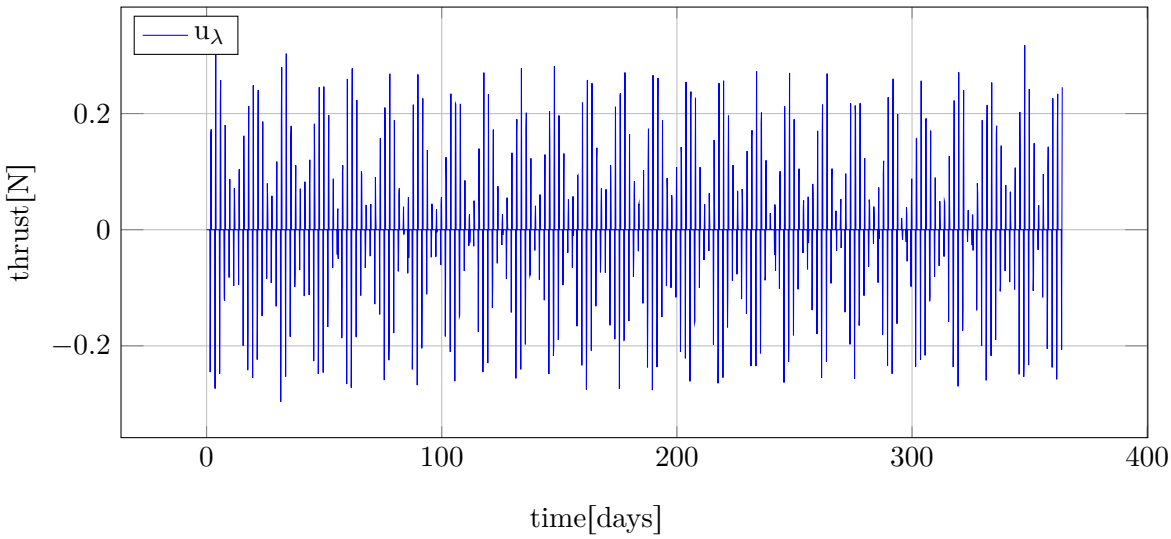

Figure 6.36: Thrust in tangential direction for one year for a geostationary satellite with the random parameter factorisation with only hard constraints and Euler integration (1200 s)

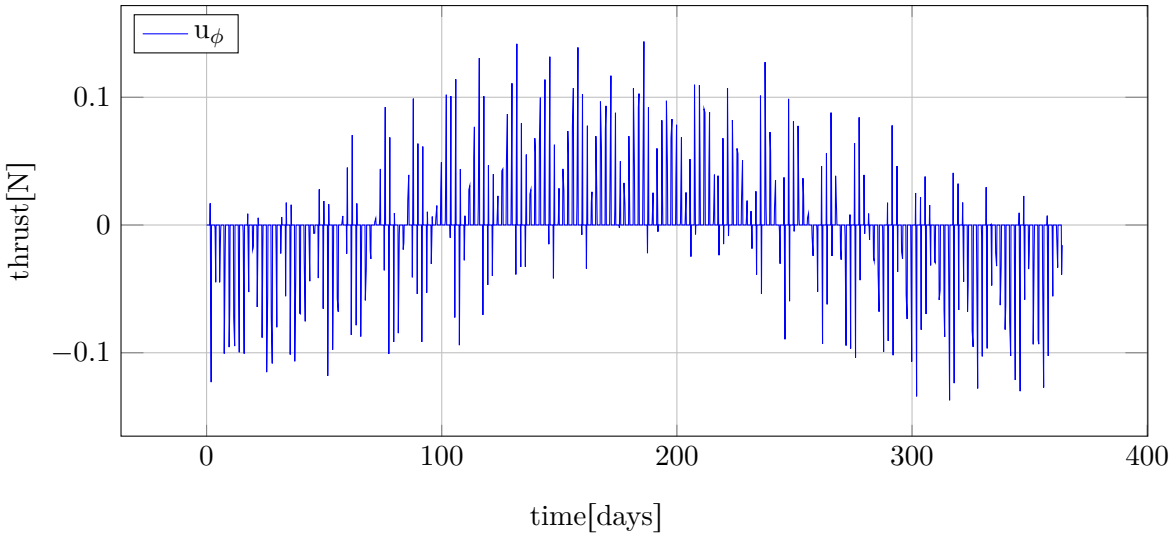

Figure 6.37: Thrust in normal direction for one year for a geostationary satellite with the random parameter factorisation with only hard constraints and Euler integration (1200 s)

7 Conclusion

7.1 Thesis Contributions

In this thesis, the possibility of holding a geostationary satellite in its control box with an electric propulsion system is shown. At the moment, this is one of the important topics for satellite providers to reduce the operational costs of a spacecraft to a minimum.
This could be achieved by using an ASRE optimisation method which is a special case of the SDRE approach. The ASRE method guarantees convergence towards its global optimum for the chosen weighting matrices and factorisation.
To optimise the station keeping problem, it is necessary to provide a perturbation model to the ASRE method. Therefore, a model including the Earth's Zonals and Tesserals up to degree and order of three, the Sun and the Moon as point masses as well as the solar radiation pressure with the eclipse constraint is used and a validation of these forces is presented. Furthermore, the ASRE approach is derived from the SDRE method. A way to implement the used method is given as well as the restrictions like controllability which have to hold. It is proven that factorisations add degrees of freedom to the pseudo-linearised non-linear model. Subsequently, the improvement of the usage of transition matrices is discussed. The non-trivial implementation of this approach is given and validated via an example which is factorised in different ways and proven why they are good factorisations. As far as the author knows, up to now there was no attempt to provide hard and soft constraints to this non-linear problem and to solve it in an optimal way with the ASRE method. The different constraints show diverse behaviour of the optimisation of the non-linear problem. For example, the hard constrained problem uses a high effort to bring the system to its final state whereas the soft constraints have a small cost because they are more flexible.
To the author's best knowledge, this is the first time that the implementation of the ASRE method including the transition matrices is given in a summarised, detailed and written form. So far, the guidelines of how to use this method are fragmental and not very precise. In addition, the spacecraft dynamics are derived with and without perturbations as well as with control input. The used pseudo-linearised factorisation is one possibility out of infinite valid ones and is chosen to the authors best knowledge.
For the final simulation, the perturbation model is included to the chosen factorisation. This complete model projects the all the external influences which act on a geostationary spacecraft and could be also used for other missions. For low Earth orbits, other forces like the drag which is neglectable for geostationary orbits have to be included, then it can be used without any restrictions. Hence, this simulation can optimise the fuel consumption for the station keeping of a geostationary satellite via the ASRE method. The simulation is tested for free drifting as well as to command the spacecraft from one position to another. As far as the author knows it is the first time that the umbra and penumbra are considered in the ASRE approach. This guarantees a more accurate perturbation

model and a more precise solution of the the station keeping problem. Furthermore, for the future improvement of the input weighting matrix it is important to provide a possibility to detect if the spacecraft enters the umbra as the low-thrust satellites are not allowed to use the thrusters while they are in the eclipse of the Earth.
A way to optimise the weighting matrices is presented and an optimal station keeping manoeuvre (for the used factorisation and weighting matrices) is shown. It is discussed that a different factorisation can decrease the total Δv which corresponds to a lower fuel consumption. A comparison of a random parameter factorisation with the result of Losa [14] is presented. The overall result is the ASRE optimisation approach can compete with classical optimisation methods. However, the given optimal control algorithm has to be improved by changing for example the factorisation or the weighting matrices.

7.2 Future Work

Future improvements should include a better choice of the weighting matrices $\mathbf{Q}$, $\mathbf{R}$ and $\mathbf{S}$. The input weighting matrix $\mathbf{R}$ should be adapted to real thruster configurations – like maximum and minimum burn duration as well as the available thrust. The calculation if the spacecraft is in the eclipse can be used to restrict the model even further. Real satellites are not allowed to use their propulsion system while they are in the umbra of the Earth, because without the sunlight not enough electricity is provided. The factorisation of the non-linear station keeping problem is very important for the result. Due to the fact that there are infinite different possibilities to factorise the problem, it is challenging to find the probably best solution. Especially a "good" choice can reduce the amount of needed propellant by more than 50 % compared to a "bad" solution. The perturbation model which contains the Sun and Moon as points masses, the solar radiation pressure (inclusive eclipses) and the Zonal and Tesseral terms of the Earth up to the order and degree of three can be made more precise. Therefore, the Zonals and Tesserals can be described with higher order terms as wells as the Sun and the Moon can be seen as non-point masses. For the modelling of the perturbations in the free drift an Euler propagator was used. Due to the increasing error of the Euler method, it is recommended to use a Runge-Kutta method up to the order of at least 4-5. This method should be used in the integration of the ASRE approach to achieve a higher accuracy. By reducing the step size of the propagator, this can be achieved but for the cost of higher computational power.
In addition, it is possible to create an alternating algorithm to combine the soft, hard and mixed constraints to a more fuel saving approach. Thus, the spacecraft can be brought to the final state and will be controlled for a certain time with the mixed constraints. If one of the free parameters go out of a certain threshold, the hard constraints will be activated again. This will save more propellant because the soft constraints are more tolerant.
Creating a better method to determine if the spacecraft will leave the control box could be another possible research topic. At the moment, a time fixed free drift is used. This could be improved in order to make it more variable such that the spacecraft can drift as long as it stays inside the box. In the actual version the whole control box is not used for the free drift.
In the future, the used ASRE method which is a kind of fixed horizon approach can be improved by adding a receding horizon as presented in Losa [14] for her optimisation. Hence, it is possible to update the ASRE method to a receding method, too.

The shown ASRE method can be used to optimise the station keeping of geostartionary satellites with electric thrusters. The positive effect of the reduction of the needed propellant is found in lower starting costs or for extension of the mission, because more fuel is available. Additionally, the saved amount of propellant can be used to install more payload on the satellite.

A Q-Matrix

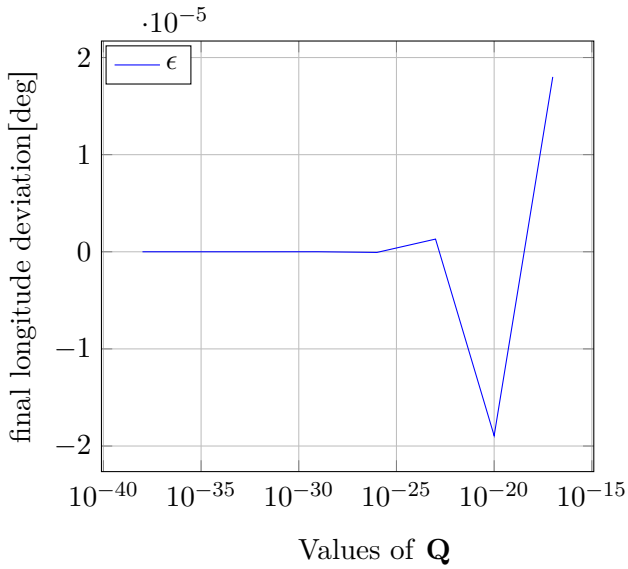

(a) Final longitude deviation values

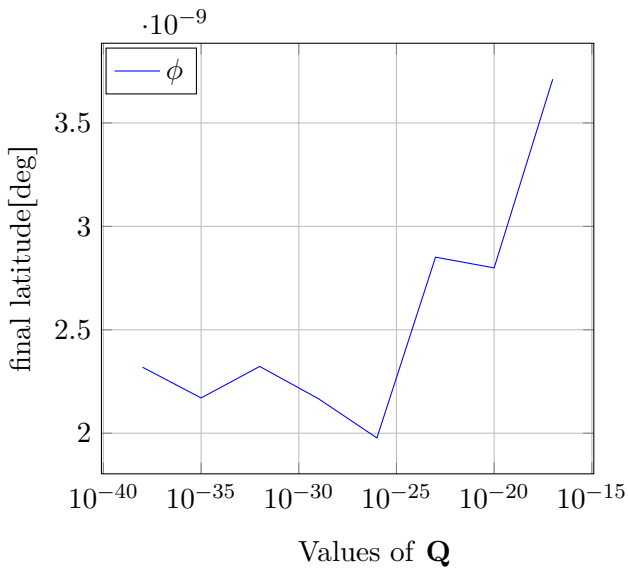

(b) Final latitude values

Figure A.1: Optimisation of weighting matrix **Q**

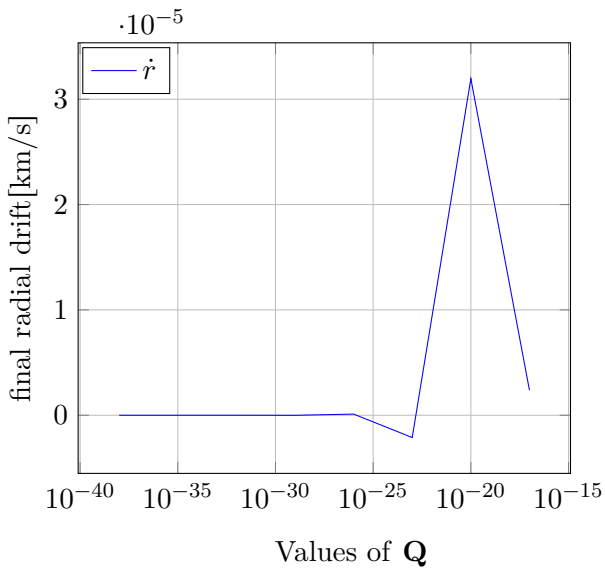

(a) Final radial drift values

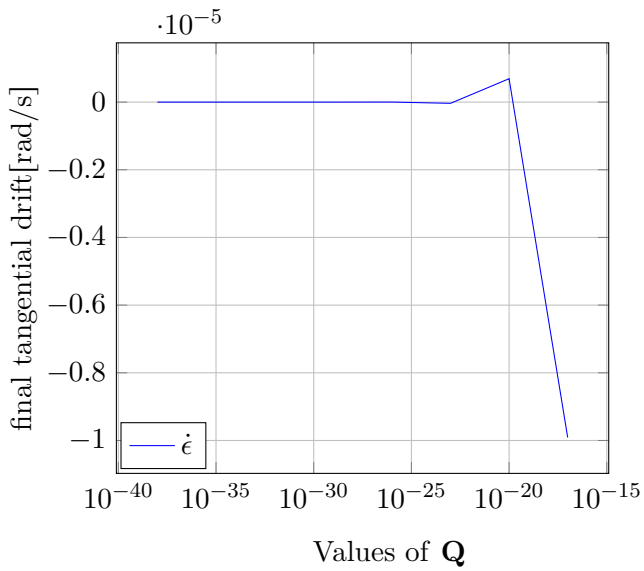

(b) Final tangential drift values

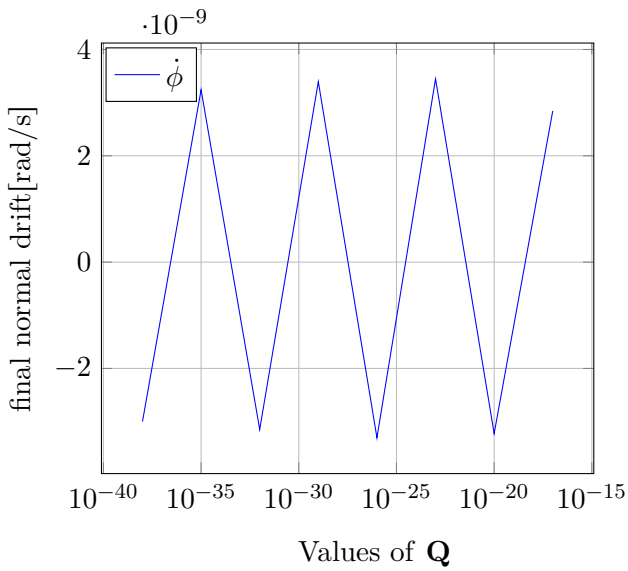

(c) Final normal drift values

Figure A.2: Optimisation of weighting matrix **Q**

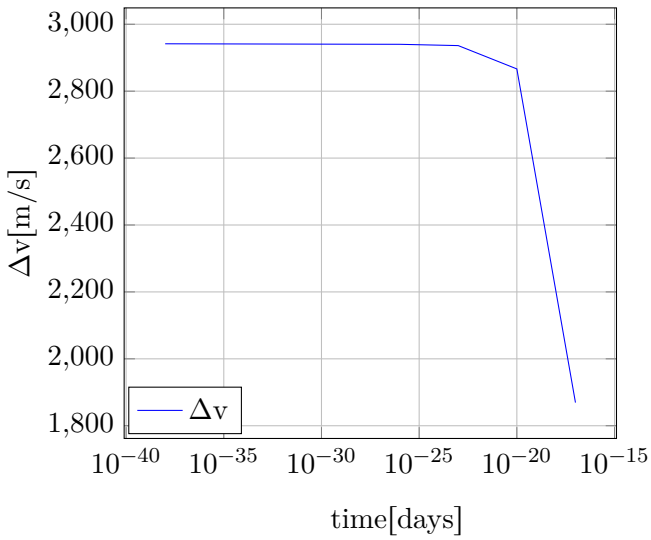

(a) Δv

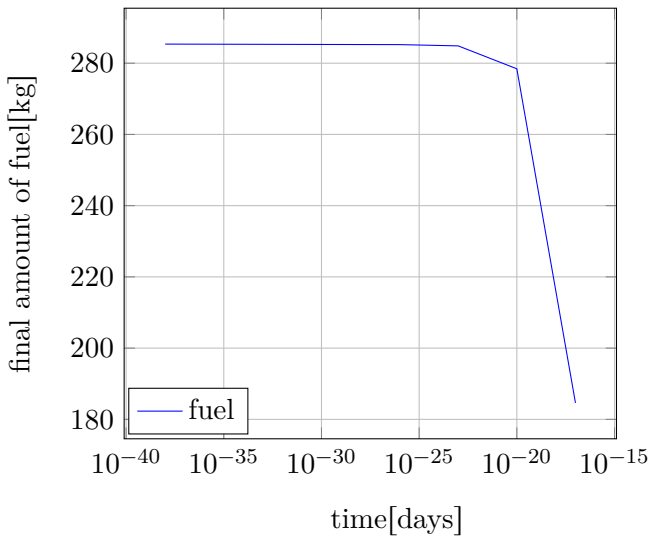

(b) Mass of needed fuel

Figure A.3: Optimisation of weighting matrix **Q** with one hard constraint (r) and Euler integration (600 s

B Symbols

Notation	Description
A	Surface area
C_r	Radiation coefficient
C_{nm}	Geopotential coefficient up to the order n and degree m of the Zonals and Tesserals
G	Gravitational constant
I_{sp}	Specific impulse
L	True longitude in EOE
$M_\oplus$	Mass of Earth
$P_\odot$	Solar radiation pressure
$P_{nm} \sin \phi$	Legendre polynomials up to the order n and degree m of the Zonals and Tesserals
$R_\oplus$	Radius of Earth
R	Radius
S_{nm}	Geopotential coefficient to the order n and degree m of the Zonals and Tesserals
U	potential function
Δv	Change of velocity vector
Ω	Right ascension of the ascending node
Φ	Solar flux
α	Angle between x-axis and projection of $\mathbf{r}_{sc}$ in the equatorial plane
$\boldsymbol{R}_{*,+}$	Rotation matrix, rotates system from * frame to + frame
$\boldsymbol{\Phi}$	Transition matrix
$\boldsymbol{\lambda}$	Co-state vector
$\boldsymbol{\zeta}$	Controllability matrix
δ	Kronecker symbol
ϵ	Reflectivity coefficient
ϵ	Error tolerance for the ASRE method
λ	Longitude
μ	Standard gravitational parameter
ν	True anomaly
ν	Shadow factor

Notation	**Description**
ω	Argument of perigee
ω	Earth angular speed
ϕ	Latitude
$\mathbf{A}$	System matrix
$\mathbf{B}$	Input matrix
$\mathbf{J}$	Cost function of the system
$\mathbf{K}$	Kalman gain
$\mathbf{P}$	Solution of the algebraic Riccati equation
$\mathbf{Q}$	Weighting matrix of the states
$\mathbf{R}$	Weighting matrix of the input
$\mathbf{S}$	Weighting matrix of the soft constraints
$\mathbf{a}$	Acceleration vector
$\mathbf{r}_{\odot}$	Vector from Earth centre to Sun in ECI
$\mathbf{r}_{☽}$	Vector from Earth centre to Moon in ECI
$\mathbf{r}_{cb}$	Vector from Earth centre to celestial body in ECI
$\mathbf{r}_{sc}$	Vector from Earth centre to spacecraft in ECI
$\mathbf{u}$	Input vector
$\mathbf{x}$	State vector
θ	GHA
a	Semi-major axis
a	Acceleration
c	Speed of light
e	Eccentricity
g	Acceleration at Earth surface
i	Inclination
m_p	Mass of used propellant
m	Mass of spacecraft
$r_{☽}$	Distance between Moon and satellite
r	Distance from centre of Earth to satellite
v	Velocity
x	Coordinate in ECI
y	Coordinate in ECI
z	Coordinate in ECI
$\lvert..\rvert$	Norm of a vector

C Acronyms

Notation	Description
ASRE	Approximate Sequence of Riccati Equation
COE	Classical Orbital Elements
ECEF	Earth-Centred Earth-Fixed
ECI	Earth-Centered Inertial
EOE	Equinoctial Orbital Elements
GHA	Greenwich Hour Angle
JGM	Joint Gravity Model
LQ control	Linear Quadratic control
LQR	Linear Quadratic Regulator
RTN	Radial-Tangential-Normal
SDC	State-Dependent Coefficient
SDRE	State-Dependent Riccati Equations

D Bibliography

[1] J. R. Cloutier. State-Dependent Riccati Equation Techniques: An Overview. In *Proceedings of the American Control Conference*, pages 932–936, June 1997.

[2] J. R. Cloutier. The Capabilities and Art of State-Dependent Riccati Equation-Based Design. In *Proceedings of the American Control Conference*, pages 86–91, May 2002.

[3] J. R. Cloutier, C. N. D'Souza, and C. P. Mracek. Nonlinear regulation and nonlinear h_∞ control via the state-dependent riccati equation technique. In *IFAC World Congress*, 1996.

[4] M. Eckstein and F. Hechler. Station acquisition and station keeping with low-thrust systems. In *Proc. Int. Symp. Spacecraft Flight Dynamics, Darmstadt, FRG*, May 1981.

[5] C. Gazzino, D. Arzelier, D. Losa, C. Louembet, C. Pittet, and L. Cerri. Optimal Control for Minimum-Fuel Geostationary Station Keeping of Satellites Equipped with Electric Propulsion. working paper or preprint, Jan. 2016.

[6] K. D. Hammett. *Control of Nonlinear Systems via State Feedback State-Dependent Riccati Equation Techniques*. Ph.D. Thesis, Graduate School of Engineering, Dept. of Aeronautics and Astronautics, U.S. Air Force Inst. of Technology, Wright–Patterson AFB, Ohio, June 1997.

[7] K. D. Hammett, C. D. Hall, and D. B. Ridgely. Controllability issues in nonlinear state-dependent riccati equation control. *Journal of Guidance, Control and Dynamics*, pages 767–773, 1998.

[8] A. Heydari and S. N. Balakrishnan. Approximate closed-form solutions to finite-horizon optimal control of nonlinear systems. In *2012 American Control Conference (ACC)*, pages 2657–2662, June 2012.

[9] T. Çimen. 17th IFAC Symposium on Automatic Control in Aerospace APPROXIMATE NONLINEAR OPTIMAL SDRE TRACKING CONTROL. *IFAC Proceedings Volumes*, 40(7):147 – 152, 2007.

[10] T. Çimen. State-Dependent Riccati Equation (SDRE) Control: A Survey. In *Proceedings of the 17th World Congress*, pages 3761–3775. The International Federation of Automatic Control, July 2008.

[11] T. Çimen and S. P. Banks. Global optimal feedback control for general nonlinear systems with nonquadratic performance criteria. *Systems & Control Letters*, 53(5):327 – 346, 2004.

[12] T. Çimen and S. P. Banks. Nonlinear optimal tracking control with application to super-tankers for autopilot design. *Automatica*, 40(11):1845 – 1863, 2004.

[13] F. L. Lewis, D. Vrabie, and V. L. Syrmos, editors. *Optimal control*. John Wiley & Sons, 3 edition, 2012.

[14] D. Losa. *High vs Low Thrust Station Keeping Maneuver Planning for Geostationary Satellites*. Automation, École Nationale Supérieure des Mines de Paris, 2007. English. <NNT: 2007ENMP1451>. <tel-00173537>.

[15] D. Losa, M. Lovera, R. Drai, T. Dargent, and J. Amalric. Electric station keeping of geostationary satellites: a differential inclusion approach. In *Proceedings of the 44th IEEE Conference on Decision and Control*, pages 7484–7489, Dec 2005.

[16] D. Losa, M. Lovera, J. P. Marmorat, T. Dargent, and J. Amalric. Station keeping of geostationary satellites with on-off electric thrusters. In *2006 IEEE Conference on Computer Aided Control System Design, 2006 IEEE International Conference on Control Applications, 2006 IEEE International Symposium on Intelligent Control*, pages 2890–2895, Oct 2006.

[17] J. Lunze. *Regelungstechnik 2*. Springer Berlin Heidelberg, 2010.

[18] O. Montenbruck and E. Gill. *Satellite Orbits*. Springer, 2005.

[19] M. Pasta. *Station keeping di satelliti geostazionari mediante controllo ottimo non lineare*. Facoltà di ingegneria industriale, Politecnico di Milano, 2009.

[20] J. Pocha. *An Introduction to Mission Design for Geostationary Satellites (Space Technology Library)*. Springer, 1987.

[21] M. J. Sidi. *Spacecraft Dynamics & Control*. Cambridge University Press, 2006.

[22] E. M. Soop. *Handbook of geostationary orbits*. Kluwer Academic Publishers, 1994.

[23] B. Steinfeldt and P. Tsiotras. A State-Dependent Riccati Equation Approach to Atmospheric Entry Guidance. In *AIAA Guidance, Navigation, and Control Conference*, August 2010.

[24] A. Sukhanov and A. Prado. On one approach to the optimization of low-thrust station keeping manoeuvres. January 2012.

[25] F. Topputo and F. Bernelli-Zazzera. Optimal low-thrust station keeping of geostationary satellites. In *CEAS 2011 The International Conference of the European Aerospace Societies*, 2011.

[26] F. Topputo and F. Bernelli-Zazzera. A method to solve nonlinear optimal control problems in astrodynamics. In *1st IAA Conference on Dynamics and Control of Space Systems*, 2012.

[27] F. Topputo and F. Bernelli-Zazzera. Approximate Solutions to Nonlinear Optimal Control Problems in Astrodynamics. *ISRN Aerospace Engineering*, 2013, 2013.

[28] F. Topputo, M. Miani, and F. Bernelli-Zazzera. Optimal Selection of the Coefficient Matrix in State-Dependent Control Methods. *Journal of Guidance Control and Dynamics*, 38:861–873, 2014.

[29] A. Weiss, U. Kalabic, and S. Di Cairano. Model Predictive Control for Simultaneous Station Keeping and Momentum Management of Low-Thrust Spacecraft. *MITSUBISHI ELECTRIC RESEARCH LABORATORIES*, July 2015.

[30] J. R. Wertz, editor. *Spacecraft Attitude Determination and Control*. D. Reidel, 1978 edition, 2002.

[31] S. Widnall, J. Deyst, and E. Greitzer. 16.07 Dynamics. (Massachusetts Institute of Technology: MIT OpenCourseWare), `http://ocw.mit.edu`. (Accessed 2 May, 2016). License: Creative Commons BY-NC-SA.